Bio-hybrid polymer membranes as tools for mimicking cell compartments

Inauguraldissertation

zur

Erlangung der Würde eines Doktors der Philosophie

vorgelegt der

Philosophisch-Naturwissenschaftlichen Fakultät

der Universität Basel

von

Mihai Lomora

aus Rumänien

Basel, 2017

Genehmigt von der Philosophisch-Naturwissenschaftlichen Fakultät
auf Antrag von

Prof. Dr. Cornelia G. Palivan (Universität Basel)

und

Prof. Dr. Abhay Pandit (National University of Ireland, Galway)

Basel, den 21. März 2017

Prof. Dr. Martin Spiess

Dekan

SUMMARY

"Many of the cells are very tiny, but they are very active; they manufacture various substances; they walk around; they wiggle; and they do all kinds of marvelous things - all on a very small scale. Also, they store information. Consider the possibility that we too can make a thing very small which does what we want - that we can manufacture an object that maneuvers at that level!" - There's plenty of room at the bottom, Richard P. Feynman, 1959.

In cells, membrane proteins naturally insert in lipid bilayers. The thickness of a lipid bilayer cell membrane is around 5 nm, with little variation in the hydrophobic mismatch (difference between the hydrophobic region of the membrane protein and the hydrophobic region of the spanned membrane) allowing them to function properly. In this work, the challenge was to identify the proper conditions in which selected ion channels (gramicidin), ion carriers (ionomycin), and other biopores (engineered α-hemolysins and glycerol facilitator) maintain their function in synthetic membranes of polymersomes with thicknesses up to 16 nm. This raised a set of questions. Gramicidin has a length of 2.5 nm, therefore: is it possible to insert and function in membranes up to 6 times thicker than the ion-channel's size? Is there a limit of membrane thickness at which the inserted membrane protein does not function anymore? Does a biopore preserve its full known function in thicker membranes? How does an ionophore of 1.5 nm in diameter, such as ionomycin, move through a thick hydropobic layer of a polymerosme membrane? Is it possible to explain the mechanism of permeabilization in thick polymer membranes? Moreover, these biopores require solubilization in organic solvents or detergents which might also impact the permeabilization of the synthetic membranes. Is there a way of avoiding detergent/organic solvent induced permeabilization and thus preservation of the architecture of the vesicles? Is the permeability induced only by the successful insertion of biopores? The insertion of membrane proteins is just a part of the challenge, as the final 3D architecture of polymersomes might also be affected in presence of additional biomolecules. The system becomes even more complex once enzymes are involved, or the designed vesicular systems are attached on solid supports. Therefore, the list of questions can be extended. As a result, this thesis aims to answer many of the above listed questions. The proposed solutions, described in this body of work, represent the foundation for the development of nano-scaled biosensors, nanoreactors and active surfaces.

TABLE OF CONTENTS

ABBREVIATIONS

$(k_{cat})_{app}$	Apparent kinetic constants
6-PG	6-Glucose phosphogluconate
7-ADCA	7-Aminodesacetoxycephalosporanic acid
A_2	Second virial coefficient
ABTS	2,2′-Azino-bis(3-ethylbenzthiazoline-6-sulfonic acid)
ACG	Asante Calcium Green
ADH	Alcohol dehydrogenase
AEC	3-amino-9-ethyl carbazole
AFM	Atomic force microscopy
ALP	Alkaline phosphatase
ANG-2	Asante Natrium Green-2
APG-2	Asante Potassium Green-2
AqpZ	Aquaporin Z
ATP	Adenosine triphosphate
ATRP	Atom transfer radical polymerization
Bcl-xL	B-cell lymphoma-extra large inhibitor
BCP	Block copolymer
Bd	Poly(butadiene)
BODIPY	Boron-dipyrromethene
BR	Bacteriorhodopsin
BSA	Bovine serum albumin
CAL B	Candida antarctica lipase B
CAT	Catalase
CC	Cytochrome C
CF	5(6)-Carboxyfluorescein
Cho	Cholesteryl
CLSM	Confocal laser scanning microscopy
CMA	Coumarin

CMC	Critical micellar concentration
CPO	Caldariomyces fumago
cryo-TEM	Cryo-transmission electron microscopy
Cu/Zn SOD	Cu/Zn super oxide dismutase
Cu^{II}ENZm	Copper enzyme mimic
Cy5	Cyanine 5
DAPN	2,3-Diaminophenazine
DEAEM	2-(Diethylamino)ethyl methacrylate
D_{eff}	Effective diffusion coefficient
DiFMU	6,8-Difluoro-4-Methylumbelliferyl
DLD	Dye labeled dextran
DLS	Dynamic light scattering
DMIBM	3,4-Dimethyl maleic imidobutyl methacrylate
DMIEM	3,4-Dimethyl maleic imidoethyl methacrylate
D_{MP}	Diffusion of membrane protein
DMSO	Dimethyl sulfoxide
DNA	Deoxyribonucleic acid
DOX	Doxorubicin
EDTA	Ethylenediaminetetraacetic acid
EE	Encapsulation efficiency
EEP	Process encapsulation efficiency
EO	Poly(ethylene oxide)
EPR	Electron paramagnetic resonance
EPR	Enhanced permeability and retention
EtOH	Ethanol
FCS	Fluorescence correlation spectroscopy
FhuA	Ferrichrome-iron receptor

G	Glycolysis
$G_{1,6}$-di-PO_4	Glucose-1,6-bisphosphate
G1P	α-D-glucose-1-phosphate
G6P	α-D-glucose-6-phosphate
G6PDH	Glucose-6-phosphate dehydrogenase
gA	Gramicidin
GdnHCl	Guanidinium chloride
GlpF	Glycerol facilitator
GOx	Glucose oxidase
GUVs	Giant unilamellar vesicles
H_2O_2	Hydrogen peroxide
Hb	Hemoglobin
HEPES	4-(2-Hydroxyethyl)-1-piperazineethanesulfonic acid
His	Histidine
HMDER	Rhodol bearing a hydroxymethyl group
$HO^{\cdot}$	Hydroxyl radical
HRP	Horseradish peroxidise
IAA	Isocyano-L-alanine-L-ananine
IAH	Isocyano-L-alanine-L-histidine
IgG	Immunoglobulin G
IPTG	Isopropyl β-D-1-thiogalactopyranoside
LPO	Lactoperoxidase
LPSA	Lipopolysaccharide-amine
Lys	Lysozyme
MHB	Müller-Hinton medium
M_n	Number average molecular weight
MNGIE	Neurogastrointestinal encephalomyopathy disease

MP	Membrane protein
mPEG	Methoxy-poly(ethylene glycol)
MSCs	Mesenchymal stem cells
M_w	Molecular weight
Myo	Myoglobin
n	Number of measurements
$Na_2S_2O_4$	Sodium hydrosulfite
$NADP^+$	Nicotinamide adenine dinucleotide phosphate
NADPH	Nicotinamide adenine dinucleotide phosphate (reduced form)
N_{agg}	Aggregation number
NEVs	Nuclear envelope-like vesicles
NO_2	Nitrogen dioxide
NR	Nanoreactor
$O_2^{\cdot -}$	Superoxide anion
OA	Oxidized sodium alginate
OG	n-Octyl-β-D-Glucopyranoside
OG488	Oregon Green®488
OmpF	Outer membrane protein F
OPD	o-Phenylenediamine
OVA	Ovalbumin
P(Asp)	Poly(α,β-aspartic acid)
P(Asp)-AP	Poly(poly([2-aminopentyl]-α,β-aspartamide)
PAA	Poly(acrylic acid)
PAA	Poly(acrylic acid)
PAD	Poly(N-amidino)dodecyl acrylamide
PB	Polybutadiene
PBLA	33Poly(β-benzyl-L-apsartate)

PCL	Poly(ε-caprolactone)
PDEA	Poly(2-(diethylamino) ethyl methacrylate
PDEAEMA	Poly(2-(diethylamino)ethyl) methacrylate
PDI	Polydispersity index
PDMIBM	Poly- 3,4-dimethylmaleinimidobutylmethacrylate
PDMIEM	Poly-3,4-dimethylmaleinimidoethylmethacrylate
PDMS	Poly(dimethylsiloxane)
PDPA	Poly(2-(diisopropylamino)ethyl methacrylate)
PDT	PhotoDynamic Therapy
PEG	Poly(ethyleneglycol)
PEGA	Poly(ethylene glycol) methyl ether acrylate
pEGFP	Enhanced green-fluorescence protein plasmid
PEI	Polyethyleneimine
PEO	Poly(ethylene oxide)
PEtOz	Poly(2-ethyl-2-oxazoline)
PGM	α-Phosphoglucomutase
PGME	Phenylglycine methyl ester
PIAH	Poly(isocyano-L-alanine-L-histidine)
PIAT	Poly(3-(isocyano-lalanyl-aminoethyl)thiophene)
PIB	Polyisobutylene
PIC	Polyion complex
PICsomes	Polyion complex vesicles
PLA	Poly(lactic acid)
PLL	Poly(lysine)
PMOXA	Poly-(2-methyloxazoline)
PMPC	Poly(2-methacryloyloxyethyl phosphorylcholine)
PNBOC	Poly(2-nitrobenzyloxycarbonyl aminoethyl methacrylate)

PNIPAM	Poly(N-isopropylacrylamide)
PNVP	Poly(N-vinylpyrrolidone)
Polsp	Selective permeable membranes
POPC	1-Palmitoyl-2-oleoyl-sn-glycero-3-phosphocholine
PP-OH	2-Hydroxy-4′-2-(hydroxyethoxy)-2-methylpropiophenone
PPP	Pentose phosphate pathway
PPS	Poly(propylene sulfide)
PS	Poly(styrene)
PSBA	Poly(styrene boronic acid)
RB–BSA	Rose Bengal - bovine serum albumin conjugate
RDH	Ribitol 2-dehydrogenase
R_g	Radius of gyration
R_h	Hydrodynamic radius
Rhod-PE	1,2-Dioleoyl-sn-glycero-3-phosphoethanolamine-N-(lissamine rhodamine B sulfonyl) (ammonium salt)
RNS	Reactive nitrogen species
ROS	Reactive oxygen species
RT	Room temperature
SD	Standard deviation
SDS	Sodium dodecyl sulphate
SEM	Scanning electron microscopy
siRNA	Small interfering ribonucleic acid
SLS	Static light scattering
SRB	Sulforhodamine B
TEM	Transmission electron microscopy
TMB	3,3′,5,5′-Tetramethylbenzidine
TMSPMA	3-(Trimethoxysilyl)propyl methacrylate)

TP	Thymidine phosphorylase
Tsx	Nucleoside-specific protein
TvNH	*Trypanosoma vivax*
UV	Ultraviolet
WST-1	2-(4-Iodophenyl)-3-(4-nitrophenyl)-5-(2,4-disulfophenyl)-(2H-tetrazolium)
z-FCS	z-Scan fluorescence correlation spectroscopy
β Gal	β -Galactosidase
α-HL	α-Hemolysin

I. INTRODUCTION

1. Cell compartments as a source of inspiration for the design of synthetic molecular factories

Design of molecular factories at the nano- or microscale requires a multi-step approach (Figure 1) [1]. First of all, it assumes the identification of a source of inspiration. Cells represent a global complex architecture from where we can draw innovation, as their cellular and molecular mechanisms, lie at the basis of life.

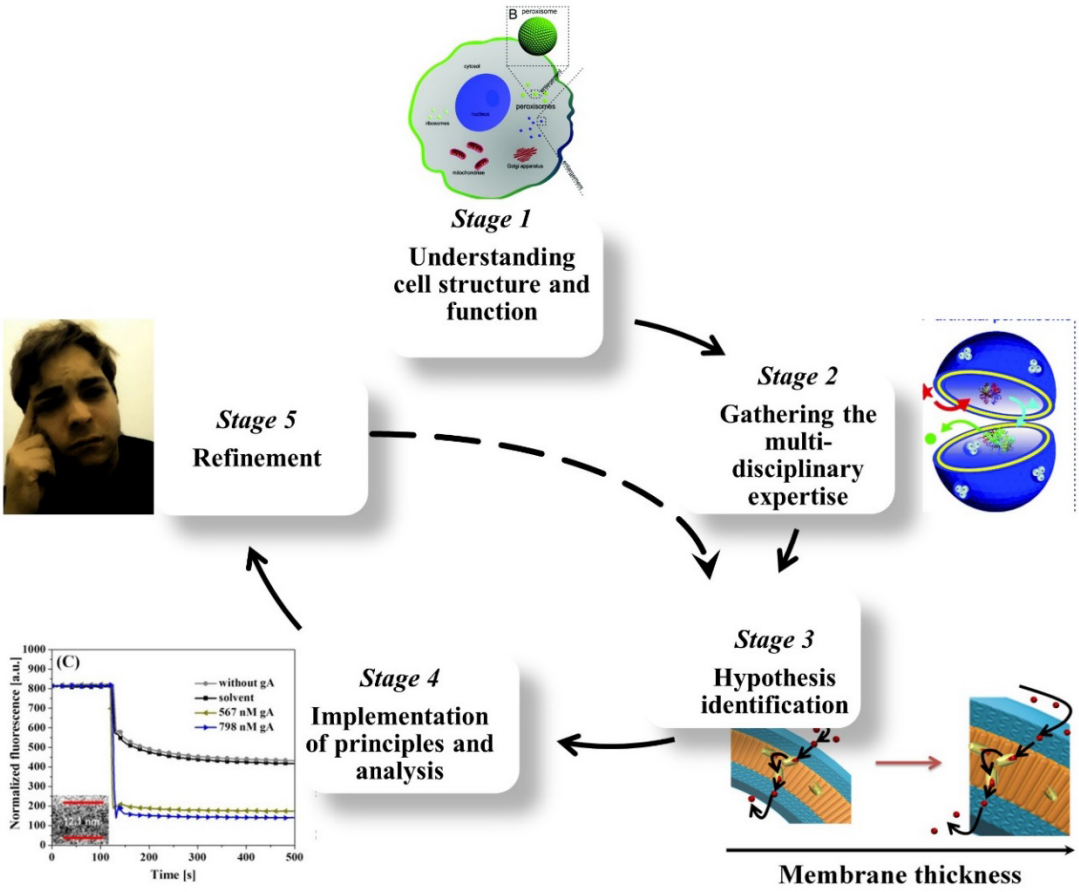

Fig. 1. General stages for the design of bio-hybrid polymer membranes using cell compartments as a source of inspiration. Modified and adapted based on ref. [1], ref. [2] Copyright (2017) American Chemical Society, ref. [3] Copyright (2017) with permission from Elsevier, and ref. [4] Copyright John Wiley and Sons.

Biological complex molecular factories consist of a membrane enclosing a mixture of smaller compartments known as organelles, each able to carry out specific and intricate functions.

The protective membrane, surrounding the organelles and cells, consists of self-assembled amphiphilic lipid molecules that accommodate membrane proteins to enable signaling and communication between the interior and outside environment. The first step in designing synthetic membranes and compartments, molecular machines or other biological inspired devices, is understanding of cell structure, physiology, or cellular communication pathways. Trying to mimick organelles or the entire cell in terms of structure or function is almost impossible due to the dynamic nature of biological systems [5]. In fact, by attempting to reproduce the structure or functions of biological systems, new non-existent in Nature functions could be discovered.

The second step in the design of synthetic molecular systems requires a multi-disciplinary perspective and involvement of researchers with various backgrounds. For example, the combination of polymer membranes with sensitive biomacromolecules (bio-hybrid polymer membranes), the expertise and interdisciplinary contribution of fields such as, but not limited only to these: biology, materials science, physical chemistry and nanoscience, should be considered (Figure 1, Stage 2). Among bio-inspired structures, liposomes (self-assembled vesicles from cholesterol and natural pshospolipids) and their combination with biological entities, are a great example of a progressive bio-inspired advanced technology [6, 7]. They are characterized by a bilayered membrane with known instability. Strategies to stabilize them are under current investigation including: tuning their composition, such as cholesterol content, or from a chemical (hydrolysis, oxidation) or physical (pH, temperature, ionic strength, buffer composition) point of view [8–11]. However, to overcome the disadvantage of liposomes' instability, more stable synthetic systems such as those based on polymers are currently being explored. Amphiphilic block-copolymers have much higher molecular weights, and they can also assemble into polymer vesicles, with much higher stability and tunable physical, chemical and biological properties than liposomes (Figure 2) [12]. As a result, combination of polymersomes with biomacromolecules does provide a better solution for the design of cellular mimicking compartments.

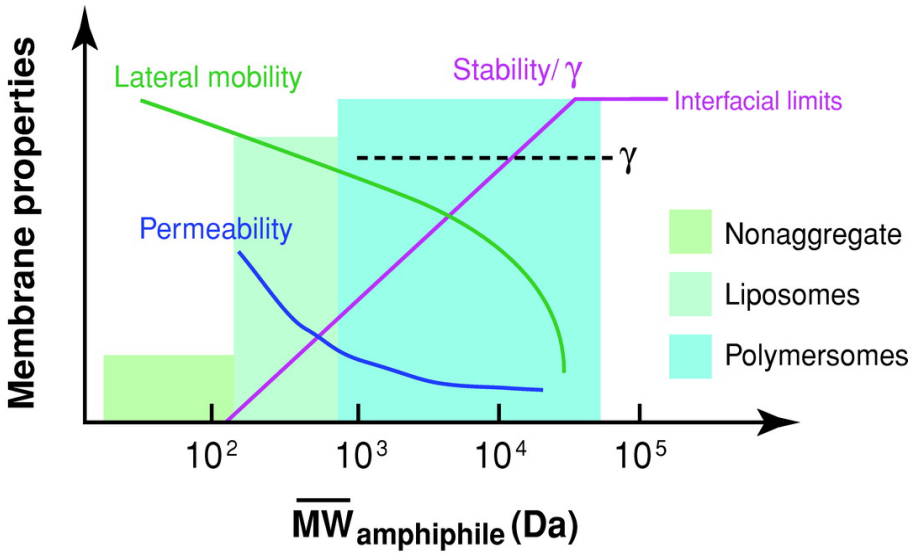

Fig. 2. Due to the higher molecular weight of polymers, their self-assembled structures into polymersomes provide more stable 3D architectures than liposomes, but at the expense of their membrane permeability and fluidity. Reprinted with permission from [13].

Once the necessary expertise has been gathered, the third step in designing synthetic molecular factories can be tackled. This step consists of the identification of proper hypotheses, assuming a thoroughly understanding of the structure and function of cellular systems (Figure 1, Stage 3). For instance, we do know that neuron-to-neuron communication occurs by sending electrical and chemical signals through their synapses. Would it be possible to re-create this communication using a completely artificial system, such as embedding the proper neuronal enzymes in synthetic vesicles? Would we be able to create a synthetic synaptic vesicle able to send signal and replace part of the neuronal functionality? Likewise, by translating single functionalities of complex artificial organelles, it was possible to design and develop a very simplistic artificial peroxisome, which might serve in the future as a novel system for treatment of currently incurable diseases, such as Parkinson, AIDS, or cancer [2]. Therefore, through the testing of these hypotheses, new principles are identified, implemented and analyzed (Figure 1, Stage 4), followed by an ongoing cycle of continuous improvement (Figure 1, Stage 5).

Though presented here as a very simplistic approach, this design strategy offers an approach overview for the design of synthetic bio-hybrid membranes and molecular factories using cell compartments as a source of inspiration.

2. Bio-hybrid spherical synthetic compartments and their applications

This subsection has been reprinted and modified by permission of The Royal Society of Chemistry from the following publication:

G. Gunkel-Grabole, S. Sigg, **M. Lomora**, S. Lörcher, C.G. Palivan, W. Meier, *Polymeric 3D nano-architectures for transport and delivery of therapeutically relevant biomacromolecules*, Biomaterials Science, **2015**, 3, 25-40.

The understanding of living cells self-assembly to block-copolymers chains joined together in solution is just a slight requirement for the breakthroughs in nanocience for curing currently killing diseases, or simply offering us a better life [14, 15]. Through the self-assembly process, polymers, peptides and their combinations can form spherical structures and accommodate biological macromolecules (eg. enzymes, oligonucleotides) inside their interior. Moreover, for those synthetic architectures surrounded by a membrane, reconstitution of membrane proteins enhances the functionality of these mimetic micro- or nanostructures for specific medical applications.

2.1. Globular synthetic compartments (polymersomes)

The self-assembly process is strongly influenced by the equilibrium between the free energy contributions to the self-assembly and kinetic factors [16–18]. Hence, introduction of additional blocks, variation of the block lengths (volume ratio of the hydrophilic to hydrophobic block) within the block-copolymer structure induces morphological changes of the final vesicular structures (Figure 3) [19, 20].

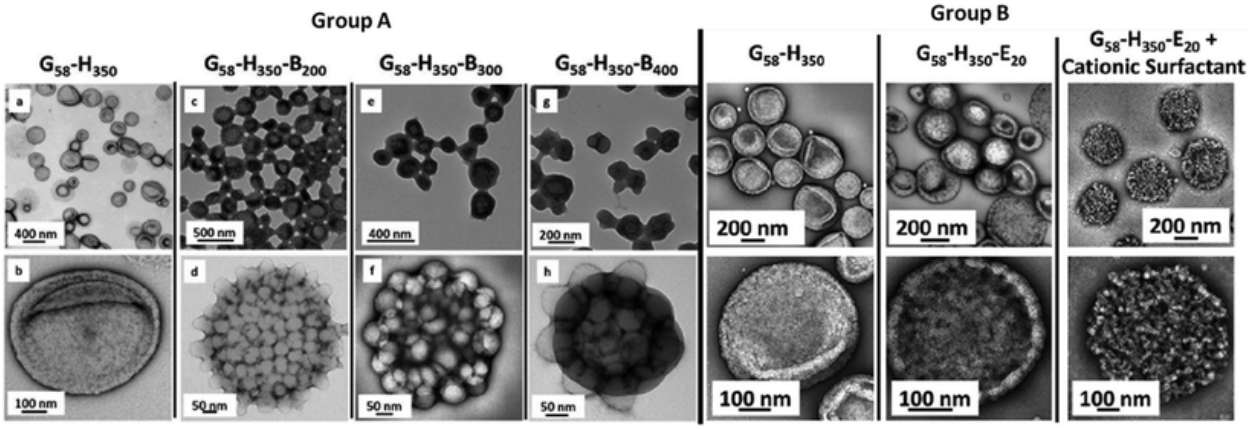

Fig. 3. Transmission electron microscopy (TEM) micrographs of various 3D vesicular nanoarchitectures. The block copolymers used to assemble these structures are composed of glycerol monomethacrylate (G), 2-hydroxypropyl methacrylate (H), benzyl methacrylate (B) and ethylene glycol dimethacrylate (E). The top row of TEM micrographs represents an overview of the vesicle samples, while the images below provide details of single vesicles. On the left (group A) it is shown that the introduction of an additional B block and changing the polymer block length induces conformational changes in the structure. On the left (group B), similar behaviour is observed by replacement of the B block with the E block. Further, the influence of surfactant on the final conformation of the architecture is demonstrated. Adapted with permission from [19]. Copyright 2012 of the American Chemical Society.

Self-assembled artificial systems, such as spherical micelles, vesicles or nanoparticles have been intensively investigated as potential candidates for their combination with biomacromolecules and as protective and defined synthetic reaction spaces (Figure 4) [21]. Among these, polymer vesicles or polymersomes - as they were first named in 1999 [22] - deserve special interest, because hydrophilic molecules can be entrapped in their inner cavity [23], and/or hydrophobic compounds can be inserted in their membrane [24]. Polymer vesicles are micro- (giant unilamer vesicles) or nanosized (polymersomes), spherical and hollow 3D architectures. An aqueous solution is enclosed by a membrane composed of amphiphilic block copolymers [12].

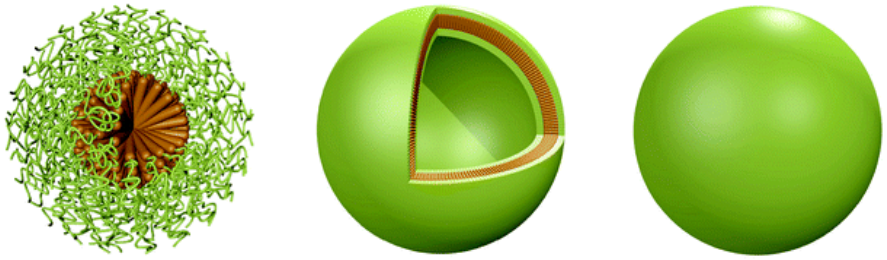

Fig. 4. Representative 3D synthetic architectures of candidates for providing defined synthetic reaction spaces: spherical micelles, vesicles and nanoparticles (from left to right). Other architectures are also accessible and used, however for simplicity only globular objects are drawn.

Frequently methods for polymersome preparation include: direct dissolution and film rehydration, which differ in their use or avoidance of organic solvents [25]. For direct

dissolution, the block copolymer can be dissolved in an aqueous solution directly, resulting from self-assembly into different accumulation of assemblies. Film rehydration method consists of the hydration of a pre-casted copolymer film using an aqueous solution under mechanical stirring. Another common used medthod is that of electroformation, where application of an electrical field induces mostly giant unilamelar vesicles (GUVs) formation. Organic solvent based methods can also be applied and involve the use of emulsion templates or dissolution of the polymers in a suitable organic solvent, followed by the injection of this solution into an aqueous phase (co-solvent or the phase inversion technique). It has to be taken into account, however, that residual organic solvent can impede the activity of biomolecular cargo. In addition, it is possible to generate hybrid polymer and lipid vesicles by introduction of amphiphilic compounds (for example lipids) at the hydrophobic-hydrophilic interface [26]. While the membrane of some polymersomes is rigid, in order to allow insertion of membrane proteins it has to be flexible and undergo conformational changes, by choosing the proper block copolymer type used for obtaining the final self-assembled structure [27, 28]. Depending on the specific application as conventional drug delivery system (carriers), nanoreactors, artificial organelles, or compartment in compartment systems, polymersomes have to fulfill specific requirements regarding their stability, membrane permeability, biocompatibility and flexibility.

2.2. Delivery applications of polymersomes

PROTEINS AND ENZYMES. Polymersomes are applied as protective 3D architectures when used as protein carriers, protecting proteins from proteolytic enzyme attacks. By the encapsulation of sensitive proteins, they maintain structural integrity and activity. Importantly, high protein encapsulation efficiencies ranging from approximately 60 to 100% have been reported for the encapsulation of bovine serum albumin (BSA), cytochrome C (CC), lysozyme (Lys), and ovalbumin (OVA) in biodegradable polymersomes composed of poly(ethyleneglycol)-b-poly(ε-caprolactone)-b-poly(2- (diethylamino) ethyl methacrylate) (PEG-b-PCL-b-PDEA) triblock copolymers [29] and poly(ethylene glycol)-b-poly(acrylic acid)-b-poly(N-isopropylacrylamide) (PEG-b-PAA-b-PNIPAM) triblock copolymers crosslinked with cysteamine [30].

Further, antibody delivery has been achieved using polymer vesicles self-assembled from a diblock copolymer with a biocompatible poly[2-(methacryloyloxy)ethyl phosphorylcholine]

(PMPC) domain and a pH-sensitive poly[2-(diisopropylamino)ethyl methacrylate] (PDPA) domain [31]. Additionally, immunoglobulin G (IgG) has been encapsulated at a high loading capacity of 89.6% in PEG-b-PCL-b-PDEA vesicles [29]. PEG linked to a pH sensitive PDEA block (pKa ≈ 7.2 in water) generated vesicles for encapsulation and release upon a dual release route (reduction or pH change) of BSA and CC [32]. Release upon exposure to oxidative conditions was facilitated by polymersomes based on poly(propylene sulfide) (PPS) and PEG, which contained encapsulated OVA [33]. These examples reveal that among the parameters influencing the encapsulation of proteins depends on the chemical structure of the copolymers, method used for the self-assembly of the block-copolymers, properties of the membrane, internal available volume of the cavity, or preservation of the activity of entrapped biomacromolecules. Systems responding to a variety of stimuli including pH [29, 31, 32], temperature [30], reductive [30, 32] or oxidative environment [33], have been generated. Moreover, the responsiveness can be tuned to increase the efficiency of cellular uptake of nanocarriers or to avoid endosomal sequestration and degradation [34]. An important aspect in the design of 3D assemblies for medical applications is the biocompatibility of their components. Variations in the preparation conditions (i.e. cross-linking density, UV irradiation time, solvent) during polymer vesicle formation determine their cytotoxic behaviour as shown for poly(ethylene glycol)-b-poly(diethylaminomethacrylate-statpoly- 3,4-dimethylmaleinimidobutylmethacrylate) (PEG-b-PDEAMA-s-PDMIBM) and poly(ethylene glycol)-bpoly(diethylaminomethacrylate-stat-poly-3,4-dimethylmaleinimidoethylmethacrylate) (PEG-b-PDEAMA-s-PDMIEM) poylmersomes [35]. Here, long UV irradiation times and the presence of phosphate buffer during the vesicle preparation might induce formation of toxic byproducts.

NUCLEIC ACIDS. Polymersomes are carrier systems able to deliver hydrophilic and hydrophobic active compounds simultaneously. Polymeric vesicles of a pH responsive, biodegradable amphiphilic methoxy-poly(ethylene glycol)-bpoly(lactic acid) (mPEG-b-PLA) copolymer were reported to co-deliver B-cell lymphoma-extra large inhibitor (Bcl-xL) -siRNA specific (Bcl-xLsiRNA) and hydrophobic doxorubicin (DOX) [24]. Co-loaded polymersomes exhibited a beneficial interaction and promising results in all assays regarding cytotoxicity, steady release and cell apoptosis. A complex copolymer composed of lipopolysaccharide-amine (LPSA) with a negatively charged backbone (oxidized sodium alginate (OA)) and a hydrophobic side chain (cholesteryl(Cho)) linked to another positively charged hydrophilic moiety

(polyethyleneimine, PEI) was proposed for achieving high transfection efficiencies [36]. Self assembly of this polymer into vesicles was induced by electrostatic interaction of anionic enhanced green-fluorescence protein plasmid (pEGFP) with cationic PEI. The vesicular membrane was composed of a central, hydrophobic Cho block and two hydrophilic OA layers surrounded by charged PEI corona. Lysosomal escape of the vesicles was facilitated by the positively charged amino groups of the PEI block via the proton sponge effect. These nanocarriers were able to transfect mesenchymal stem cells (MSCs) with an efficiency of 95%. In a related study, tumour microenvironments characterized by an acidic nature were addressed by pH sensitive polymersomes of di- or triblock copolymers consisting of PEG, poly(imidazole-butyl) methacrylate and poly(glycidylmethacrylate) blocks [37]. Double stranded DNA was encapsulated in these vesicles and release of their payloads occurred only under specific pH conditions. Non-viral vectors based on polymersomes have been shown to act as efficient nanocarriers in vitro, but most of these systems do not live up to the expectations to accomplish their task in vivo. Indeed, polymer vesicles can safely deliver nucleic acids into cells, however, the unprotected cargo is unstable after release. Therefore, further optimization is required in terms of stability, biocompatibility, and function of polymersomes as gene delivery vectors with respect of their application in vivo.

2.3. Nanoreactors and artificial organelles

Recently, polymer vesicles have been proposed as compartments for reactions ranging from nanoreactors [38] to artificial organelles [2, 39, 40] and cell mimics [41] (Figure 5). A nanoreactor consists of a synthetic compartment designed to carry out defined bio-chemical reactions on a micro- or nano-scale, optimized to have an efficient encapsulation of active compounds (proteins, enzymes, mimics), and protecting the encapsulated entity from the environmental factors (pH, temperature), whilst maintaining the activity of the encapsulated entity. At the same time, it has to provide a stable membrane through which to allow the passage of substrates and products and enable the nanoreactor to act *in situ*. A non-toxic nanoreactor succesfuly up-taken by cells, simultaneously stable and with preserved activity *in situ*, becomes a functional artificial organelle. More polymersomes or nanoreactors inside a bigger compartment could be regarded as a “polymersome – in -polymersome” or “compartment – in – compartment” system, to illustrate a very simplistic cell mimic.

Permeability of the membrane can be controlled by the specific chemical nature of amphiphilic copolymers [42–44], chemical modification of the membrane after vesicle formation [45, 46], insertion of channel proteins within the synthetic membrane [38, 47–50, 50], use of organic solvents [51], or mixing lipids with copolymers (lipid-copolymer hybrids) followed by the extraction of the incorporated lipids [52].

In addition to single enzyme type nanoreactors [40, 49, 53], entrapped combinations of enzymes participating in reactions have been described [54, 55].

Haemoglobin was encapsulated in vesicles assembled from poly-(2-methyloxazoline)-*b*-poly(dimethylsiloxane)-*b*-poly(2-methyl-oxazoline) (PMOXA-*b*-PDMS-*b*-PMOXA) triblock copolymers, where it fulfilled a dual role: detoxified peroxynitrites present in the vesicular environment and stored oxygen [56]. Nanoreactors with triggered activity were produced by encapsulation of Rose Bengal - bovine serum albumin conjugate (RB–BSA) inside polymersomes composed of PMOXA-*b*-PDMS-*b*-PMOXA block copolymers. This membrane is permeable to oxygen, enabling the release of reactive oxygen species (ROS) generated *in situ* "on demand", thereby promoting cellular toxicity at selected time and location for PhotoDynamic Therapy (PDT) [57]. These systems are also stable, for example thymidine phosphorylase encapsulated in polymersomes of the same triblock copolymer maintained stability in blood serum for several days with only a slight decrease in enzyme activity over time [58]. Interestingly, an increase of catalytic activity after enzyme encapsulation was reported for trypsin in polystyreneb-poly(acrylic acid) (PS-*b*-PAA) block copolymer (BCP) vesicles [59]. Successful nanoreactors were also formed with trypanosome vivax nucleoside hydrolase in PMOXA-*b*-PDMS-*b*-PMOXA vesicles, which can be applied in enzyme replacement therapy [60] and by entrapment of β-lactamase in similar vesicles used for hydrolysis of antibiotics [38].

Examples of NRs containing two or more enzymes were intended to design artificial organelles, or to enable cascade reactions across the membrane. The first example of an artificial organelle mimicking natural peroxisomes was realised by coencapsulation of antioxidant enzymes (Cu/Zn SOD, and lactoperoxidase, LPO, or catalase, CAT) in polymersomes (Figure 5 centre) [2]. These enzymes are the main proteins inside peroxisomes and indeed, upon uptake in HeLa cells, the enzymes acted in tandem inside and allowed simultaneous detection and detoxification of $O_2^{\cdot-}$ and H_2O_2.

A three-enzyme cascade reaction system has been developed by the encapsulation of glucose oxidase (GOx) in the inner cavity, insertion of CAL B in the bilayer membrane and immobilisation of horseradish peroxidise (HRP) on the surface of PS-*b*-PIAT copolymer vesicles [54].

2.4. Polymersome-in-polymersome systems

Polymersome-in-polymersome systems are used to perform cascade reactions across multiple compartments and represent an approach to mimic eukaryotic cells (Figure 5 right).

Enzymes such as Candida antarctica lipase B (CAL B), alcalase and alcohol dehydrogenase (ADH) were encapsulated in polystyrene-*b*-poly(3-(isocyano-lalanyl-aminoethyl)thiophene) (PS-*b*-PIAT) polymersomes with sizes ranging from 180 to 300 nm [41]. Subsequently, these vesicles were encapsulated in micrometer sized polybutadiene-*b*-poly(ethylene oxide) (PB-*b*-PEO) polymersomes together with free enzymes and reagents. This design provides a protected environment for the enzymes. The reactions are initiated once reactants and products diffuse across the inner polymersomes membrane. An initial profluorescent substrate undergoes a multi-step, enzyme catalysed reaction to yield resorufin as a final, fluorescent product.

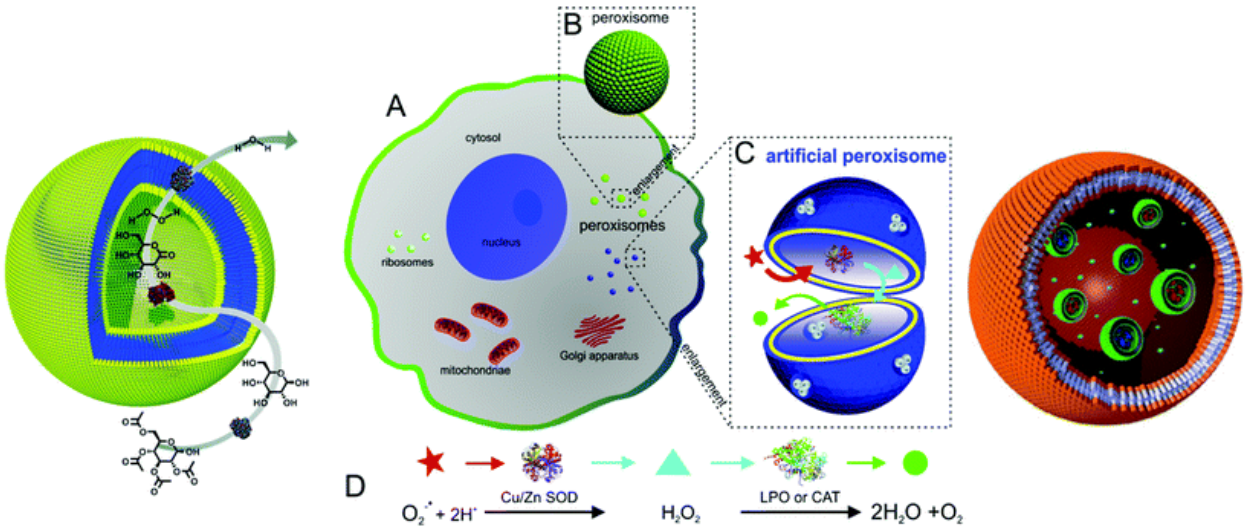

Fig. 5. Typical applications of polymersomes as a nanoreactors (left, reprinted with permission from [61]), as an artificial peroxisome (centre, reprinted with permission from [2], copyright 2013 American Chemical Society) and as a cell mimic (right, reprinted with permission from [41]).

3. Permeability of synthetic membranes and reactions inside bio-hybrid compartments

This subsection has been modified/expanded and submitted for publication:

A. Larrañaga, **M. Lomora**, J.R. Sarasua, C.G. Palivan, A. Pandit, *Polymer capsules as micro-/nanoreactors for therapeutic applications: Current strategies to control membrane permeability*, **submitted**.

Although a low permeability is sometimes needed, as in the case of viral capsides [62], quite often this may limit their use of NRs in several biomedical applications because it blocks the molecular exchange with the environment. Herein, different strategies have been adopted to control the membrane´s permeability of polymersomes, but not all of them were demonstrated as further applicability for micro-/nanoreactors development.

3.1. Intrinsic permeability of the polymersome membrane

The level of molecule diffusivity through the polymersome membrane varies depending on the type of copolymer used for the self-assembly. Some block-copolymers have reduced or no permeability for small molecules while others can self-assemble into membranes that allow specific molecules to pass. There are two membrane permeability scenarios: i) porous membrane and, ii) membranes permeable only to specific ions, molecules.

i) The category of copolymers forming a porous membrane are amphiphilic block copolymers containing a poly(styrene) (PS) tail and a charged helical poly(isocyanide) headgroup [63]. First, isocyanides were polymerized from dipeptides [isocyano-L-alanine-L-ananine (IAA) and isocyano-L-alanine-L-histidine (IAH)] resulting in the formation of helical peptide polymers. Then, a series of poly(styrene)-*block*-poly(isocyanide) copolymers was prepared employing poly(styrene) derivatives of well-defined length (40 repeating units). Finally, the protected block copolymer was deprotected by treatment with a 1 M aqueous NaOH-toluene mixture that removed the ester functional groups of the copolymers, yielding a superamphiphile with a negatively charged helical headgroup, in the case of PS-*b*-PIAA, and a superamphiphile with a zwitterionic headgroup, in the case of PS-*b*-poly(isocyano-L-alanine-L-histidine) PS-*b*-PIAH. The synthesized amphiphilic block copolymer self-assembled into various morphologies (e.g., spherical or rod-like micelles, vesicles, superhelices) depending on the length of poly(isocyanide) block, pH and the anion-headgroup interactions.

Similarly, synthesis of rod-coil block copolymers that consist of 40 styrene and 50 3-(isocyano-L-alanyl-amino-ethyl)-thiopene units (PS-*b*-PIAT) have been widely reported in the literature to self-assemble in water into polymer vesicles (polymersomes) [64–66]. The membrane is composed of PS-*b*-PIAT in which the PS blocks are oriented towards the center of the membrane and the poly(isocyanide) blocks toward the solvent. The potential of these polymersomes to serve as compartments for the development of nanoreactors was proved via the encapsulation of CAL B and subsequent reaction with 6,8-Difluoro-4-Methylumbelliferyl Octanoate (DiFMU octanoate) [66], which fluoresces when hydrolytically cleaved by CAL B. The possibility to encapsulate enzymes within polymersomes with a porous membrane has been employed to perform single reactions of permeable substrates with specific enzymes, as for example ring-opening polymerization of 8-octanolactone and dodecalactone to yield oligomers via the reaction with encapsulated CAL B [65]. In another study, Caldariomyces fumago (CPO) was encapsulated within PS-*b*-PIAT polymersomes and the reaction with pyrogallol and thioanisole was investigated [64]. In the case of pyrogallol, the reaction with CPO is limited by the diffusion of the substrate molecules along the membrane, whereas for thioanisole the limiting factor is the reaction with the enzyme.

Cascade reactions inside porous polymersomes have been exemplified by GOx and horseradish peroxidase (HRP) independently encapsulated within PS-*b*-PIAT polymersomes [67]. First, by reacting with GOx, glucose was converted into gluconolactone and H_2O_2, which further reacted with HRP and 2,2′-azino-bis(3-ethylbenzthiazoline-6-sulfonic acid) **(**ABTS) to form the ABTS radical cation ($ABTS^{\cdot+}$).

A three-enzyme cascade reaction was conducted within a single PS-*b*-PIAT polymersome. HRP was covalently bound to the surface of polymersomes via click chemistry between acetylene-functionalized anchors on the surface of polymersomes and azido functions of HRP; CAL B was located in the membrane, and GOx was located in the lumen [54]. First, glucose acetate was deprotected by CAL B to form glucose; second, glucose was oxidized by GOx yielding gluconolactone and H_2O_2; third, ABTS was oxidized to $ABTS^{\cdot+}$ in the presence of H_2O_2.

PS-*b*-PIAT polymersomes containing Cu/Zn SOD and CAT in their inner cavity have been proposed as model devices to combat overproduction of ROS within the cellular environment [68]. Although high encapsulation efficiency and confirmation of a low probability for empty or single enzyme is reported, the activities of the final PS-*b*-PEG or PS-*b*-PIAT nanoreactors are

still less efficient when compared with the enzymatic cascade reaction in bulk. In addition, no activity inside cells was reported to establish the *in vitro* activity of the nanoreactor.

ii) In another interesting study, poly(N-vinylpyrrolidone)-*b*-poly(dimetheylsiloxane)-*b*-poly(N-vinylpyrrolidone) (PNVP-*b*-PDMS-*b*-PNVP) polymersomes were employed to encapsulate ceria nanoparticles, which are known to act as superantioxidant particles [69]. In addition, ceria nanoparticles were reported to participate in a Fenton-like reaction with H_2O_2, resulting in production of $HO^{\cdot}$ and $O_2^{\cdot -}$ radicals that are cytotoxic. Their encapsulation inside polymersomes was intended to decrease their toxicity while still benefiting from their super-antioxidant property, due to the specific permeability of PDMS to $O_2^{\cdot -}$ and impermeability to H_2O_2, the encapsulation of ceria nanoparticles within PNVP-*b*-PDMS-*b*-PNVP polymersomes served as a promising strategy to take advantage of the super-antioxidant properties of ceria nanoparticles while avoiding their related cytotoxicity. Ceria loaded polymersomes were uptaken by HeLa cells and, as assessed by MTS assay, they were not cytotoxic after 72 h of exposure. Finally, HeLa cells were exposed to oxidative stress induced by the addition of paraquat. Interestingly, the viability of HeLa cells exposed to paraquat was reduced to 60% after 24 h of incubation, whereas those cells pretreated with ceria-loaded polymersomes maintained a viability of 96%. These results indicated that ceria nanoparticles-loaded polymersomes act as an efficient ROS detoxification system.

The intrinsic permeability of PDMS to $O_2^{\cdot -}$ has also been exploited to design nanoreactors for PhotoDynamic Therapy (PDT) under various irradiation conditions (for example, mild illumination with a light dose: 23.7 - 70 $J \cdot cm^{-2}$, illumination time < 25 min) [57, 70]. This has been achieved by encapsulating conjugates of a protein with photosensitizers to serve as a source of singlet oxygen “on demand”: only upon irradiation, encapsulated photosensitizers produce singlet oxygen, otherwise the system is not active. Rose Bengal (RB), a photosensitizer known to produce singlet oxygen with a high quantum yield upon irradiation at a specific wavelength, was conjugated to bovine serum albumin (BSA) and encapsulated in polymersomes self-assembled from a library of PMOXA-*b*-PDMS-*b*-PMOXA and PNVP-*b*-PDMS-*b*-PNVP triblock copolymers. RB was therefore protected by the cavity of polymersomes, eliminating the inherent systemic toxicity typical of photosensitizers. RB conjugation to bovine serum albumin served to increase its solubility and encapsulation efficiency inside polymersomes, without affecting the

photosensitizing activity. RB–BSA nanoreactors uptaken by HeLa cells and irradiated induced formation of blebs and initiation of apoptosis (Figure 6).

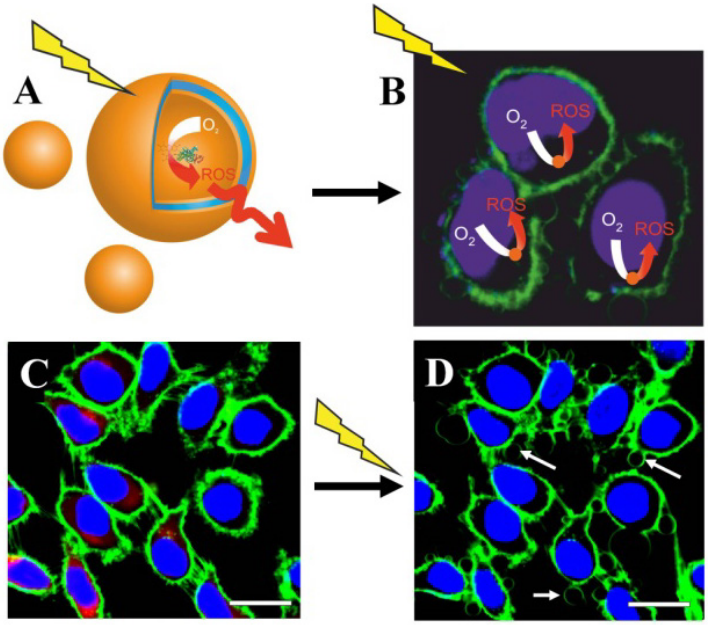

Fig. 6. Polymer nanoreactors for "*in situ*" production of reactive oxygen species "on demand" (A) when up-taken by cells (B) and irradiated with the appropriate wavelength. HeLa cells treated with nanoreactors before (C) and after irradiation (D). White arrows indicate formation of blebs, as a sign for apoptosis (D). Scale bar: 20 μm. Adapted by permission of The Royal Society of Chemistry from [57].

Due to the polymersome formation at neutral pH, PNVP-*b*-PDMS-*b*-PNVP copolymers (pK_a~ 6.8) assembled in polymersomes with an overall negative charge, which induced a low encapsulation efficiency of the RB-BSA conjugate due to electrostatic repulsion (pK_a for BSA ~ 4.7). This issue was solved by using neutral PMOXA-*b*-PDMS-*b*-PMOXA based nanoreactors, of approximately 200 nm in diameter, which were better candidates in terms of size, high encapsulation efficiency of the photosensitizer, cellular uptake, permeability towards ROS and thus, high activity inside the cells.

PMOXA-*b*-PDMS-*b*-PMOXA is known to generate polymersomes of controlled size thickness and a membrane permeable to oxygen species [71] or specific molecules, such as guanidinium chloride (GdnHCl) [72] that can diffuse through, whilst being impermeable for other small

molecular weight molecules, as for example H_2O or H_2O_2. In the particular case of $O_2^{\cdot-}$, its diffusion can be tuned via precise control of copolymer composition. With this in mind, three $PMOXA_x$-*b*-$PDMS_y$-*b*-$PMOXA_x$ copolymers were synthesized with various lengths of hydrophobic blocks (i.e., y = 22, 55, 165) and the permeability of $O_2^{\cdot-}$ toward the membrane was analyzed [71]. For that purpose, 2-(4-iodophenyl)-3-(4-nitrophenyl)-5-(2,4-disulfophenyl)-(2H-tetrazolium) (WST-1) was encapsulated within PMOXA-*b*-PDMS-*b*-PMOXA polymersomes and its reduction to formazan due to the presence of $O_2^{\cdot-}$ was analyzed by spectrophotometric assays. As expected, longer lengths of hydrophobic blocks resulted in a decrease in permeability. A potential biomedical application of these selectively permeable polymersomes is their use as NRs for the regulation of ROS species [73]. SOD was successfully encapsulated within PMOXA-*b*-PDMS-*b*-PMOXA polymersomes, with its structural and functional integrity unaffected upon encapsulation. Accordingly, due to the permeability of the membrane toward $O_2^{\cdot-}$, these polymersomes were able to scavenge $O_2^{\cdot-}$ and act as efficient antioxidant nanoreactors, whilst keeping H_2O_2 inside.

3.2. Polymersomes with a membrane rendered permeable by chemical modification/reactions

A versatile strategy to render a polymersome membrane permeable consists in the photoreaction of a photoinitiator with the polymeric membrane [45, 74]. In this approach, a water-soluble type I photoinitiator (i.e., 2-hydroxy-4′-2-(hydroxyethoxy)-2-methylpropiophenone (PP-OH)) is first added to a solution containing PMOXA-*b*-PDMS-*b*-PMOXA polymersomes and then is irradiated with UV light. As a result, ketyl and alcohol radicals are produced that further attack the membrane of the polymersome causing an increase in its permeability. To demonstrate the enhanced permeability of PMOXA-*b*-PDMS-*b*-PMOXA polymersome upon photoreaction with PP-OH, HRP was encapsulated and the reaction with four molecules of different hydrophilicity: ABTS, 3-amino-9-ethyl carbazole (AEC), pyrogallol and 3,3′,5,5′-tetramethylbenzidine (TMB) was monitored. For those polymersomes none photoreacted with PP-OH, the reaction between the aforementioned molecules and HRP did not occur, demonstrating the low permeability of the polymersome membrane. In contrast, the UV-induced photoreaction rendered the vesicles permeable and, accordingly, without affecting the reaction between HRP and the substrates. By using this approach, poly(ethylene glycol) methyl ether acrylate (poly(PEGA)) was successfully

polymerized by enzyme-catalyzed atom transfer radical polymerization (ATRP) within PMOXA-*b*-PDMS-*b*-PMOXA polymersomes [74], demonstrating the potential application of these photo-reacted polymersomes as nanoreactors.

3.3. Biomimetic membrane permeabilization by insertion of biomolecules

An elegant way to render permeable an impermeable polymersome membrane is to use a biomimetic strategy of insertion of membrane proteins (MPs) and biopores/ion-carriers. Such biomolecule-decorated membranes allow a selective or partially selective diffusion through of specific molecules and offer the possibility of inducing stimuli-responsiveness for a non-permeable synthetic membrane (Figure 7).

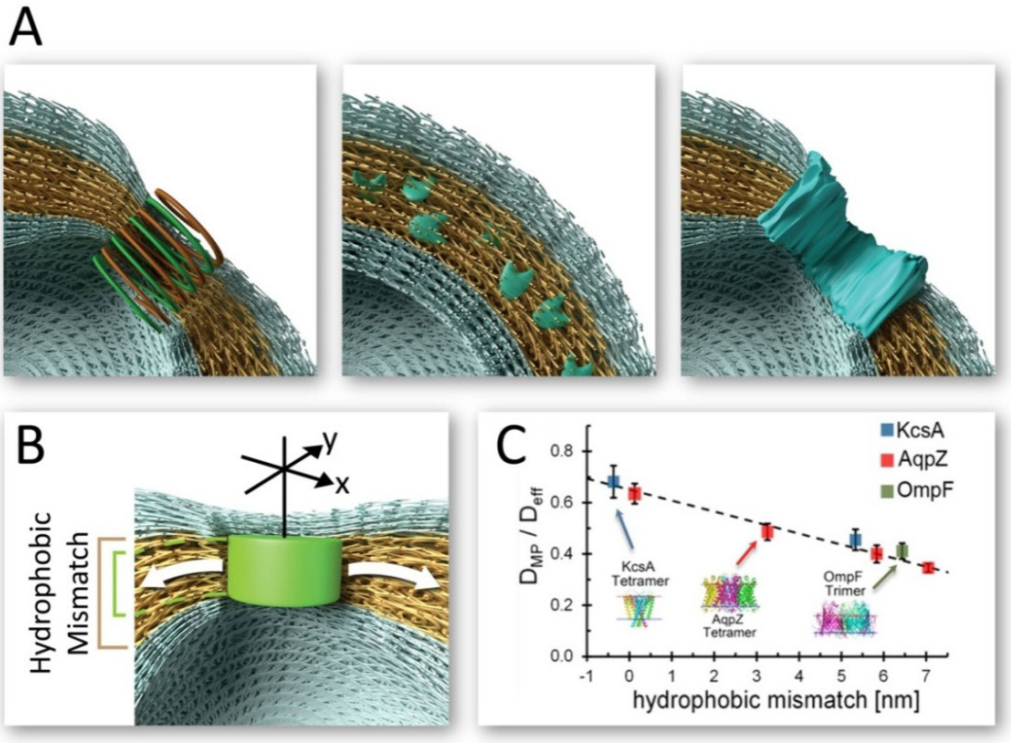

Fig. 7. Smart hybrid membranes with induced stimuli-responsiveness through insertion of ion carriers, ion channels, or membrane proteins to induce selective permeability to ions or biomolecules (A). The membrane of the polymer vesicle is able to compress (B) and an increase in thickness induces a reduction in the relative, effective diffusion coefficient, D_{MP}/D_{eff} (C). Adapted with permission from ref. [75]. Copyright (2016) American Chemical Society.

Since their introduction by Meier *et al*. [76], various channel proteins, such as aquaporin Z (AqpZ), outer membrane protein F (OmpF), nucleoside-specific protein (Tsx), ferrichrome-iron receptor (FhuA), have been incorporated in the membrane of polymer vesicles to tune their permeability (Table 1).

Although a few examples exist in the literature reporting the incorporation of channel proteins in the membrane of other block copolymers [e.g. PB-*b*-PEO [77], polyisobutylene-polyethyleneglycol-polyisobutylene (PIB-PEG-PIB) [78]], PMOXA-*b*-PDMS-*b*-PMOXA has been the copolymer of choice in most cases [79]. Considering that the thickness of the membrane in synthetic block copolymers is 2-10 times that of phospholipid bilayers, there is a large mismatch (in the range from 3.3 to 7.1 nm) between the membrane thickness and the size of the protein channels that makes the insertion of channel proteins within the membrane of block copolymers difficult, if not impossible. It has been shown that the hydrophobic mismatch might result either by a contraction of the block copolymer macromolecules in the vicinity of the channel protein, by the arrangement of smaller block copolymer chains around the protein or by a combination thereof. Mean-field analysis derived models or molecular dynamics simulation studies have focused on adaptability of the polymer membranes due to the insertion of membrane proteins [27, 80]. These studies indicated that a large hydrophobic mismatch (more than 1.3 nm) can be overcome and a successful insertion of MPs is possible for the particular analysed systems. Indeed, despite significant hydrophobic mismatch (up to 5 times), MPs have been successfully inserted and, importantly, they maintained their function. As demonstrated by a combination of cryo-transmission electron microscopy (cryo-TEM) and z-scan fluorescence correlation spectroscopy (z-FCS), this hydrophobic size mismatch can be overcome by a high flexibility and fluidity of the hydrophobic domain (for example PDMS block within PMOXA-*b*-PDMS-*b*-PMOXA block copolymers) [75]. It has been demonstrated using PDMS-containing amphiphilic block copolymer membranes (9-13 nm) that the relative diffusion coefficient (diffusion of membrane protein, D_{MP}, divided by the effective diffusion coefficient of the corresponding membrane, D_{eff}) decreases with increasing hydrophobic mismatch. This is due to the flexible arrangement of block copolymer chains forming domains around the protein, which guide the protein through the membrane, and slows it down once the polymer membrane thickness increases.

Table 1. Permeabilized membranes formed by inserting membrane proteins and biopores [21].

Polymer composition used for polymersome formation	**Membrane protein/biopore**	**Proven function**	**Nano-/micro-reactors**	**Reference**
PEO-*b*-PB	dendritic helical pore	H^+, H_2O	No	[81]
PEG-*b*-PDMS	Calcimycin	Ca^{2+}	Yes	[82]
PMOXA-*b*-PDMS-*b*-PMOXA	asalocid A, N,N-dicyclohexyl-N',N'-dioctadecyl-3-oxapentane-1,5-diamide, Alamethicin	Ca^{2+}	Yes	[83]
PEtOz-*b*-PDMS-*b*-PEtOz	Bacteriorhodopsin	H^+ gradient	No	[84]
PMOXA-*b*-PDMS-*b*-PMOXA	Complex I	electron transfer	No	[85]
PMOXA-*b*-PDMS-*b*-PMOXA, PEO-*b*-PB	Aquaporin	H_2O	No	[77, 86, 87]
PEO-*b*-PB	α-hemolysin	Calcein	No	[88]
PMOXA-*b*-PDMS-*b*-PMOXA, DNA-PIB	OmpF	molecules up to 600-700 Da	Yes	[38, 53, 55, 60, 89–91]
PMOXA-*b*-PDMS-*b*-PMOXA	LamB	DNA translocation	No	[50]
PMOXA-*b*-PDMS-*b*-PMOXA	Tsx	inosine, adenosine, guanosine, 2-fluoroadenosine	Yes	[60]
PMOXA-*b*-PDMS-*b*-PMOXA, PIB-*b*-PEO-*b*-PIB	FhuA	various dyes	Yes	[48, 78]
PMPC-*b*-PDPA	DNA nanopores	1.5 nm sized molecules	Yes	[92]

A strategy to favour biopore insertion is to increase the size of the pore with respect to the membrane thickness, thus to increase the hydrophobic region of the protein in order to overcome

the mismatch with the hydrophobic domain of the synthetic membrane. For instance, the FhuA protein (4 nm in length) was extended by increasing the number of hydrophobic amino acids in the structure and therefore increasing its length by 1 nm more, being able to match the 5 nm thickness of the polymersome membrane assembled from PIB_{1000}-*b*-PEG_{6000}-*b*-PIB_{1000} triblock-copolymer [78]. Although this strategy might affect the pore function, in this case the modified Outer membrane protein OmpF is the most extensively studied channel porin for the design of nanoreactors and artificial organelles because it allows passive, concentration-driven transport, where molecules with molecular weight above 600 Da are sterically excluded. OmpF is a homo-trimeric channel protein found in the outer membrane of Gram-negative bacteria such as *E. coli* [38, 93]. Additionally, OmpF channels can be closed above a critical transmembrane voltage of about 100 mV [94], allowing the protein channel to act as an on/off switch that can be controlled externally.

The transport across OmpF channel protein was also turned from passive to pH-driven function via an engineered OmpF channel in which six amino acids were substituted to pH responsive histidines (OmpF 6His) [95]. Channel cross-section of OmpF 6His increased from 0.9 x 1.3 nm at pH = 5 to 1.2 x 1.4 nm at pH = 7, resulting in an increased release of a model cargo (acridine orange) from 33.6 to 79.2% when the pH was increased from 5 to 7. Very recently, the OmpF channel was chemically modified by embedding a pH sensitive Cy5-hydrazide molecular cap to control the passive diffusion of molecules once it is inserted in the membrane of PMOXA-*b*-PDMS-*b*-PMOXA polymersomes [91]. This strategy allowed the restriction of molecule diffusion at a pH value of 7.4, while at pH 5.0, the cap was released from the pore, resulting in an open conformation that allows the passage of molecules. The ability to control permeability of the membrane has been further demonstrated by the encapsulation of HRP model enzyme within polymer vesicles in presence of absence modified OmpF embedded in their membrane. The formation of fluorescent or colored products upon addition of two specific substrates: TMB and Amplex Red, was monitored. When using the TMB chromogenic substrate, in presence of H_2O_2, the formation of a colored product can be monitored if it encounters the encapsulated enzyme. TMB and H_2O_2 indeed could not pass through the PMOXA-*b*-PDMS-*b*-PMOXA membrane, and they could only reach the protected enzyme when the Cy5-hydrazide molecular cap of the successfully reconstituted OmpF inside the polymersome membrane was cleaved due to a drop in pH, from 7.4 to 5.0.

Selective permeability of the polymersome membrane can exploited for development of water purification nanodevices. For example, AqpZ, a homotetrameric protein that allows the diffusion of water across biological membranes has been successfully incorporated within the membrane of PMOXA-*b*-PDMS-*b*-PMOXA polymersomes [96]. Permeability measurements of the membrane conducted via stopped-flow light-scattering experiments revealed that the incorporation of AqpZ into PMOXA-*b*-PDMS-*b*-PMOXA polymersomes resulted in a 90 times increase (from 0.8 μm/s to 74 μm/s) in the permeability of the polymeric membrane. Furthermore, AqpZ incorporated in the membrane was highly selective to water, allowing the diffusion of water while avoiding the transport of small solutes such as salts, glucose, urea and glycerol. This opens new bio-nanoscience based solutions for water purification processes.

A completely different application was intended when Tsx, a small substrate specific (31.4 kDa) channel protein involved in the transport of nucleosides and nucleotides that serve as carbon and nitrogen sources and as precursors for nucleic acid synthesis, was inserted into synthetic membranes [60]. The specific transport of several substrates (e.g., inosine, adenosine, guanosine, 2-fluoroadenosine, thymidine, deoxyuridine) along PMOXA-*b*-PDMS-*b*-PMOXA polymersomes incorporating Tsx has been demonstrated in a few studies[58, 60]. In this sense, *Trypanosoma vivax* (TvNH) was encapsulated in PMOXA-*b*-PDMS-*b*-PMOXA polymersomes that contained Tsx in their membrane [60]. The apparent kinetic constants [$(k_{cat})_{app}$] of the reaction between encapsulated TvNH and inosine, adenosine, guanosine or 2-fluoroadenosine were evaluated and compared with the $(k_{cat})_{app}$ of the same enzyme encapsulated in PMOXA-*b*-PDMS-*b*-PMOXA polymersomes incorporating OmpF instead of Tsx. Due to the specificity of Tsx to nucleosides and nucleotides, the diffusion of the substrates and thus, the $(k_{cat})_{app}$ of polymersomes containing Tsx was much higher with respect to polymersomes containing OmpF. PMOXA-*b*-PDMS-*b*-PMOXA polymersomes incorporating Tsx in their membrane has been proposed to treat mitochondrial neurogastrointestinal encephalomyopathy (MNGIE) disease [58]. In this disorder, loss of function of thymidine phosphorylase (TP) resulted in the systemic accumulation of thymidine and deoxyuridine. As a proof of concept, TP was encapsulated in PMOXA-*b*-PDMS-*b*-PMOXA polymersomes. Due to the presence of Tsx in the membrane of the polymersome, thymidine was able to diffuse into the polymersome and react with TP, resulting in the formation of thymine. Moreover, the developed polymersomes did not affect the

viability of primary hepatocytes nor did they cause stimulatory effect on macrophages and, therefore, may be useful to control thymidine levels in MNGIE disorders.

An interesting approach has been introduced by incorporating LamB in the membrane of PMOXA-*b*-PDMS-*b*-PMOXA polymersomes [50]. LamB forms a trimeric channel in biological membranes and is involved in the transport of maltose and maltodextrines. Additionally, it also serves as a receptor for λ phage. Phages are able to bind to LamB via their tails and, afterwards, they are able to inject their genome into the polymersomes, demonstrating that the function of LamB is preserved in the artificial block copolymer.

While various membrane proteins allow passive bidirectional transport, others serve for unidirectional active transport and so, their orientation might affect the function and compromise the final objective of their intended application. For instance, the model proton pump, bacteriorhodopsin (BR), inserted in the membrane of poly(2-ethyl-2-oxazoline)-*b*-poly(dimethylsiloxane)-*b*-poly(2-ethyl-2-oxazoline) (PEtOz-PDMS-PEtOz) polymersomes, pumped protons inwardly or outwardly based on protein fractions with different orientations [97]. Therefore, a random orientation inside synthetic membranes can be avoided by adopting a proper method of preparation [97], protein modification [98], or by ensuring specific charges on the membrane surface [99].

An approach worth mentioning consists of using an asymmetric triblock copolymer to force a controlled interaction of the protein with a desired directionality. This is the case with a PEG-*b*-PDMS-*b*-PMOXA triblock copolymer able to self-assemble into polymersomes and which provided a membrane with the right conditions to orient an Aquaporin type pore [100]. Of course, the use of one single strategy might not be sufficient, and most often a combination of various parameters needs to be considered to obtain the correct orientation of the MPs, which have a final impact on the efficiency of desired system. In the case of NRs, their efficiency will also be affected by other parameters, such as the self-assembly process of copolymers and proteins, MPs incorporation efficiency, vesicular membrane thickness, and interaction with the polymer membrane etc. Therefore, to fully understand all these interaction factors, more detailed investigations are necessary both for the synthetic membranes and of the MPs.

3.4. Stimulus-driven permeability or activity without compromising the architecture of the polymer compartment

Small changes in the environmental conditions induced by external stimuli such as light, pH, temperature, presence of a biological molecule (e.g. glucose) affect compartments self-assembled from "smart" block-copolymer which are specifically designed to respond to such stimuli [101]. This type of block copolymers cannot be used to obtain polymersomes with both stimuli-responsiveness and preserved architecture. Other approaches should be used to design polymer compartments with a membrane, which, upon a specific stimulus, has an increased permeabilization without affecting the overall architecture over a certain range of conditions. For example, a feasible solution for a concomitant increased stability and permeability has been reported by an appropriate structural design of block copolymers containing motifs triggered by specific stimuli [102, 103]. Following this approach a so-called light-regulated "traceless" crosslinking strategy has been developed (Figure 8, left) [103]. This consists in triggering motifs using amphiphilic block-copolymer based on poly(ethylene oxide)-*b*-poly(2-nitrobenzyloxycarbonyl aminoethyl methacrylate) PEO-*b*-PNBOC containing photolabile carbamate-caged primary amine moieties. These moieties will initially be part of the hydrophobic domain, which under UV irradiation will release the primary amine, initiate amidation reactions, and induce vesicle crosslinking directly correlated with a hydrophobic-to-hydrophilic transition within the membrane. This strategy allowed encapsulation of hydrophilic such as doxorubicin hydrochloride (inner cavity) or hydrophobic entities, Nile red (within the hydrophobic part of the membrane) inside polymersomes that after the UV-initiated chemical reaction, were released due to an enhanced permeability of the membrane. By encapsulation of alkaline phosphatase (ALP), these crosslinked polymersomes served as a basis to design stable and stimuli-responsive nanoreactors. Once permeabilization of crosslinked bilayer occurred under UV irradiation, water-soluble non-fluorescent phosphate-caged fluorescein substrate diffused across the membrane and was converted by ALP into a highly fluorescent fluorescein product, which was monitored by a spectrophotometer (Figure 8, right). The release of a dye labeled dextran (DLD), with five times lower molecular weight than the molecular weight of the enzyme, indicated no ALP leaked from the inner cavity of the vesicles upon membrane permeabilization.

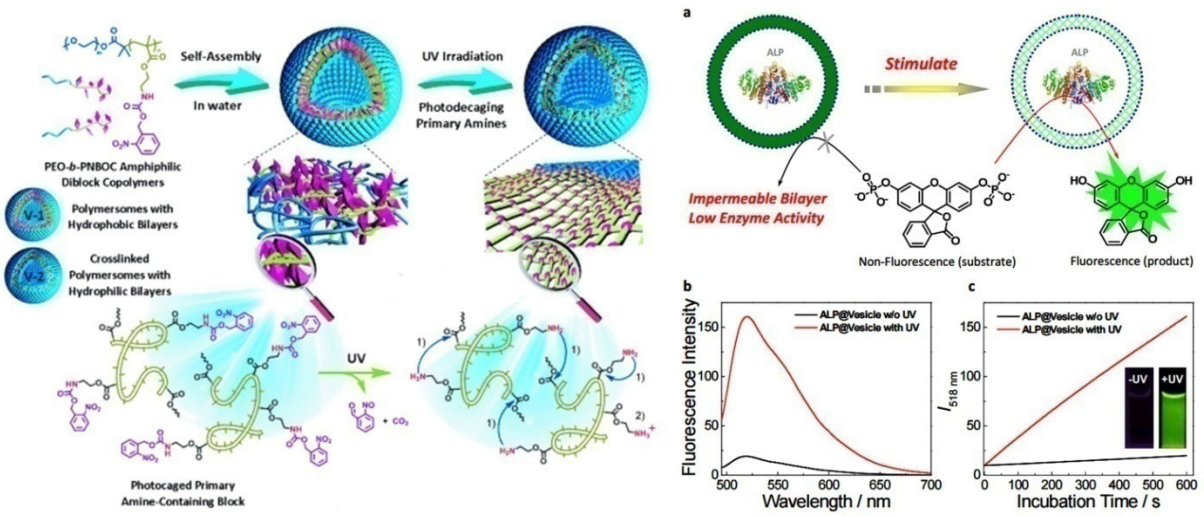

Fig. 8. Simultaneous crosslinking and permeabilization of polymersomes based on PEO-b-PNBOC block copolymers, triggered by UV irradiation (left). Encapsulation of ALP enzymes inside polymersomes (a) and enzyme activity monitored by the formation of a fluorescent product (b and c) before (black curve) and after (red curve) UV-induced permeabilization. Reprinted with permission from ref. [103]. Copyright (2016) John Wiley and Sons.

However, once permeability is increased, it cannot be reversed. Other approaches have been reported to achieve a reversible permeability of the polymer based membrane. In order to increase the stability of pH-responsive polymersomes and to prevent their dissociation upon a pH change, incorporation of a crosslinkable comonomer has been proposed, with proven application in the biomedical field due to their cyto-compatibility and mechanical stability [35, 104, 105]. These polymersomes have been utilized as NRs where single [46] or cascade [106] enzymatic reactions have been conducted. As a proof of concept, GOx and myoglobin (Myo) or HRP were encapsulated within PEG-*b*-PDEAEM-*stat*-PDMIBM polymersomes, in which 3,4-dimethyl maleic imidobutyl methacrylate (DMIBM) was employed as a photo-crosslinkable unit. GOx turned D-glucose into D-glucono-δ-lactone and hydrogen peroxide, which acted as a co-substrate for Myo to oxidize guaiacol and for HRP to oxidize ABTS, respectively. At pH = 8, no enzymatic reaction was observed, indicating that at this pH the substrates (D-glucose and guaiacol) cannot diffuse along the membrane. However, at pH = 6, when the tertiary amine of DEAEM was protonated and the block turned hydrophilic, while maintaining the stability, the

substrates were able to permeate into the membrane initiating the enzymatic reactions. Interestingly, the reaction was abruptly stopped at pH = 8, describing a switch between an off (pH = 8) and on (pH = 6) state of the polymersomes.

Following a similar concept, synthetic nuclear envelope-like vesicles (NEVs) have been proposed [107]. The strategy to encapsulate biomolecules within polymersomes was based on mimicking the gateway connecting the cell nucleus and the cytoplasm in eukaryotes (nuclear envelope-like structures). Photo-crosslinkable coumarin (CMA) was employed to yield PEO-*b*-PDEAEM-*stat*-CMA polymersomes. Due to nanophase segregation during the polymersome formation, the resulting membrane consists of a CMA-rich matrix with CMA-poor patches. The CMA-poor patches act as giant valves, mimicking the nucleus pore complex and facilitating the diffusion of biomolecules [GOx and Hb], by tuning the pH. The cascade enzymatic reaction within the polymersome was confirmed as follows: first, glucose reacts with GOx to yield H_2O_2 and gluconic acid; second, H_2O_2, together with Hb, oxidizes o-phenylenediamine (OPD) forming 2,3-diaminophenazine (DAPN), easily detected via UV-Vis spectroscopy. The proposed approach represents a promising strategy to encapsulate fragile biomolecules (e.g., proteins, RNAs, enzymes, etc.) in pure aqueous solutions triggered by slight pH changes.

Carbon dioxide (CO_2), CO_2/NO_2 and/or pH driven permeability of synthetic membranes has also been reported in the literature [108–110]. In a particular case, an amphiphilic block copolymer of PEG and CO_2-sensitive poly(N-amidino)dodecyl acrylamide (PAD) was synthesized via ATRP. The hydrodynamic radius (R_h) of the resulting polymersomes increased at a rate of 2.5 $nm \cdot min^{-1}$ when CO_2 was passed through the solution at a flow rate of 1 $ml \cdot min^{-1}$ due to the transition of part of PAD blocks from unprotonated, entangled state (polyamidine) to a protonated, stretched state (polyamidinium). This enabled the tuning of the thickness and corresponding permeability of the membrane upon CO_2 bubbling, allowing the separation of molecules of different sizes. Myo was encapsulated in poly(ethyleneglycol)-*b*-poly[(N-amidino)dodecyl acrylamide] (PEG-*b*-PAD) polymersomes, and the reaction was monitored over 5 minutes in the presence of CO_2, which induced swelling of the vesicles and “opening” of their pores. Opening of the pores allowed the diffusion of glutathione across the membrane. Incubation of oxymyoglobin with tripsin results in complete disappearance of the O_2-binding activity. However, due to the larger size of trypsin compared to glutathione, 15 min of CO_2 bubbling was necessary to allow the reaction to proceed to completion.

Amphiphilic dendritic star-block terpolymers consisting of a hydrophobic poly(ε-caprolactone) (PCL) block, an intermediate CO_2/pH-sensitive bridging poly(2-(diethylamino)ethyl) methacrylate (PDEAEMA) block, and a hydrophilic PEG end block self-assembled into vesicular nanostructures which undergo reversible morphological transitions (vesicles, swelled vesicles, macroporous vesicles) upon alternating CO_2/N_2 stimulation [110]. It would be interesting to see a future design of a NR based on this special self-assembly, based on the potential this system holds for encapsulating biomacromolecules and controlling the passage of subtrates/products via a CO_2-adjustable size of the inner cavity and membrane poration.

A fruitful strategy for NRs design is to mix conventional amphiphilic block copolymers with stimuli-responsive block copolymers, the latter being the component which upon a certain stimulus, poration is induced in the final self-assembled architecture, whilst maintaining its integrity. The use of phenylboronic acid derivatives permits the development of glucose responsive polymers due to the strong binding between boronic acid and monosaccharides through the formation of reversible covalent bonds [43]. PEG-*b*-PS amphiphilic copolymers have been blended with glucose-responsive PEG-*b*-poly(styrene boronic acid) (PEG-*b*-PSBA). At a PSBA concentration of ~10%, phase-separated PSBA domains were dispersed along the PS matrix in the membrane. These moieties are disassembled upon an increase in pH to 12.6 or by exposure to D-glucose or D-fructose, generating pores in the membrane of the polymersome and increasing, accordingly, its permeability. As a proof of concept, CAL B was encapsulated within the aforementioned polymersomes and its reaction with DiFMU octanoate was allowed only after the disassembly of PSBA moieties. Additionally, the permeability of the membrane can be tuned by changing the weight ratio between the two block copolymers.

Of course the stimulus does not necessarily have to influence the permeabilization of the membrane, but can influence the overall activity of the nanoreactor as is the case with the light-responsive NRs containing the encapsulated photosensitizer RB-BSA. Such NR becomes active upon light irradiation and produces ROS *"on demand"*, able to pass through the intrinsic permeability of the PMOXA-*b*-PDMS-*b*-PMOXA membranes for these species (see section 3.1) [57, 70].

4. Polymersome-based networks and active surfaces

POLYMERSOME-BASED NETWORKS. Cells are organized in a controlled spatial topology to promote proper structure and function of tissues. Cellular positional distribution is mediated through adhesive molecules or gap junctions with crucial role in connecting two adjacent membranes and enabling communication between compartments. A way to mimick this biological connection is through the design of synthetic networks. For instance, by decorating the surface of polymersomes with complementary single-stranded (ssDNA), followed by ssDNA hybridization, formation of clusters with controlled distance between the polymer vesicles was achieved (Figure 9) [111]. Mixing the same or differently sized polymersomes with ssDNA strands, two main configurations were observed: chain-like (Figure 9: b, c) or satellite-like polymersome clusters (Figure 9: d, e), respectively. These are exciting results, as DNA acted as a protective layer between polymersomes without allowing membrane fusion. Additionally, no large aggregates were generated because of the low ssDNA density on the surface of the polymersomes, as well as the migration of ssDNA strands towards the bridging area, prohibiting the binding of more polymersomes to the formed clusters. This sets the stage for designing clusters from nanoreactors with controlled positioning for more advanced bio-mimetic applications, such as controlled simulation of required cellular signaling processes between synthetic compartments.

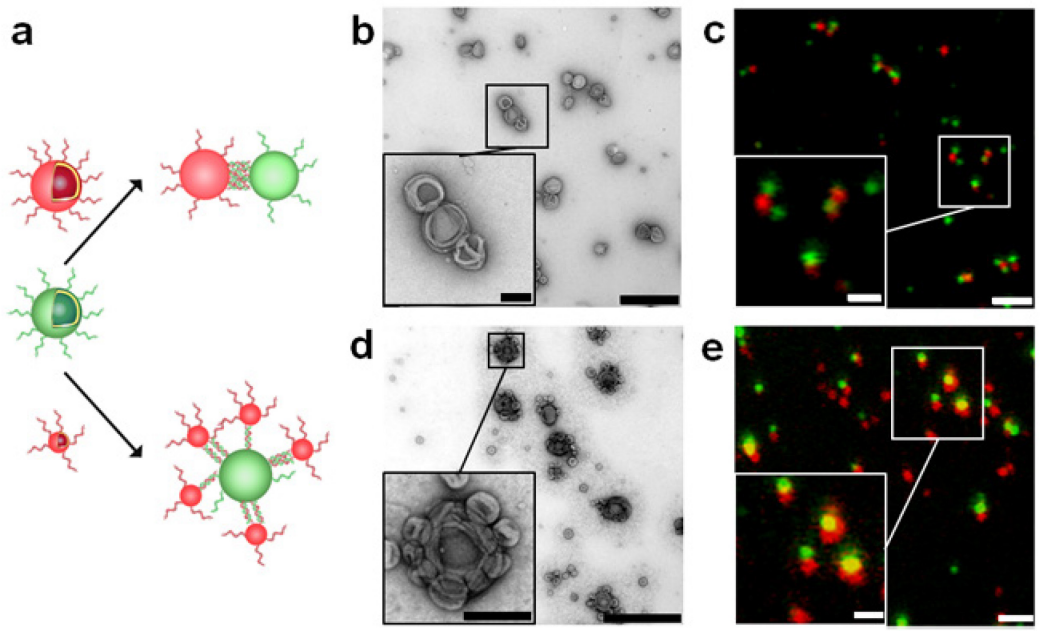

Fig. 9. Complementary DNA mediated connection of polymersomes to form synthetic networks: polymersomes with complementary DNA strands on their surface and their corresponding linkage configurations (a) as observed by TEM (b, d) and CLSM (c, e). Scale bar: 1000 and 200 nm in the inset (TEM); 2000 and 1000 nm in the inset (CLSM). Reprinted with permission from [111]. Copyright (2016) American Chemical Society.

ACTIVE SURFACES. Up to now, examples that illustrate the versatility of polymersomes as carriers, nanoreactors, artificial organelles, or clusters were described for systems in solution, however a similar approach has been applied for surfaces. For instance, immobilization of protein-polymer nanoreactors via covalent chemical interactions on a solid support, without disintegration of the vesicles, led to the generation of "smart or active surfaces" with desired functionality [112]. This is of relevance especially for designing medical implants with nonfouling properties, with attached reservoirs for sustained release of drugs [113]. Among the first successful active surface was developed using PMOXA-*b*-PDMS-*b*-PMOXA nanoreactors containing an OmpF permeabilized membrane and their immobilization on a glass surface, via a receptor-ligand pair, biotin-streptavidin [49]. Streptavidin-structured glass surfaces were incubated with biotinylated vesicles to allow the specific binding of the polymersomes on the solid substrate. Polymersomes were loaded with acid phosphatase to perform a model dephosphorylation reaction with the fluorogenic substrate ELF97. As demonstrated via time-

resolved fluorometric studies, this strategy permitted reactions to be performed on surfaces at precise locations (Figure 10).

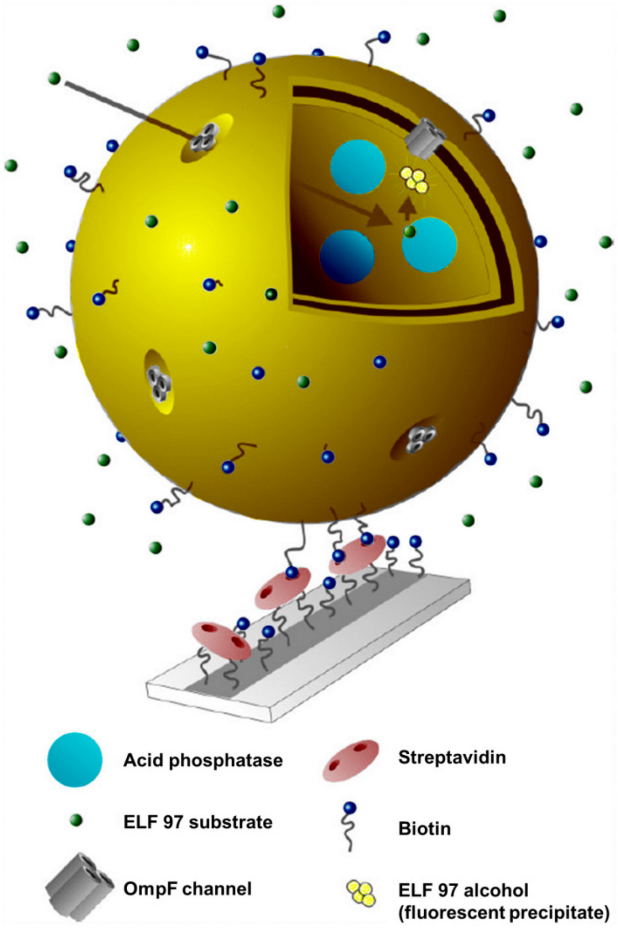

Fig. 10. Protein-polymer nanoreactor immobilized on a solid support: Biotinylated nanoreactors with encapsulated acid phosphatase and OmpF permeabilized membrane are immobilized on the surface of a streptavidin functionalized glass support. Reprinted with permission from [49]. Copyright John Wiley and Sons.

In another study, PMOXA-*b*-PDMS-*b*-PMOXA polymersomes containing OmpF protein channels in their membrane were employed to develop active surfaces to prevent bacteria-associated medical implant infections [53, 113]. In this case, the immobilization strategy was based on Schiff-base formation between aldehyde groups on the outer surface of polymersomes and amino groups on a silicon surface, followed by reductive amination: first, hydroxyl-terminal groups of the polymer were oxidized to aldehyde by Dess-Martin oxidation; these polymersomes

were then incubated with aminated silicon surface to form imine bonds; finally, upon reductive amination, strong and stable amino bonds were formed between the polymersomes and the silicon substrate. The enzyme penicillin acylase was encapsulated in these polymersomes. Due to the presence of OmpF in the membrane of the polymersomes, the substrates 7-ADCA and PGME were able to diffuse into the polymersome and react with the enzyme, resulting in the release of the antibiotic cephalexin. Hence, these surfaces, where nanoreactors were immobilized, inhibited bacterial growth and prevented biofilm formation up to seven days, a process far more efficient at maintaining enzymatic activity than the free enzyme alone, which becomes inactive after less than two days. Immobilizing such nanoreactors on surfaces of implants should increase the effectiveness of antibiotics due to their localized production, and thereby could significantly reduce systemic side-effects [113]. Based on these approaches active surfaces based on attached polymersome networks through which inter-vesicular cascade reactions are expected to be developed.

II. AIM OF THIS THESIS

In this work, design of supra-molecular assemblies using polymersomes with induced membrane permeability through the insertion of membrane proteins, is presented. Moreover, interactions of biomolecules/enzymatic reactions inside nanocavities were studied in detail. These studies led to the design and exciting results for: i) polymersomes with stimuli-responsivness towards monovalent (H^+, Na^+, K^+) and divalent cations (Ca^{2+}), ii) nanoreactors in solution, iii) nanoreactors attached on solid supports.

The aim of this thesis was to design $PMOXA_x$-$PDMS_y$-$PMOXA_x$ polymersomes that permit:

- ✓ proton and ion exchange without affecting their size or morphology, based on gramicidin (**Chapter III**). These selectively permeable polymersomes with preserved architecture were stimuli-responsive for protons (H^+) and monovalent cations, such as Na^+ and K^+.
- ✓ selective permeability to divalent cations, mediated through the presence of ionomycin ion carriers (**Chapter IV**). These selectively permeable polymersomes with preserved architecture were stimuli-responsive for Ca^{2+} ions.
- ✓ permeability towards molecules, such as glucose derivatives, based on a mixture of engineered α-hemolysins. These permeable polymersomes, allowed the design of nanoreactors for the production *in situ* of metabolic relevant compounds (glucose derivatives and NAPDH, as a source of energy) (**Chapter V**).
- ✓ permeability for sugar alcohols, with the help of a glycerol facilitator. These selectively permeable polymersomes were further developed into nanoreactors and attached on solid glass surfaces to produce active surfaces for sugar alcohol sensing (**Chapter VI**) (Figure 11).

These aims were achieved by using a biomimetic approach through the insertion of ion channels (gramicidin), ion carriers (ionomycin), and other biopores (engineered α-hemolysins and glycerol facilitator) in the membrane of the synthetic polymer vesicles. Thus, allowing a selective permeability, ions and biomolecules can access sensitive and protected probes and/or enzymes encapsulated inside the cavity of synthetic vesicles. These systems are ideal candidates for the development of biosensors, applied nanoreactors to replace impaired metabolic pathway

or as energy sources, active surfaces for local implants, in applications from environmental science, catalysis, and biomedical field.

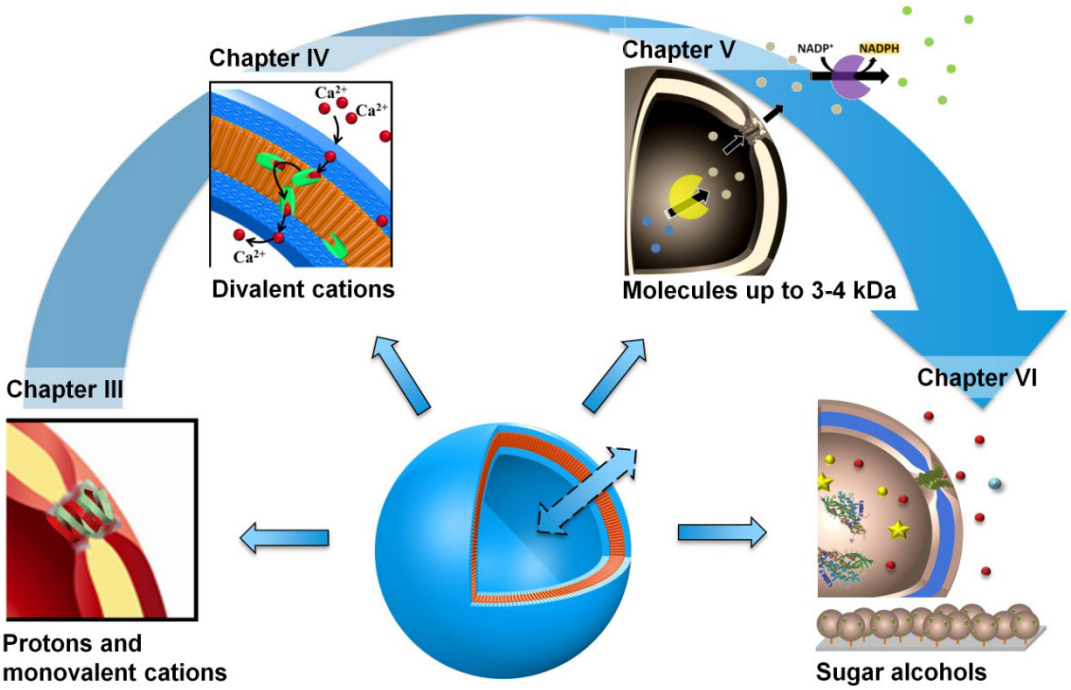

Fig. 11. Biomimetic membrane permeabilization of polymersomes to protons and monovalent ions (**Chapter III**), divalent cations (**Chapter IV**), molecules up to 3-4 kDa (**Chapter V**), and sugar alcohols (**Chapter VI**). Reproduced and modified from ref. [3] Copyright (2017) with permission from Elsevier, ref. [114] CC-BY-NC 3.0 license, and ref. [115] Copyright (2017) with permission from Elsevier.

III. HYBRID SYNTHETIC MEMBRANES WITH RESPONSIVENESS TO PROTONS AND MONOVALENT CATIONS

The results of this investigation have been reprinted and modified from the following publication [3] Copyright (2017) with permission from Elsevier:

M. Lomora, M. Garni, F. Itel, P. Tanner, M. Spulber, C. G. Palivan, *Polymersomes with engineered ion selective permeability as stimuli-responsive nanocompartments with preserved architecture,* Biomaterials, **2015**, 53, 406-414.

1. Introduction

The ability of ions or biomolecules to pass through cellular membranes is due to the various pore-forming peptides or other membrane proteins that serve to maintain the homeostasis, or to preserve the stability of the internal cell's environment. In order to serve as nanoreactors, biosensors or artificial organelles, polymer compartments must preserve their structural integrity and the permeability of their membrane has to be specifically engineered. One way to achieve selective permeabilization of polymersome membranes is by inserting biopores, as in the case of cell membranes. As regards to MP insertion, the permeability is determined by the diameter, specificity, or mode of transport of the MPs' pores, based on which it allows a passive, active, selective or non-selective exchange of small mass molecules through the synthetic membrane. Here, we selected as a biopore model, gramicidin (gA), which allows a controlled passage of protons and monovalent ions (Figure 12). We have used a library of $PMOXA_x$-$PDMS_y$-$PMOXA_x$ triblock copolymers that self-assemble in polymersomes with membrane thicknesses ranging from 9.2 to 16.2 nm. This library was used in order to understand whether the membrane thickness affects the biopore insertion. A combination of light scattering, transmission electron microscopy, and fluorescence correlation spectroscopy was used to characterize the polymersomes with and without inserted gA to establish if the biopore insertion affects their architecture and size. Exchange across the membranes of protons, Na^+ and K^+ was studied using fluorescence spectroscopy by monitoring changes in fluorescence intensity of an encapsulated sensitive dye as a result of pH change or the presence of ions in the environment of the polymersomes. In addition, gA was inserted in single giant unilamellar vesicles (GUVs), and the

change of fluorescence intensity of the encapsulated dye was visualised in real time. The design of polymersomes with membranes permeable to protons and monovalent cations represents a new approach for producing compartments with specific responses, whilst preserving their morphology, and therefore the encapsulated active compounds. Such systems represent ideal candidates for developing applications in which specificity and responsiveness are key factors, as for example in biosensors, or specialised artificial organelles.

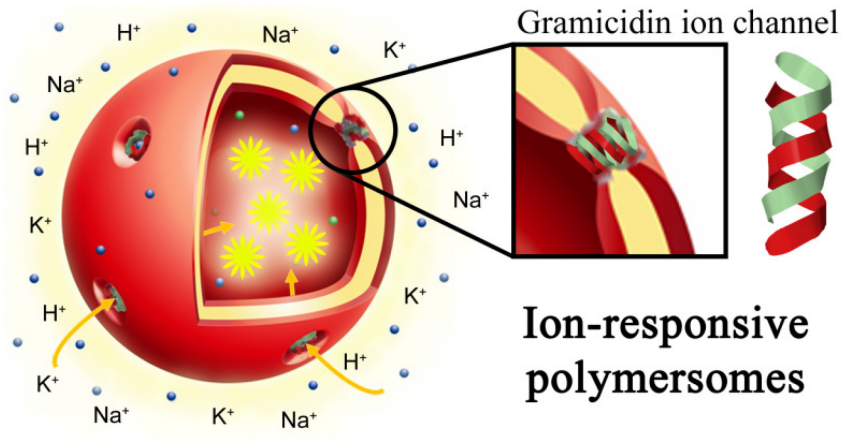

Fig. 12. Polymersomes with membranes permeable to protons and ions, such as Na^+ or K^+, through the insertion gramicidin (gA) biopore insertion.

2. Results and discussion

2.1. Going against Nature with the insertion of gramicidin in a 21.1 nm thick membrane of polymersomes

gA is a model ion channel chosen because of its simplicity (only 15 amino acids in its compositions), and versatility [116]. As mentioned in the introduction, gA allows a controlled passage of protons and monovalent ions trough synthetic membranes [117]. An approach to proof the successful incorporation of gA in a synthetic membrane of a polymersome is by encapsulating within the inner cavity specific ion sensitive probes, which could give a response in the presence of protons and monovalent cations. For instance, pyranine, a pH sensitive marker with fluorescence intensity at high pH (≈8.2), while at pH = 6.2 its fluorescence is quenched [118]. Therefore, the proper insertion and function of gA biopores in the membrane of vesicles was investigated by measuring quenching of fluorescence of encapsulated pyranine upon decreasing the pH (from 8.3 to 6.2) [119]. A combination of fluorescence spectroscopy and stopped-flow spectroscopy was used to assess any change in intensity of pyranine fluorescence as a function of time, and to correlate it with proton transfer across the polymeric membrane resulting from functional gA biopore insertion.

Additionaly, a close look at the published reports in which gA has been extensively studied in lipid membranes [120–123], surfactants mimics of unsaturated lipids [124, 125], and liposomes [125], indicated that a successful insertion of the biopore is favoured by a reduced thickness mismatch between gA size and lipid membranes. However, there was only one report on the insertion of gA in symmetric block copolymer membrane arrays, offering no indication of the thickness of the membrane, the number of inserted gA pores or their localization inside the membrane [126].

Meanwhile, I have gathered more published information about the synthesized polymer library with their corresponding polymersomes much more thicker than a liposome membrane, as determined via cryo-TEM (Table 2, Figure 13) [3, 79], and focused my initial experiments on gA insertion in the membrane of PMOXA$_{14}$-PDMS$_{65}$ (A$_{14}$B$_{65}$) polymersomes (21.3 nm thick membrane). Therefore, I was expecting that gA, of ≈ 2.6 nm in length, should incorporate into a 21.3 nm thick membrane of the A$_{14}$B$_{65}$ polymersomes, an attempt which was without success.

Table 2. Membrane thickness of liposomes versus $PMOXA_x$-$PDMS_y$ (A_xB_y) diblock and $PMOXA_x$-$PDMS_y$-$PMOXA_x$ ($A_xB_yA_x$) triblock copolymers as candidates for the formation of polymersomes

Lipid/Polymer composition used for liposome/polymersomes formation	Mw [g/mol]	Membrane thickness (d) [nm]
POPC	770	4.0
$A_{14}B_{65}$	6200	21.3
$A_6B_{34}A_6$	3800	9.2
$A_7B_{42}A_7$	4500	10.3
$A_6B_{44}A_6$	4500	10.7
$A_7B_{49}A_7$	5100	12.1
$A_{12}B_{63}A_{12}$	6900	13.4
$A_{12}B_{87}A_{12}$	8700	16.2

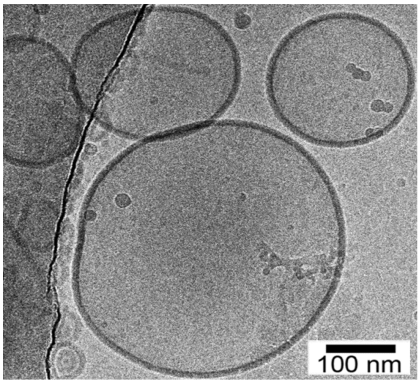

Fig. 13. Example of a cryo-TEM for $A_7B_{42}A_7$

2.2. Feasibility of gramicidin insertion in a thinner (< 21.1 nm) polymersome' membrane

As a result of previous findings, the same pyranine assay was applied to attempt to insert gA in a thinner polymersome membrane. As an initial candidate, $A_7B_{42}A_7$ triblock copolymer was chosen as it forms polymersomes with a 10.3 nm membrane thickness, half as $A_{14}B_{65}$ polymersomes, but still twice as thick as a typical liposome membrane.

A biopore, such as gA, requires the presence of a stable self-assembled membrane which is in this case, part of a polymer vesicle with a specific size and morphology. gA presence in various concentrations, the organic solvent used for its solubilisation, the chosen sensitive probe and the change in pH (from 8.2 to 6.2) can all have an influence upon the self-assembly of the synthetic polymers in terms of their morphology, size, and stability, which had to be investigated by a combination of TEM and light scattering under conditions optimized for the gA function assay. 3D supramolecular assemblies of the tested $A_7B_{42}A_7$ triblock copolymer containing loaded pyranine without (in the presence of DMSO:EtOH (1:1) only) and with gA in DMSO:EtOH (1:1) at pH = 8.2, or with gA at pH = 6.2 revealed from their TEM micrographs formation of spherical structures with radii around 100 nm (Figure 14).

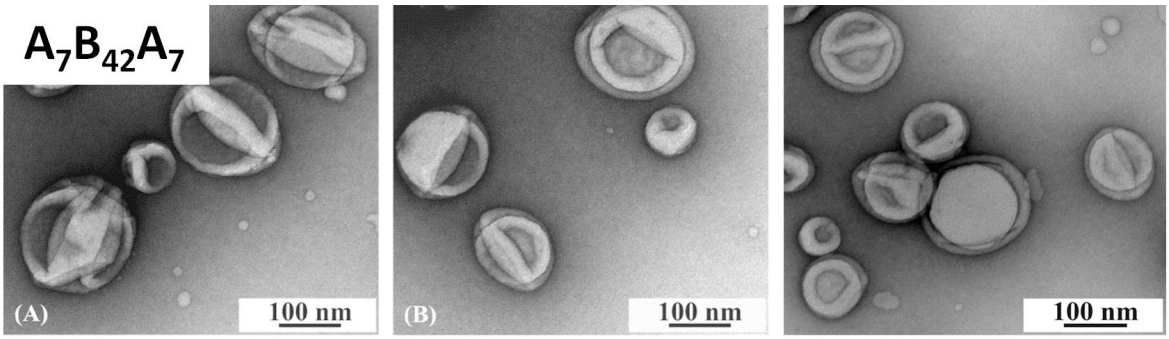

Fig. 14. TEM micrographs of pyranine loaded polymersomes (pH = 8.2) of $A_7B_{42}A_7$ (A), in the presence of gA (B), in the presence of gA and pH = 6.2 (C).

It has to be noted that the concentration of 798 nM gA was chosen as the maximum safe concentration for the insertion assay, as damaged membranes of pyranine loaded $A_7B_{42}A_7$ polymersomes were observed at 1.5 μM initial gA concentration (Figure 15).

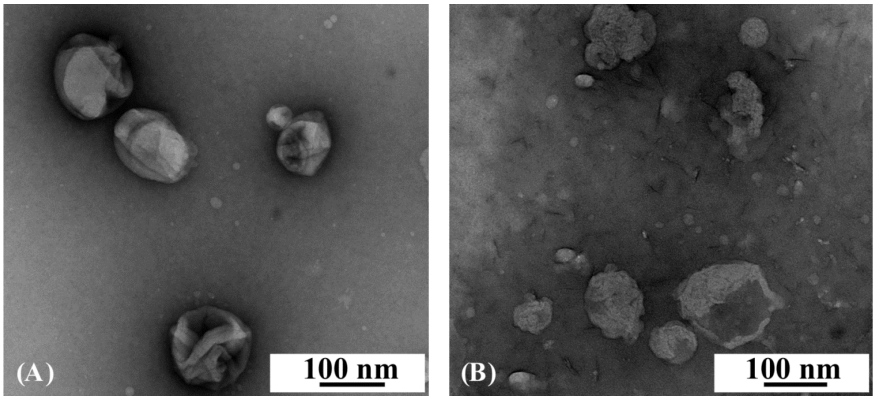

Fig. 15. Preserved architecture of pyranine loaded $A_7B_{42}A_7$ polymersomes in the presence of 798 nM (0.798 μM) (A) versus damaged pyranine loaded $A_7B_{42}A_7$ polymersomes in the presence of 1.5 μM gA (B).

Static light-scattering (SLS) enables the radius of gyration (R_g) to be measured, dynamic light scattering (DLS) allows the hydrodynamic radius (R_h) of the self-assembled objects to be determined, and R_g/R_h (ρ-parameter) reveals the morphology of the 3D assemblies. $A_7B_{42}A_7$ triblock copolymer self-assembled in spherical supramolecular structures with R_g around 100 nm, and a ρ value of 0.93, close to the expected values of 1.0 for hollow spheres (Table 3), confirming the results obtained via TEM characterization.

Table 3. Molecular parameters for 3D assemblies of $A_7B_{42}A_7$ without and with gA.

Components or polymer composition	DLS/SLS			
	R_h [nm]	R_g [nm]	PDI	$\rho = R_g/R_h$
$A_7B_{42}A_7$ (Pyranine)	111.4 ± 1.3*	104.0 ± 0.8	0.14 ± 0.01	0.93 ± 0.01
$A_7B_{42}A_7$ (Pyranine) + gA	110.9 ± 2.6	101.7 ± 0.8	0.17 ± 0.02	0.91 ± ± 0.02

**± SD, n=3. An example of DLS/SLS raw data has been presented in Appendix A.*

Pyranine encapsulation in polymersomes was studied by fluorescence correlation spectroscopy (FCS) (Figure 16) [127]. In this method, variations in fluorescence emission from single fluorophores diffusing through a confocal detection volume are recorded as a function of time, making it possible to determine rotational and lateral diffusion, conformational dynamics, molecular associations and disasociations, concentrations and other molecular properties of single fluorescent molecules *in vitro* and in living cells (Figure 16A) [128–132]. The diffusion time for free pyranine in buffer (room temperature) was τ_d = 16 μs (Table 4), a value which is much lower than the diffusion times obtained when pyranine was loaded in polymersomes during their self-assembly process ($\tau_d \approx$ 2900 μs).

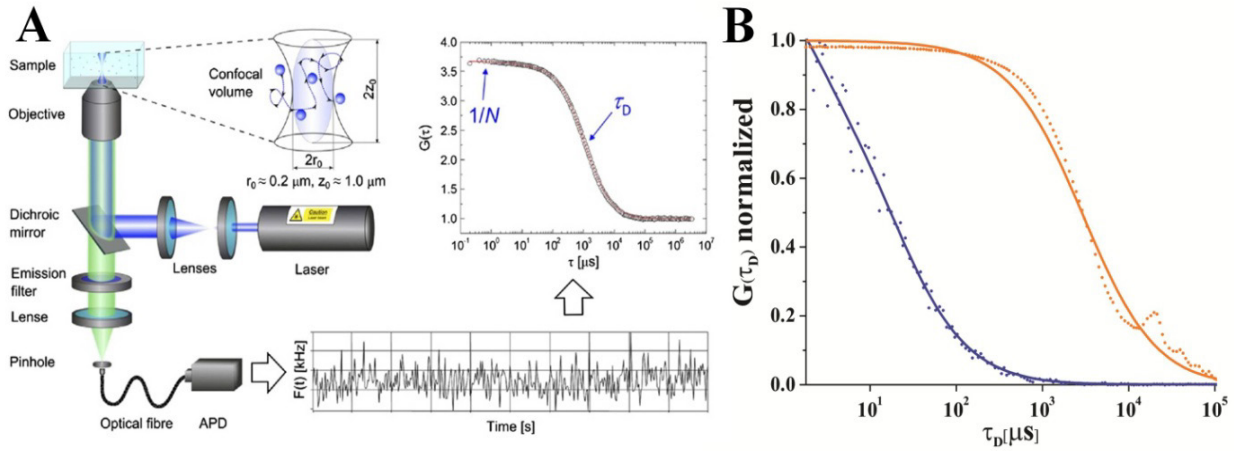

Fig. 16. FCS schematic principle: Fluorescent molecules diffuse through the laser (continuous-wave or pulsed laser) focus and the intensity fluctuations, as the molecules go in and out through the confocal volume, are recorded as a function of time and autocorrelated in terms of strength and duration. Reprinted with permission from [133] Elsevier (A) and autocorrelation curves and fits for pyranine (blue curve) versus pyranine loaded polymersomes of $A_7B_{42}A_7$ (orange curve) (B).

In complex polymersome systems studied by FCS, low amounts of free dye (less than 1%) are not detectable because of the high signal intensity from the bright vesicles [127]. As the autocorrelation curve (Figure 16B) was fitted with only one population of diffusing particles, a successful encapsulation of pyranine was demonstrated during polymersomes formation. Hydrodynamic radius of pyranine-loaded polymersomes (R_h) of 109 nm was obtained using the Stokes-Einstein equation (Equation 1, Table 4), in good agreement with the light scattering results [127]:

$$R_H = \frac{k_B T}{6\pi\eta D_{trans}} \quad (1)$$

Where: R_H - hydrodynamic radius, k_B - Boltzman constant, T – temperature, η - viscosity of the solution, and D_{trans}- translational diffusion constant.

The process encapsulation efficiency (EEP) of pyranine, which represents the fraction of encapsulated dye divided by the amount for encapsulation, was determined to be 20 % according to FCS combined with UV/Vis spectroscopy, using Equation 2 (Table 4):

$$EEP[\%] = \frac{c_{ep}}{c_i} \quad (2)$$

Where: c_{ep}- concentration of pyranine in polymersomes after encapsulation and purification [mol/L], and c_i - initial concentration of pyranine used for the film rehydration [mol/L].
The concentration ofencapsulated pyranine was determined using an extinction coefficient of 2.55×10^{-3} $M^{-1}cm^{-1}$, obtained experimentally at 456 nm wavelength.
Using brightness measurements (ratio of the average fluorescent intensity and the number of species for an individual specimen) [133], 12% encapsulation efficiency of pyranine was determined (Table 4). The encapsulation efficiency (EE) was experimentally determined by fluorescence correlation spectroscopy (FCS) and calculated using Equation 3:

$$EE[\%] = \frac{\#Pyr_{exp}}{\#Pyr_{calc}} \quad (3)$$

where #Pyr was calculated according with the formula:

$$\#Pyr_{exp} = \frac{CPM_{pol}}{CPM_{dye}} \quad (4)$$

in which CPM_{pol} [kHz] are the counts per molecule of the encapsulated dye inside polymersomes, and CPM_{dye} [kHz] represents the counts per molecule of the free dye, as determined experimentally from brightness measurements using the fluorescence correlation spectroscopy technique [2].

The total number of pyranine (#Pyr) per polymersome was calculated according with the Equation 5:

$$\#Pyr_{calc} = C * N_A * \frac{4}{3}(\pi * R_H^3) \quad (5)$$

Where: C is the concentration of pyranine encapsulated [mol/L], N_A is the Avogadro number, and R_H is the hydrodynamic radius [nm] of the polymersomes determined from light scattering experiments [70].

Compared to values for the process encapsulation efficiency, determined by UV/Vis spectroscopy, the encapsulation efficiency value determined by FCS is slightly lower, probably due to bleaching of the encapsulated pyranine. A simple calculation of the number of gA channels/polymersome was obtained by dividing the number of gA channels to the number of polymersomes. In more detail, to estimate the number of gA channels per polymersome, we used a theoretical approach as described for lipid mixture [134]. Briefly, the number of gA per total surface area ($\#gA_{ves}$) of $PMOXA_x$-$PDMS_y$-$PMOXA_x$ polymer membrane was determined by dividing the number of gA channels (n_{gA}^0) by the number of vesicles formed in the system (N_{ves}), and taking into account the efficiency of the interaction between vesicles and gA in a Brownian movement (η) (Equation 6):

$$\#gA_{ves} = \frac{n_{gA}^0 \cdot \eta}{N_{ves}} \quad (6)$$

The number of polymersomes (N_{ves}) was calculated by dividing the concentration of the polymer to the number of polymer chains. The number of polymer chains was obtained by dividing the area of a vesicle by the aria of a polymer chain, using $R_g = N^a \frac{b}{6}$, where N is the number of PDMS units, b the Si-O-Si segment length (b = 0.311 nm) [135].

The efficiency of the interaction between polymersomes and gA molecules in Brownian motion (η) was obtained by taking into account the hydrophobic forces inducing the insertion of gA inside the polymersome membrane.

The probability of interaction between the vesicles and the gA molecules is governed by hydrophobic forces (they normally act in a domain around the interacting particles with $r_{hydropbobic} = 10\ nm$ [136]. Therefore, the interaction radius for vesicles and gA, respectively, become:

$$R_{ves}^{i} = R_H + r_{hydropbobic} \quad (7)$$

$$R_{gA}^{i} = R_{gA} + r_{hydropbobic} \quad (8)$$

The efficiency of the interaction between polymersomes and gA molecules in Brownian motion (η) is obtained by dividing the cross section of vesicles (σ_{ves}) to the cross section of gA molecules (σ_{gA}), considering that the probability of interaction between them is proportional to the cross sections:

$$\eta = \frac{\sigma_{ves}}{\sigma_{gA}} \quad (9)$$

where the cross section of vesicles is:

$$\sigma_{ves} = N_{ves} A_{ves}^{i} \quad (10)$$

and the cross section of gA molecules is:

$$\sigma_{gA} = n_{gA} A_{gA}^{i} \quad (11)$$

A_{ves}^{i} and A_{gA}^{i} are the area of the transversal section of vesicles and gA molecules, respectively.

Therefore, for an initial concentration of gA of 798 nM, the number of gA channels/polymersome was ≈ 110.

Table 4. Encapsulation efficiency of pyranine in $A_7B_{42}A_7$ polymersomes

Components or polymer composition	FCS				UV/VIS	DLS/SLS + theoretical approach
	τ_d [µs]	R_h [nm]	#pyranine molecules per polymersome	EE [%]*	EEP [%]**	#gA channels/polymersome#
pyranine	16 ± 1#	N/A***	N/A	N/A	N/A	N/A
$A_7B_{42}A_7$	2908 ± 298	109	114	11.8	20	110

**EE [%]- Encapsulation Efficiency [%]; **EEP [%]- Encapsulation Efficiency of the Process [%]; ***N/A - Not applicable; #calculated in the presence of 798 nM gA for the polymersomes self-assembled from the listed triblock copolymers; # ± SD, n=3. An example of FCS raw data has been presented in Appendix B.*

Fluorescence quenching of free pyranine, which was induced by a pH decrease from 8.2 to 6.2, under similar conditions to those used for assessing gA function in dye loaded polymersomes was evaluated. Quenching of pyranine fluorescence was investigated in the presence of DMSO:EtOH (1:1). As expected neither DMSO:EtOH (1:1) nor gA had any influence on pyranine fluorescence (Figure 17).

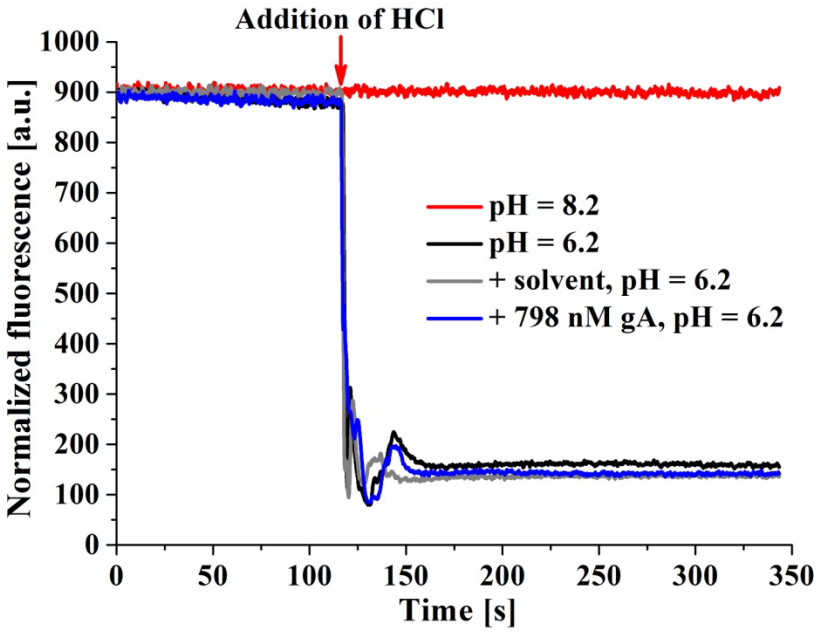

Fig. 17. Fluorescence quenching of the free pyranine solution with the same volume and concentration of HCl in the presence of solvent and gA.

The proper insertion and function of gA biopores in polymersome membrane was then investigated by the quenching of fluorescence of encapsulated pyranine upon decreasing the pH. A combination of fluorescence spectroscopy and stopped-flow spectroscopy was used to assess any change in intensity of pyranine fluorescence as a function of time, and to correlate it with proton transfer across the polymeric membrane resulting from functional gA biopore insertion.

At pH 8.2, pyranine loaded $A_7B_{42}A_7$ polymersomes without gA had a high fluorescence intensity (Figure 18A). This decreased slightly when pH was lowered to 6.2, as a result of quenching of any free pyranine that was not completely removed during purification. The fluorescence intensity of pyranine decreased after addition of 128 nM gA to the polymersome solution, thus indicating a proton influx through the membrane inserted gA biopores. Pyranine fluorescence intensity decreased when gA concentration was increased up to 567 nM, due to insertion of a higher number of biopores, which allowed a greater proton transfer to the inner aqueous cavity of the polymersomes. This behavior is similar to that of gA-permeabilized unilamellar giant lipid vesicles, where quenching rate is proportional with the number of gA conducting channels [137]. However, no difference in fluorescence intensity was observed upon further increasing the gA concentration to 798 nM, a result which suggests that a plateau is reached for proton influx through the polymersome membrane. It should also be noted that pyranine is too large (M_w = 524 Da) to diffuse out through gA biopores, which are known to only allow the passage of protons and monovalent cations. Together with the impermeability of $PMOXA_x$-$PDMS_y$-$PMOXA_x$ polymersome membrane to small molecules [86], this provides evidence that the quenching effect was entirely due to a successful insertion and function of gA biopores.

Additional stopped-flow measurements provided insights into the efficiency of proton influx through the gA biopores in the short period of time (≤10 s) after the pH decrease (Figure 18B). An instant quenching of the dye in polymersomes with inserted gA biopores was observed, in agreement with the behavior of pyranine-loaded polymersomes with gA established by fluorescence spectroscopy. The fast transport of protons through functional inserted biopores results in the ability to almost instantly regulate pH through polymersome membrane.

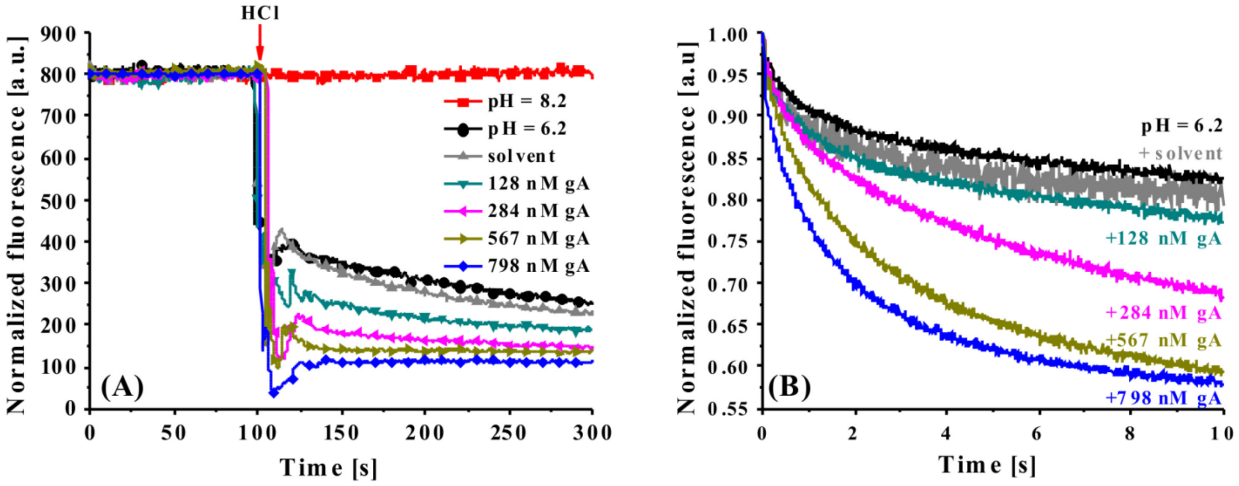

Fig. 18. Quenching of the fluorescence intensity of pyranine-loaded $A_7B_{42}A_7$ polymersomes (pH = 6.2) observed by (A): fluorimetry - before (black and grey curves), and after insertion of gA (green to dark blue curves). The fluorescence intensity of pyranine loaded polymersomes without gA at pH = 8.2 (red curve), and (B): stopped-flow spectroscopy - before (black and grey curves), and after insertion of gA (green to dark blue curves).

Since gA is also permeable to monovalent cations, I investigated Na^+ and K^+ influx through polymersome membranes upon insertion of gA. $A_7B_{42}A_7$ polymersomes were loaded with Na^+ (ANG-2) and K^+ (APG-2) sensitive dyes, which increase their fluorescence intensity in the presence of these ions. TEM and SLS/DLS showed spherical structures with radii of 100 nm were obtained by self-assembly of $A_7B_{42}A_7$. In the presence the fluorescent sensitive dyes at pH = 7.0, they preserved their morphology and size in the presence of 798 nM gA, or 798 nM gA and 5 mM monovalent cation concentration (Figure 19 and Table 5).

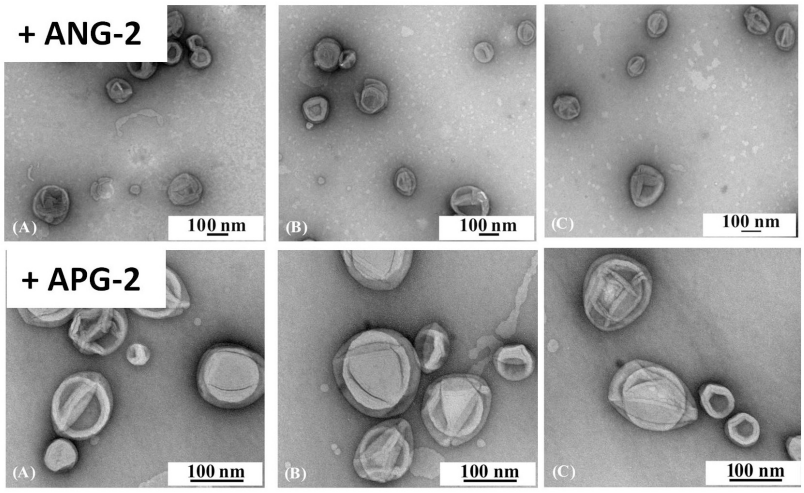

Fig. 19. TEM micrographs of APG-2/ ANG-2-loaded polymersomes of $A_7B_{42}A_7$ without gA (A), with gA (B), with gA and 5 mM Na^+/ K^+ (C).

Table 5. Molecular parameters for 3D assemblies of APG-2/ ANG-2-loaded polymersomes of $A_7B_{42}A_7$ without and with gA.

Components or polymer composition	**DLS/SLS**			
	R_h [nm]	**R_g [nm]**	**PDI**	**$\rho = R_g/R_h$**
$A_7B_{42}A_7$ (ANG-2)	110.4 ± 1.1[#]	119.8± 0.7	0.15± 0.01	0.92± 0.04
$A_7B_{42}A_7$ (ANG-2) + gA	108.4 ± 0.5	116.9 ± 1.3	0.16± 0.03	0.93± 0.01
$A_7B_{42}A_7$ (APG-2)	113.2 ± 0.8	120.5 ± 1.5	0.14± 0.01	0.94± 0.01
$A_7B_{42}A_7$ (APG-2) + gA	113.6 ± 1.2	119.2 ± 0.5	0.13± 0.01	0.91± 0.02

[#] *± SD, n=3. An example of DLS/SLS raw data has been presented in Appendix A.*

Additionally, in the absence of gA there was no increase in fluorescence intensity of the encapsulated dye. The dye fluorescence intensity increased only upon gA insertion, thus providing evidence for passage of both types of ions across the polymersome membrane (Figure 20A and B). The difference in fluorescence intensity between the two dyes is determined by their specific sensitivity.

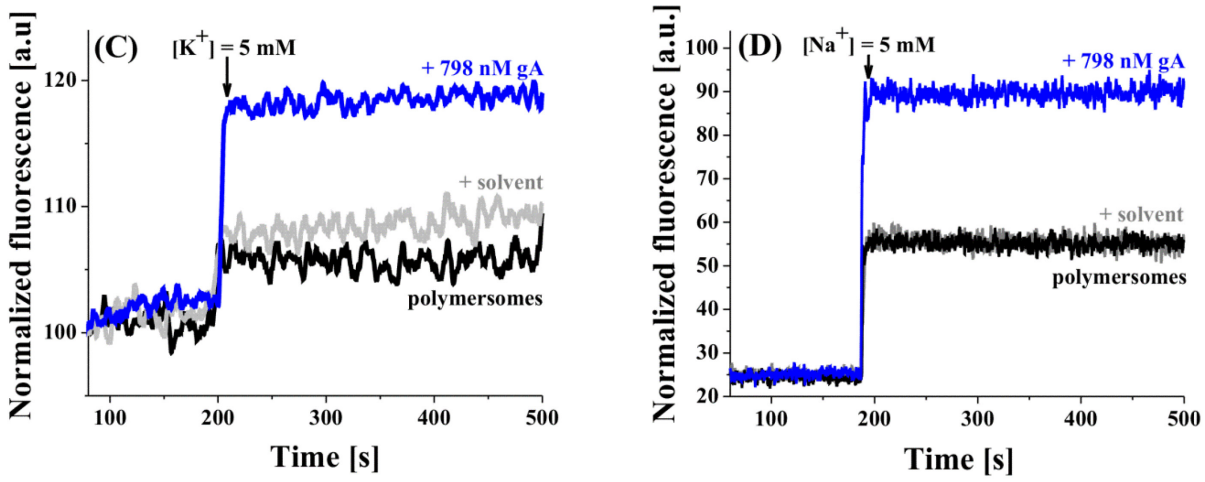

Fig. 20. Fluorescence intensity of dye-loaded polymersomes (pH = 7.0). (A) APG-2-loaded polymersomes upon addition of 5 mM K^+ (black curve), upon addition of 5 mM K^+ in the presence of DMSO:EtOH (1:1) (grey curves), and upon addition of 5 mM K^+ in the presence of DMSO:EtOH (1:1) after insertion of gA (blue curve). (B) ANG-2-loaded polymersomes upon addition of 5 mM Na^+ (black curve), upon addition of 5 mM K^+ in the presence of DMSO:EtOH (1:1) (grey curve), and upon addition of 5 mM K^+ in the presence of DMSO:EtOH (1:1) after insertion of gA (blue curve).

Owing to their large dimensions, GUVs prepared using the electroformation method (see Materials and Methods) were also used as a tool to visualize gA insertion and activity. In order to verify the function of gA when inserted into GUV membranes, 5(6)-carboxyfluorescein (CF), a pH-sensitive fluorescent dye with reduced fluorescence intensity at low pH, and high fluorescence intensity at high pH, was encapsulated in GUVs.

GUVs were formed in presence of CF at pH = 5.5 (Figure 21A). GUVs tested in presence of pure solvent (DMSO:EtOH (1:1)) were observed to have a membrane impermeable to protons (Figure 21B), showing that the solvent affects neither the GUV membrane stability nor its permeability properties, which is an important fact when performing the experiments with gA.At pH = 5.5, the fluorescence of the dye is quenched, therefore confocal laser scanning microspopy (CLSM) micrographs showed low fluorescence intensity inside GUVs (Figure 21C). It has to be noted that the CF concentration inside the GUVs is higher due to dilution of the GUV solution into the LSM observation chamber that is already filled with a CF-free buffer. Therefore, at the beginning of the experiments, the fluorescent intensity inside the GUVs was always higher than

the outside solution. In order to prove that GUVs membranes are impermeable to protons, the pH of the outer solution was increased from 5.5 by the addition of NaOH. The higher pH increases the fluorescent intensity of the background solution significantly, but the fluorescent intensity of the inner cavity of the GUVs remained unchanged, indicating that the block copolymer membrane does not allow diffusion of protons (Figure 21C, inset).

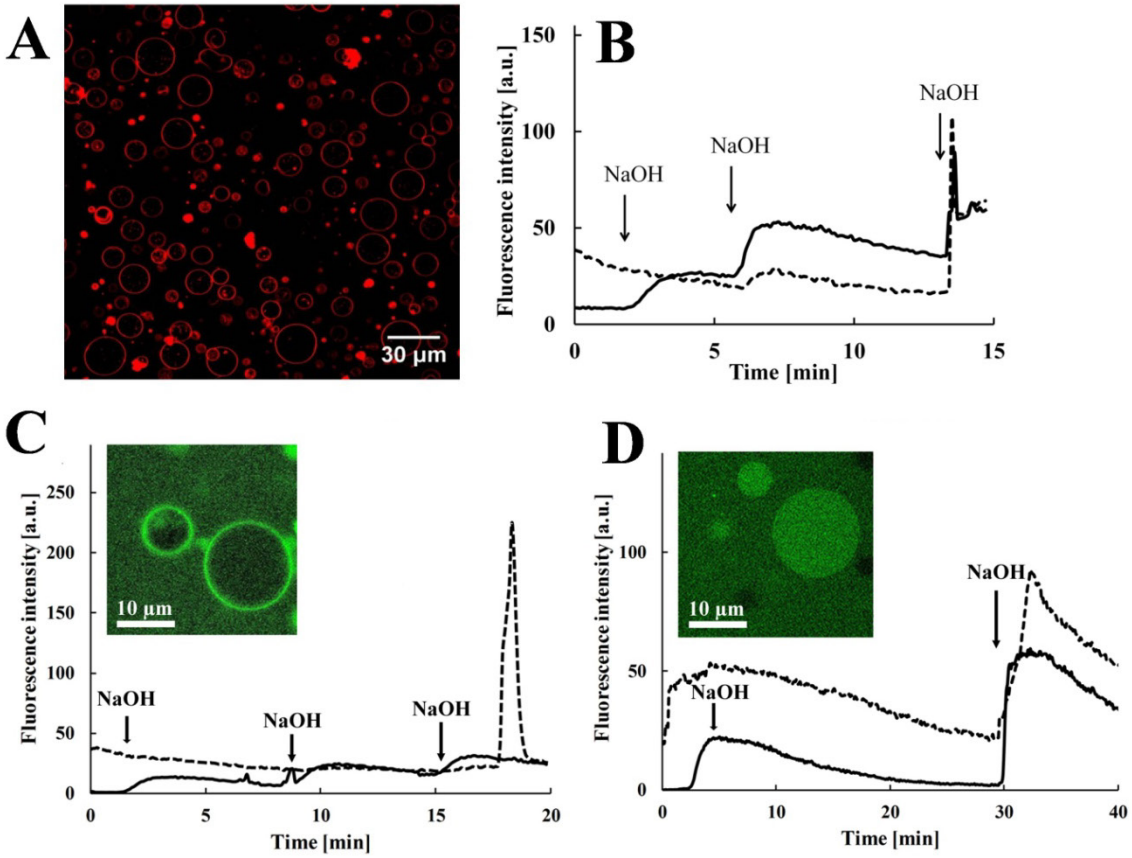

Fig. 21. CLSM images GUVs formation identified by staining the membrane with BODIPY (A); Fluorescence intensity change over time of 5(6)-carboxyfluorescein (CF) inside and outside of polymer GUVs ($A_7B_{42}A_7$) in the presence of solvent (B), absence (C), and upon insertion of gA (D). Insets: representative LSM images showing the principle of blocking the membrane to protons (C) and permeability of the membrane to protons by insertion of gA (D). Fluorescence intensity inside GUVs (dotted line), and outside GUVs (solid line).

The change of fluorescence intensity inside polymersomes upon gA insertion was also confirmed by plotting the fluorescent intensity over time (Figure 21C). Even after several additions of

NaOH, no response of the fluorescent intensity inside the GUVs was observed until the particular GUV ruptured and released its encapsulated CF, shown as a sudden intensity increase (Figure 21C). In contrast, when gA was added to the GUVs solution and the pH was increased, the fluorescent intensity inside the GUVs increased immediately after the higher pH reached the GUV membrane, shown by the higher fluorescent intensity of the outside solution. The increase in the fluorescence intensity inside GUVs clearly indicates permeability of the membrane due to successful insertion and function of gA (Figure 21D).

2.3. Identifying a limit of insertion of gramicidin in polymersome' membranes with various thicknesses

In polymersome membranes, the bilayer thickness is significantly higher and there is a higher degree of hydrophobic mismatch with the protein size. Therefore, with increasing membrane thickness the incorporation of shorter proteins becomes a challenge. gA has a length of ≈ 2.6 nm, and forms a pore with an inner diameter of 0.4 nm [138]. The polymers chosen for testing insertion have membrane thicknesses ranging from 9.2 to 12.1 nm, significantly larger than the gA biopore (Figure 22).

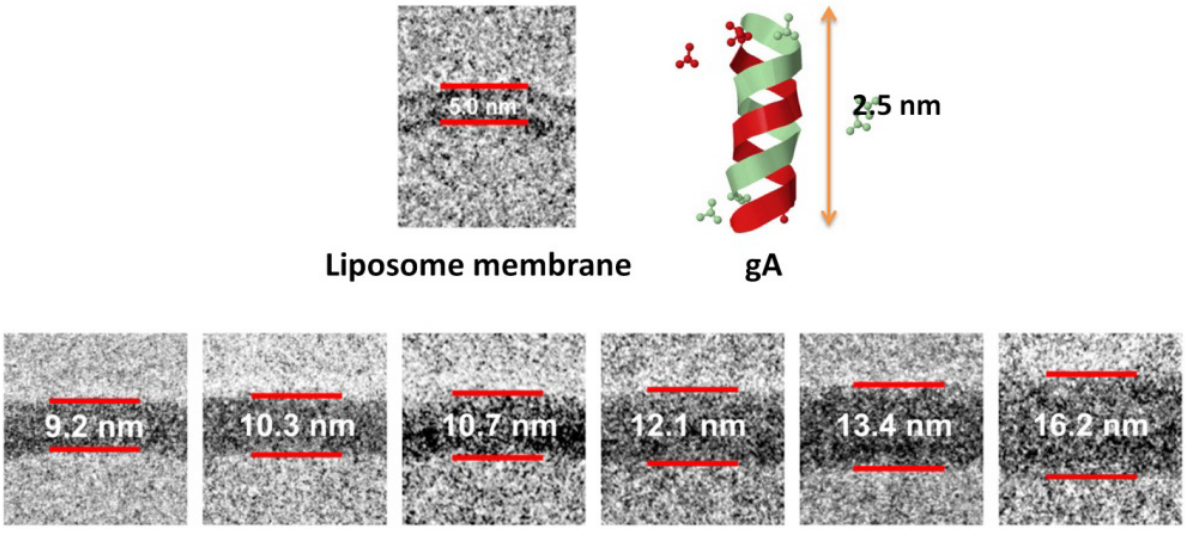

Fig. 22. gA versus liposomes versus polymersomes' membrane thickness. Adapted with permission [79]. Copyright (2014) American Chemical Society.

A membrane thickness larger than the size of the gA has been reported to be correlated with a dimeric stretched active conformation of the biopore with preserved function in the case of lipid membranes [139]. However, as polymer membranes have a significantly larger thickness than those formed from lipids, the difference between the polymer membrane and the size of the gA channel is large. Therefore, I was interested to see whether gA insertion is affected or even blocked, by complete insertion within the hydrophobic domain of the membrane as predicted by modelling the insertion of membrane proteins in polymer membranes [27]. I chose triblock copolymers resulting in polymersomes with membrane thickness between 9.2 and 16.2 nm (Table 2).

All $PMOXA_x$-$PDMS_y$-$PMOXA_x$ copolymers preserved their architecture in the presence of pyranine and gA (in the range 128 nM to 798 nM), or gA at pH = 6.2. It has to be noted that, even though all $PMOXA_x$-$PDMS_y$-$PMOXA_x$ copolymers, in the presence of pyranine, self-assemble in polymersomes, $A_{12}B_{87}A_{12}$ copolymer formed a mixture of worm-like micelles and polymersomes (Figure 23) [140].

According to the DLS/SLS results, all triblock copolymers self-assembled in spherical supramolecular structures with Rg around 100 nm, and ρ values ranging from 0.90 up to 1.09 (Table 6), (i.e. close to the expected values of 1.0 for hollow spheres), confirming the results obtained via TEM characterization.

Table 6. Molecular parameters for 3D assemblies of $PMOXA_x$-$PDMS_y$-$PMOXA_x$ without and with gA.

Components or polymer composition	DLS/SLS			
	R_h [nm]	R_g [nm]	PDI	$\rho = R_g/R_h$
$A_6B_{34}A_6$ (Pyranine)	104.2 ± 3.0[#]	95.4 ± 0.2	0.15 ± 0.01	0.91 ± 0.02
$A_6B_{44}A_6$ (Pyranine)	110.4 ± 1.8	121.3 ± 1.7	0.13 ± 0.02	1.09 ± 0.02
$A_7B_{49}A_7$ (Pyranine)	124.0 ± 1.1	125.1 ± 1.0	0.15 ± 0.01	1.00 ± 0.007
$A_{12}B_{63}A_{12}$ (Pyranine)	115.0 ± 0.8	121.8 ± 0.9	0.10 ± 0.01	1.05 ± 0.12
$A_6B_{34}A_6$ (Pyranine) + gA	112.0 ± 3.6	101.4 ± 1.5	0.15 ± 0.01	0.90 ± 0.03
$A_6B_{44}A_6$ (Pyranine) + gA	110.5 ± 1.9	121.5 ± 1.1	0.11 ± 0.01	1.09 ± 0.09
$A_7B_{49}A_7$ (Pyranine) + gA	125.6 ± 1.3	124.9 ± 1.3	0.15 ± 0.02	1.00 ± 0.01
$A_{12}B_{63}A_{12}$ (Pyranine) + gA	113 ± 0.5	119.2 ± 0.7	0.12 ± 0.03	0.93 ± 0.04

[#] *± SD, n=3. An example of DLS/SLS raw data has been presented in Appendix A.*

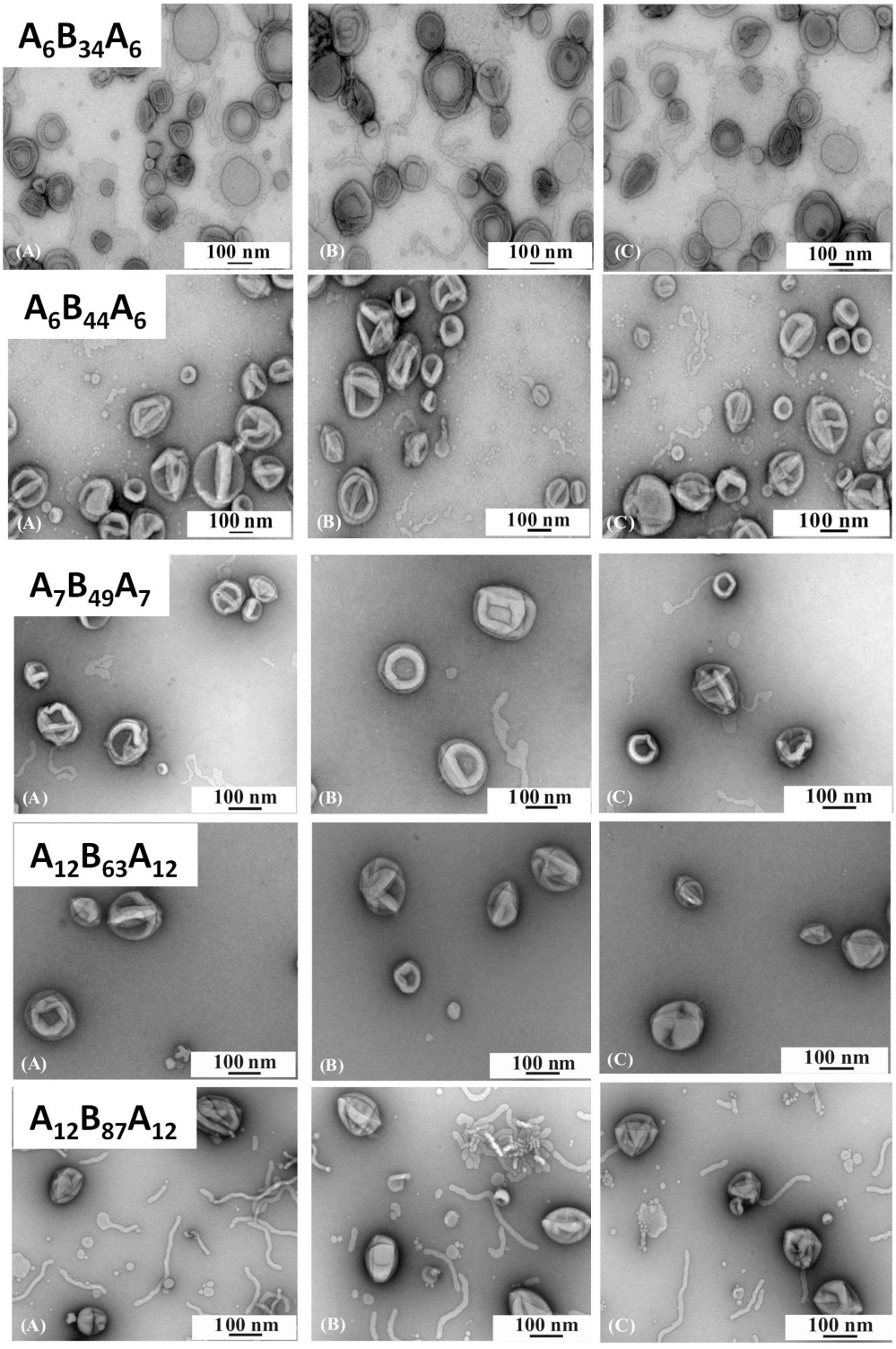

Fig. 23. TEM micrographs of pyranine loaded polymersomes (pH = 8.2) of $A_xB_yA_x$ (left column), in the presence of gA (middle column), in the presence of gA and pH = 6.2 (right column).

The diffusion times obtained when pyranine was loaded in polymersomes during the self-assembly process was in the range of 2500 – 3000 μs. This is much higher than the diffusion time for free pyranine in buffer (room temperature) of 16 μs (Table 7). The FCS autocorrelation curve was fitted with only one population of diffusing particles, as in the case of initially studied $A_7B_{42}A_7$, demonstrating as well a successful encapsulation of pyranine during polymersomes formation. The hydrodynamic radii of pyranine-loaded polymersomes (R_h) ranged from 95 nm to 113 nm, in good agreement with the light scattering results. The process encapsulation efficiency (EEP) of pyranine, as determined by using UV/Vis and FCS spectroscopy gave values ranging from 4 to 20 %, while the encapsulation efficiency (EE) of pyranine was within the range from 2 to 12 %, with a number of gA channels/polymersome from 98 – 116.

Because of different encapsulation efficiency of pyranine inside polymersomes, samples were diluted to the same pyranine final concentration before measuring fluorescence.

A significant decrease in fluorescence intensity was obtained for gA-containing $A_6B_{34}A_6$, $A_6B_{44}A_6$, $A_7B_{49}A_7$ polymersomes (membrane thickness ranging from 9.2 to 12.1 nm), as compared with the polymersomes without gA. This indicated that inserted gA mediated proton influx across the membrane (Figure 24).

Table 7. Encapsulation efficiency of pyranine in $PMOXA_x$-$PDMS_y$-$PMOXA_x$ polymersomes

Components or polymer composition	**FCS**				**UV/VIS**	**DLS/SLS + theoretical approach**
	τ_d [μs]	**R_h [nm]**	**pyranine molecules per polymersome**	**EE [%]***	**EEP [%]****	**gA channels/polymersome#**
pyranine	16 ± 1##	N/A***	N/A	N/A	N/A	N/A
$A_6B_{34}A_6$	2785 ± 378	104	50	3.5	5	98
$A_6B_{44}A_6$	2902 ± 312	109	105	6.4	10	108
$A_7B_{49}A_7$	2916 ± 610	109	87	5.3	7	116
$A_{12}B_{63}A_{12}$	3025 ± 211	113	37	2.0	4	N/A
$A_{12}B_{87}A_{12}$	2527 ± 830	95	49	4.5	6	N/A

**EE [%]- Encapsulation Efficiency [%]; **EEP [%]- Encapsulation Efficiency of the Process [%]; ***N/A - Not applicable; #calculated in the presence of 798 nM gA for the polymersomes self-assembled from the listed triblock copolymers; ## ± SD, n=3. An example of FCS raw data has been presented in Appendix B.*

Additionally, an instant quenching of pyranine inside $A_6B_{34}A_6$, $A_6B_{44}A_6$, and $A_7B_{49}A_7$ polymersomes with gA was observed by stopped-flow measurements (Figure 25).

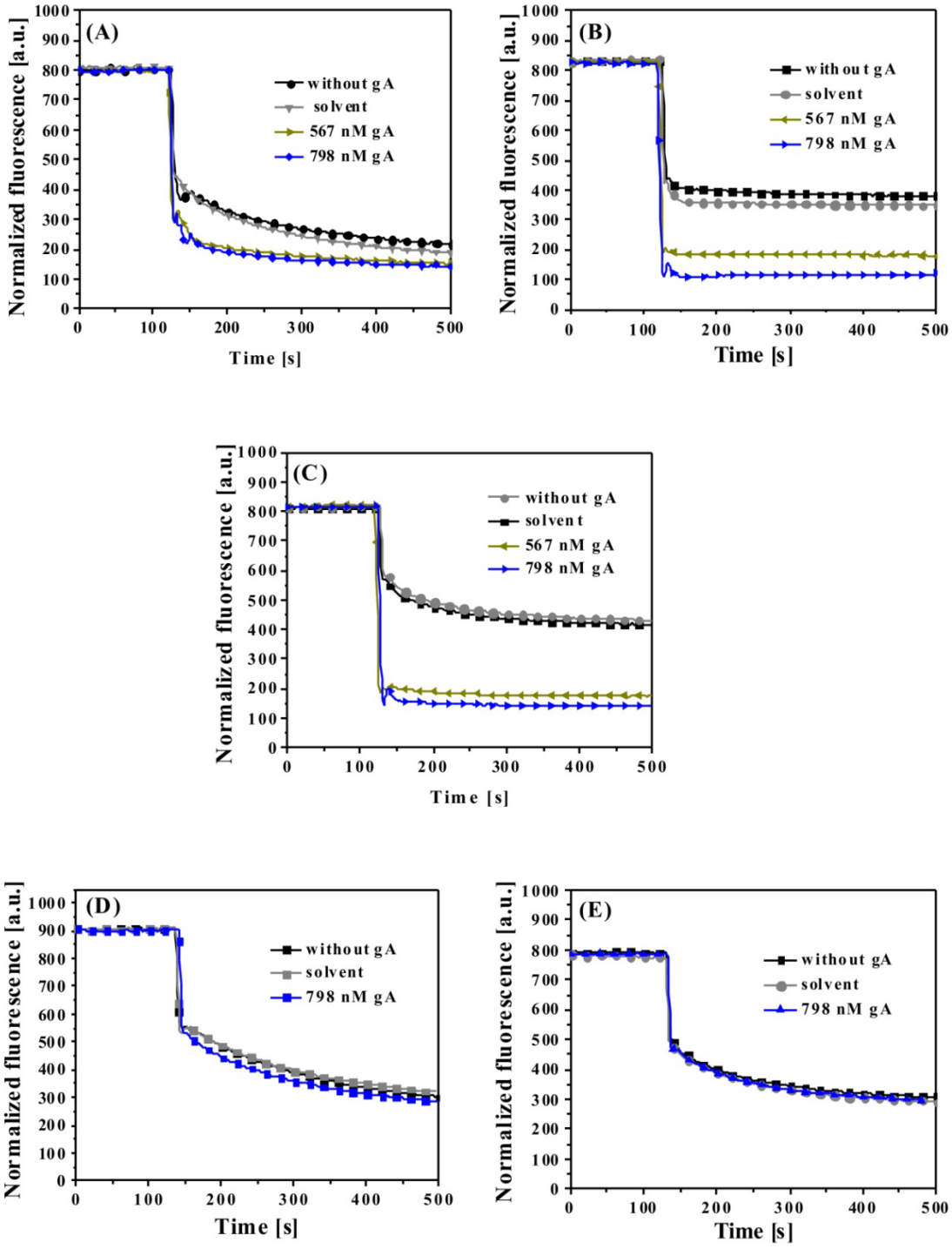

Fig. 24. Quenching of the fluorescence intensity of pyranine-loaded $PMOXA_x$-$PDMS_y$-$PMOXA_x$ polymersomes (pH = 6.2) observed by fluorimetry: pyranine-loaded $PMOXA_x$-

$PDMS_y$-$PMOXA_x$ polymersomes (black curve), pyranine-loaded $PMOXA_x$-$PDMS_y$-$PMOXA_x$ polymersomes in the presence of DMSO:EtOH (1:1) (grey curve) and pyranine-loaded $PMOXA_x$-$PDMS_y$-$PMOXA_x$ polymersomes in the presence of DMSO:EtOH (1:1) after insertion of 567 nM gA (dark yellow curve) or 798 nM gA (blue curve). The following $PMOXA_x$-$PDMS_y$-$PMOXA_x$ triblock copolymers with increasing membrane thickness were chosen: $A_6B_{34}A_6$ (A), $A_6B_{44}A_6$ (B), $A_7B_{49}A_7$ (C), $A_{12}B_{63}A_{12}$ (D), $A_{12}B_{87}A_{12}$ (E).

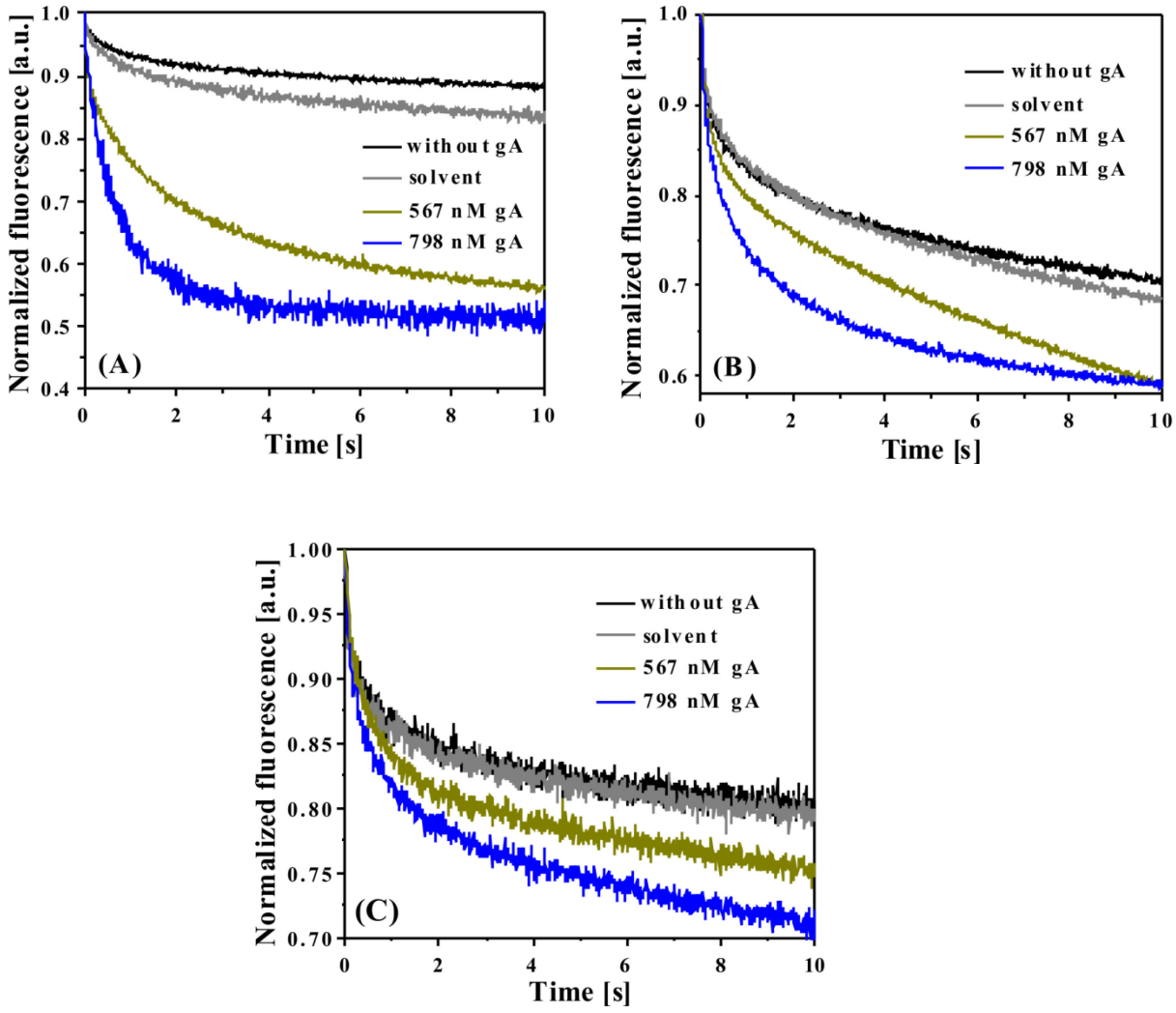

Fig. 25. Quenching of the fluorescence intensity of pyranine-loaded $A_6B_{34}A_6$ (A), $A_6B_{44}A_6$ (B), and $A_7B_{49}A_7$ (C) polymersomes (pH = 6.2) observed by stopped-flow spectroscopy: pyranine-loaded $PMOXA_x$-$PDMS_y$-$PMOXA_x$ polymersomes (black curve), pyranine-loaded $PMOXA_x$-$PDMS_y$-$PMOXA_x$ polymersomes in the presence of DMSO:EtOH (1:1) (grey curve) and

pyranine-loaded $PMOXA_x$-$PDMS_y$-$PMOXA_x$ polymersomes in the presence of DMSO:EtOH after insertion of 567 nM gA (dark yellow curve) or 798 nM gA (dark blue curve).

As expected, polymersomes generated by film-rehydration method, and GUVs obtained by electroformation technique, proved successful insertion and function of gA in block copolymer membranes with thicknesses ≤ 12 nm.

The preserved function for gA when the membrane thickness ranged from 9.2 to 12.1 nm can be explained by a bilayer compression. The compression is due to an energetic balance between the surface tension at the hydrophobic/hydrophilic interface and the chain configurations to match the biopore length. Bilayer compression results in an increase of the surface tension energy and a decrease in stretching energy. Protein insertion reduces the system free energy compensating for thickness mismatches [27]. A modulation of membrane protein activity has been reported for Complex I when inserted in $PMOXA_x$-$PDMS_y$-$PMOXA_x$ membranes, the hydrophobic block being the key domain, which provided the necessary flexibility to accommodate the significantly smaller size of the hydrophobic part of the protein [85]. For thicker polymer membrane (≥12 nm), no influx of protons across the membrane was observed by fluorescence measurements. The lack of proton transfer through gA in polymer membranes with thickness ≥ 13.4 nm indicates that there is a limit of thickness mismatch for which the membrane perturbation energy becomes a barrier for protein insertion [27]. In our polymersome membranes thickness mismatches up to 12.1 nm were compensated by the bilayer compression, while higher differences have not been matched up. The successful insertion of other membrane proteins (e.g., OmpF, AqpZ, and Complex I) in $PMOXA_x$-$PDMS_y$-$PMOXA_x$ polymersome membranes can be explained by similar compression compensation in thickness mismatches [38, 76, 85, 100].

Compared to the insertion of proteins in lipid bilayers, the significantly greater hydrophobic mismatch in polymer bilayers creates a challenge for the incorporation of proteins/biopores. However, by appropriate selection of the chemical nature and intrinsic flexibility of the hydrophobic domain it was possible to insert biopores/membrane proteins even for a high degree of mismatch between the size of biomolecule and the thickness of polymer membrane, and still preserve the integrity of the membrane.

3. Conclusions

We have engineered polymersomes with selective membrane permeability by inserting gramicidin biopores, which are known to allow transport of protons and monovalent ions, such as Na^+ and K^+. Whilst gA has been inserted in lipid membranes in a plethora of research studies, the challenge of inserting the pore into the membrane of polymer vesicles is greater because of the significant difference between the pore length and the thickness of the polymer membrane (more than 3.5 times). By using a small library of $PMOXA_x$-$PDMS_y$-$PMOXA_x$ copolymers, which self-assemble in polymersomes or GUVs with membrane thickness ranging from 9.2 to 16.2 nm, I tested the conditions in which gA can be inserted, and remains functional inside the synthetic membrane, whilst preserving the polymersome architecture. pH-, Na^+- and K^+-sensitive dyes were encapsulated inside polymersomes/GUVs, and proton or ion gradients between the environment of polymersomes/GUVs and their inner cavity served to assess the exchange of ions across the membrane upon gA insertion. The results showed that gA was successfully inserted and remained functional in polymer membranes with thickness of 9.2–12.1 nm. Larger thicknesses did not allow gA insertion, and 12.1 nm represents a limit for the mismatch between the pore length and the membrane thickness. gA-polymersomes are therefore pH and ions self-regulating polymersomes, which maintain their integrity in different pH or ion gradient conditions.

This bio-mimetic approach to use ion channels with specific selectivity (e.g. gA biopores) for insertion in polymer membranes is an elegant strategy to develop mimics of biomembranes or for supporting the design of nanoreactors or artificial organelles in which biopore function is combined with preserved membrane architecture.

IV. HYBRID SYNTHETIC MEMBRANES WITH RESPONSIVENESS TO DIVALENT CATIONS

The results of this investigation have been reprinted and modified with permission from the following publications ([114] CC-BY-NC 3.0 license and [4] Copyright John Wiley and Sons):

1. **M. Lomora**, F. Itel, I. A. Dinu, C. G. Palivan*, Selective ion-permeable membranes by insertion of biopores into polymersomes,* Phys. Chem. Chem. Phys., **2015**, 17, 15538-15546;
2. **M. Lomora**, I. A. Dinu, F. Itel, S. Rigo, M. Spulber, C. G. Palivan*, Does Membrane Thickness Affect the Transport of Selective Ions Mediated by Ionophores in Synthetic Membranes?,* Macromol. Rapid Commun. **2015**, 36, 1929−1934.

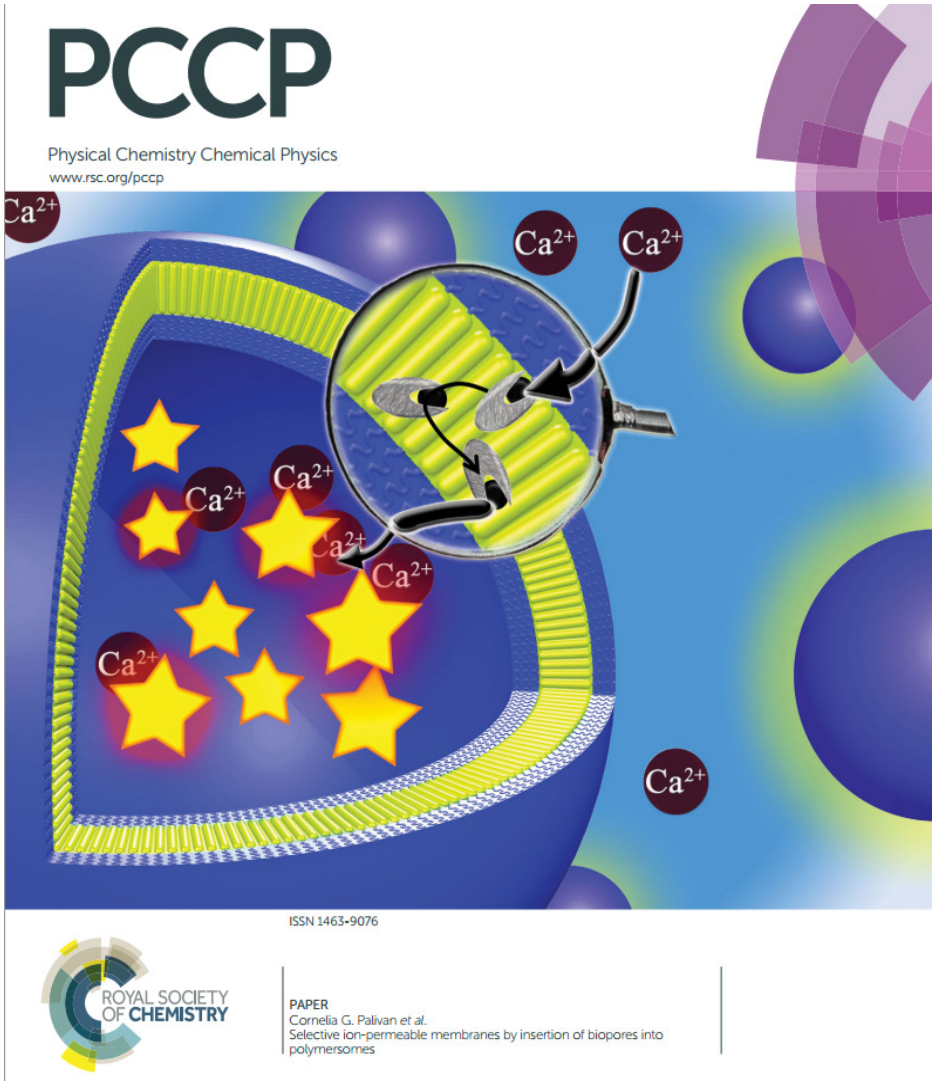

1. Introduction

Mimics of cell membranes and bio–compartments are essential for developing tailored applications in therapeutic diagnostics. The selectivity of polymersome membranes should support specific reactions inside the cavities, or the development of nano–biosensors for molecules selected by their specific permeability. In particular, biosensors are being explored for applications as diagnostic systems, because they can sense changes in biological responses, which are then converted to a detectable and measurable signal [141, 142]. Such sensors based on nanoreactors have been developed recently, but only a few examples have been reported, either in solution [42] or immobilized on surfaces [49]. However, these sensors are based on the specificity of active compounds encapsulated inside nanoreactors, and are not mediated by a selective membrane, as is the case in natural biocompartments.

Being inspired by nature, I present here biomimetic nanocompartments with Ca^{2+}–selective membrane permeability engineered by insertion of ionomycin biopores into polymersomes to support applications that require transport of a desired ion through the membrane, such as for specific *in situ* reactions or nano–sensors. I selected $PMOXA_x$–$PDMS_y$–$PMOXA_x$ for vesicle formation, and as a model biopore, able to induce selective membrane permeability, we selected ionomycin, a carboxylic acid ionophore (divalent anion polyether, M_w 787.08 Da), produced by *Streptomyces conglobatus*. Ionomycin allows specific transport of divalent ions, such as Ca^{2+} [143–145], which was chosen because it plays a pivotal role in biological systems where many cellular responses are regulated by an ON and OFF mechanism that is strongly correlated to the intracellular Ca^{2+} concentration [146]. In nature, calcium signaling is initiated by cells using both intra– and extracellular sources of Ca^{2+}, which are controlled by channels, pumps and exchangers to provide cellular calcium homeostasis for the cell integrity. Any perturbation in the calcium regulating gates results in channelopathies correlated with severe diseases, such as muscle or neurological disorders [147]. As a marker to assess the proper insertion and function of ionomycin inside the synthetic membrane, we used a Ca^{2+} – sensitive dye encapsulated inside the polymersome cavity prior to inserting the biopore.

A combination of light scattering (LS) and transmission electron microscopy (TEM) has been used to characterize the formation of biopore–equipped polymersomes and their stability. By using a combination of stopped–flow and fluorescence spectroscopy, it was shown that ionomycin can function and transport calcium ions across polymer membranes with thicknesses

in the range 10.7 - 13.4 nm (7.1 - 8.9 times larger than the size of the ionophore). Thicker membranes induced a decrease in transport, but did not inhibit it due to the intrinsic flexibility of these synthetic membranes. The ion–selective permeable polymersome presented here (Figure 26) represents a progress in the development of mimics of a cell membrane. Polymersomes equipped with ion selective membranes are ideal candidates for the development of cellular ion nano–sensors as well as for the design of nanoreactors in which ionic exchange is required to support *in situ* reactions.

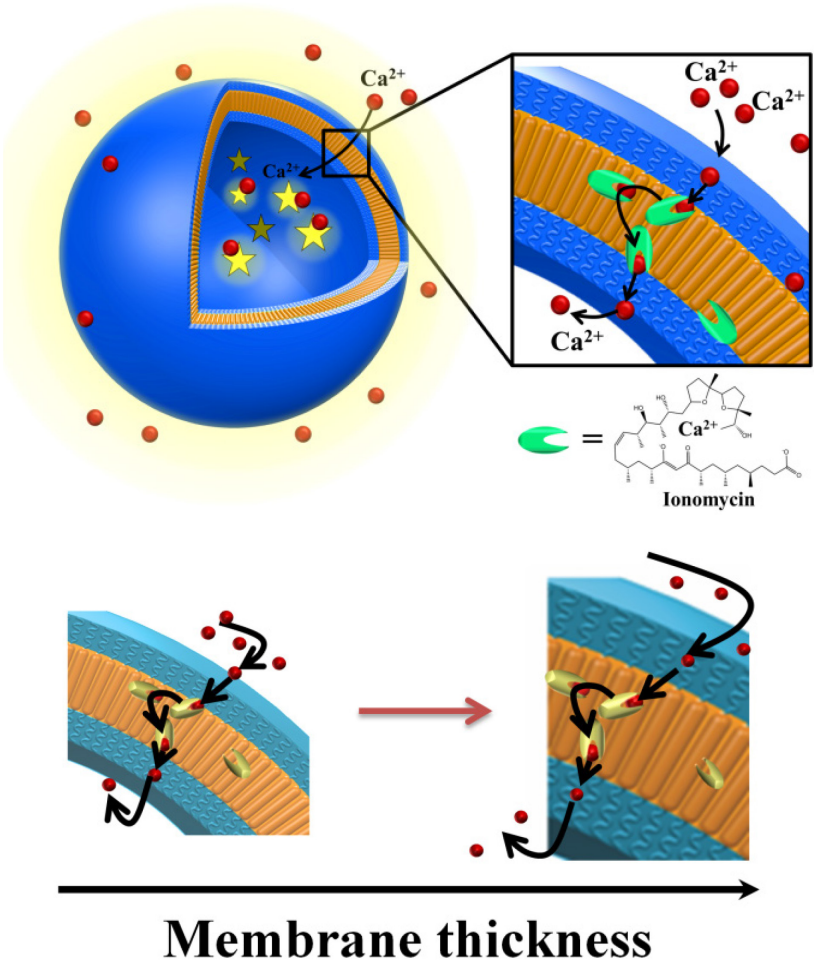

Fig. 26. Design of Ca^{2+} – selective permeable membranes by insertion of ionomycin into polymersomes (up), and by insertion of ionomycin into increasing membrane thicknesses of polymersomes (down).

2. Results and discussion

2.1. Influence of inserted and functional ionomycin pores in polymersomes with a 10.7 nm membrane thickness

The process of generating polymersomes with selective permeable membranes (Polsp) by insertion of biopores has to preserve both the architecture of the polymer vesicles and the function of the biopores which, depending on their function, should span or cross the entire membrane. The membrane permeabilization upon insertion of ionophores results from a selective transport of ions that is mediated by the ionophore through the membrane. In this respect, I selected first $PMOXA_6$–$PDMS_{44}$–$PMOXA_6$ copolymers with a membrane thickness of 10.7 nm (almost twice as thick as a lipid bilayer) [79] and ionomycin, a model ionophore for efficient membrane permeabilization for Ca^{2+} ions.

I combined light scattering (LS) and transmission electron microscopy (TEM) to evaluate the formation of polymersomes using specific conditions aimed at not affecting ionomycin function. I was interested in establishing whether the engineering of Polsp is influenced in terms of polymersomes size, shape and stability by the components of the system: *i.e.* whether the selected Asante Calcium Green (ACG) as a calcium sensitive dye, ionomycin used for polymer membranes permeabilization, or the presence of calcium ions, influences the self–assembly process.

First, 3–D supramolecular assemblies were formed in the presence of ACG. TEM indicated the formation of spherical structures upon encapsulation of ACG, with radii around 100 nm (Figure 27A), and no changes were observed in either shape or size of the 3–D supramolecular assemblies upon addition of 3.74 μM ionomycin (Figure 27B), or 3.74 μM ionomycin and 830 μM $CaCl_2$ (Figure 27C).

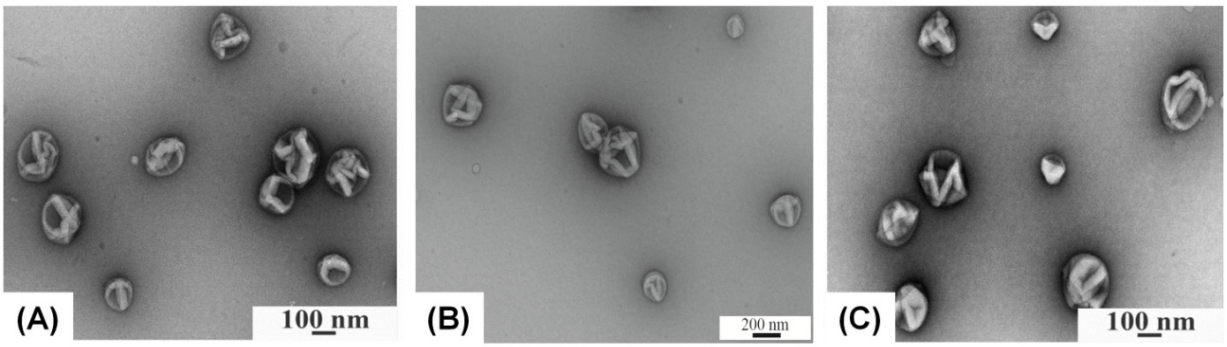

Fig. 27. TEM micrograph of $A_6B_{44}A_6$ polymersomes with encapsulated ACG (A), and in the presence of 3.74 μM ionomycin (B) and 830 μM $CaCl_2$ (C).

To gain further insight, light scattering measurements were used to determine the size, shape and stability of the 3–D supramolecular assemblies that resulted after encapsulation of ACG, in the presence of ionomycin, or/and Ca^{2+} ions. Their hydrodynamic radius (R_h) was determined by dynamic light scattering, whilst the radius of gyration (R_g) was measured by static light scattering (Table 8). The 3–D supramolecular assemblies resulting from encapsulation of ACG, and in the presence of ionomycin or/and Ca^{2+} ions, have radii of gyration around 100 nm, in agreement with the values obtained from TEM micrographs (Table 8, Figure 27). The observation of a monomodal distribution peak with a narrow size distribution indicates that only one population of 3–D supramolecular structures is present in solution. For the 3–D supramolecular assemblies, the structural parameter ρ ($\rho = R_g/R_h$) has values of 0.89 – 0.96, which are close to the value of 1.0 for hollow spheres. Therefore, the 3–D supramolecular assemblies are polymersomes after encapsulation of ACG, and there is no influence on their architecture when ionomycin is inserted into their membranes and/or Ca^{2+} ions are present in their surroundings. Moreover, within the concentration range investigated (see Materials and Methods), there was no significant variation in their radii, indicating that the measurements were in a concentration range which did not induce interactions between polymersomes. The slight increase in $M_{w,agg}$ and N_{agg} by addition of ionomycin confirms the presence of ion-carriers in the self–assembled structures, in agreement with reports indicating that R_h and N_{agg} values of nano-objects are highly dependent on the length and content of the constituent molecules [148, 149] (Table 8). By changing the hydrophobic to hydrophilic ratio of the membrane, a nonlinear increase of N_{agg} has been observed, whilst the size of the vesicles only slightly increased [149],

which is also the case for our polymersomes upon insertion of ionomycin (Table 8). In addition, the insertion of the charged molecules of ionomycin in the hydrophobic domain of the membrane decreased the ζ-potential of polymersomes, and contributed to the increase in the N_{agg} value (Table 8 and 9). The stability of supramolecular assemblies in the presence and in the absence of ionomycin, as well as upon addition of $CaCl_2$, is supported by the very small and slightly negative values of the second virial coefficients ($A_2 \sim 10^{-8}$). Both the low PDI values and the very low values of the second virial coefficient A_2 indicate no fusion of polymersomes, which would result in merger vesicles. Therefore, the change in $M_{w,agg}$ and N_{agg} values is attributed only to the insertion of the ionophore into the vesicle membrane.

Table 8. Molecular parameters of 3-D assemblies of $PMOXA_6$-$PDMS_{44}$-$PMOXA_6$ without and with ionomycin, and in the presence of 830 μM $CaCl_2$.

Size and stability of calcium sensing nanodevices	DLS/SLS*						
	R_g [nm]	R_h [nm]	$\rho = R_g/R_h$	$M_{w,agg}x10^{-8}$ [g/mol] **	$N_{agg}x10^{-4}$**	A_2x10^8 [mol·dm^3/g^2] **	PDI**
$A_6B_{44}A_6$	114.5 ± 2.5#	128.4 ± 13	0.89 ± 0.04	1.82 ± 0.16	4.04 ± 0.16	- 9.44 ± 0.34	0.09 ± 0.02
$A_6B_{44}A_6$ + ionomycin	131.9 ± 3.4	144.7 ± 6.7	0.91 ± 0.03	5.75 ± 0.05	12.77 ± 0.05	- 0.14 ± 0.59	0.12 ± 0.02
$A_6B_{44}A_6$ + ionomycin + $CaCl_2$	116.9 ± 2.0	122.4 ± 4.1	0.96 ± 0.03	4.43 ± 0.05	9.84 ± 0.05	- 0.06 ± 0.26	0.09 ± 0.01

**Dynamic – and static light scattering experiments in dilute polymersome solutions; ** $M_{w,agg}$ – apparent molecular weight, N_{agg} – the average aggregation number, A_2 – second virial coefficient, and PDI – polydispersity index for polymersomes. #± SD, n=3. An example of DLS/SLS raw data has been presented in Appendix A.*

Table 9. Surface (ζ) Potential

Parameters	ACG*	Empty $A_6B_{44}A_6$ polymersomes	$A_6B_{44}A_6$ polymersomes with entrapped ACG	$A_6B_{44}A_6$ polymersomes with entrapped ACG + 3.74 μM Ionomycin	$A_6B_{44}A_6$ polymersomes with entrapped ACG + 3.74 μM Ionomycin + $CaCl_2$
ζ [mV]	- 7.5	5.4	4.6	2.0	2.3
±SD, n=3	1.7	0.3	0.4	0.2	0.3

*Asante Calcium Green;

By dividing the fraction of encapsulated ACG by the initial amount used for encapsulation, we calculated the entrapment efficiency process of ACG as 7.5 %.

It is interesting to study whether it is still able to mediate Ca^{2+} transport when inserted in polymer membranes with double the thickness of lipid membranes. Ionomycin has a diameter of 1.5 nm, as calculated from the crystal structure of the calcium complex [150] (Figure 28).

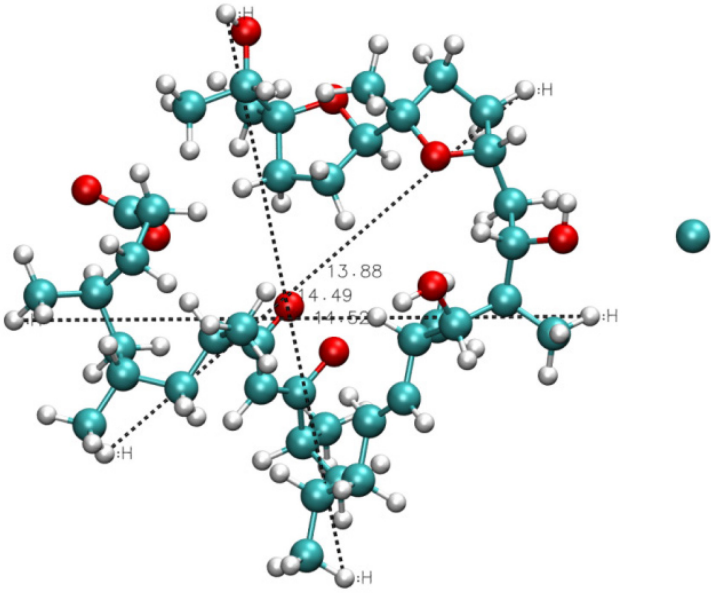

Fig. 28. Size estimation of ionomycin molecule, taking into account the molecule diameter as the largest distance from one end to another.

First, I evaluated the changes in fluorescence intensity of the free ACG, induced by the presence of a $CaCl_2$ solution under similar conditions to those used for assessing ionomycin function in ACG–loaded polymersomes. The fluorescence intensity of ACG was evaluated in the presence of ionomycin, and EtOH was used for ionomycin solubilization. Neither ionomycin nor EtOH had any influence on ACG fluorescence intensity (Figure 29).

Secondly, the change in fluorescence intensity of encapsulated dye was evaluated, both presence and absence of ionomycin, to provide evidence of eventual defects in the polymer membrane (in the absence of ionomycin), and on successful insertion of ionomycin. If ionomycin is inserted into the membrane, Ca^{2+} ions from the environment surrounding the vesicles will penetrate through membrane, resulting in an increase in fluorescence intensity of the encapsulated dye. ACG–loaded polymersomes without ionomycin had low fluorescence intensity in the presence of

830 µM $CaCl_2$ (Figure 30, black curve), and did not change in the presence of EtOH (Figure 30, red curve). The slight increase in fluorescence intensity upon addition of $CaCl_2$ may be due to a small fraction of ACG that was incompletely removed during purification of the ACG–containing polymersomes.

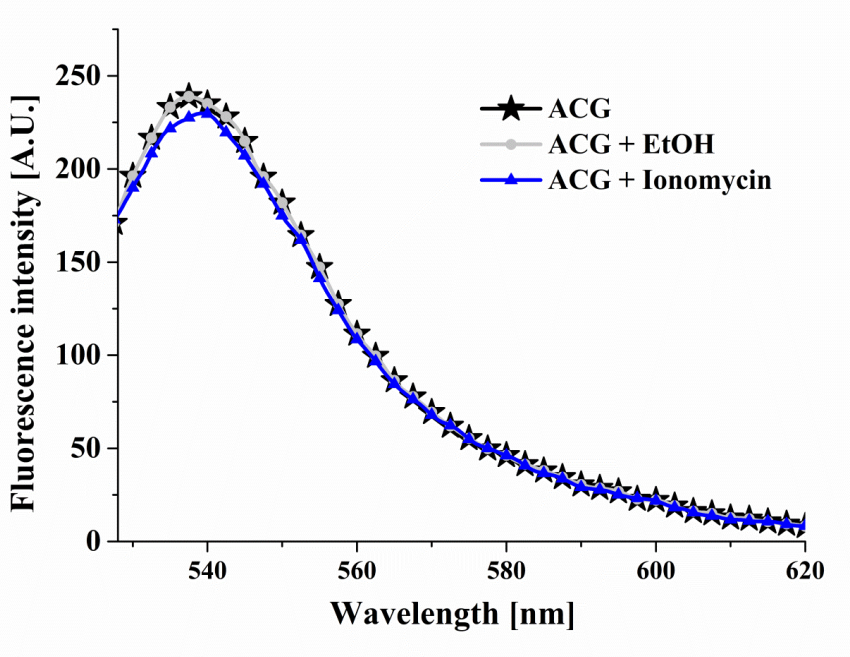

Fig. 29. Influence of EtOH and ionomycin upon fluorescence intensity increase of the free Asante Calcium Green (ACG) solution in the presence of 830 µM $CaCl_2$.

It was only when ionomycin was added that the fluorescence intensity increased significantly. This indicates a calcium influx through the ionomycin (Figure 30, blue curve), and thus demonstrates their proper insertion and function.

The fluorescence intensity of ACG–loaded polymersomes increased with increasing concentration of ionomycin in a range of 117– 3740 nM (in the presence of 830 µM $CaCl_2$), at which the maximum of fluorescence intensity was reached (Figure 31).

For low initial amounts of ionomycin, an insertion efficiency close to 100% was obtained, which slightly decreased upon increasing the amount of ionomycin (for 3.74 µM, the insertion efficiency was of 93%). To calculate the number of ionomycin molecules/polymersome we used a simple model based on uniform distribution of ionomycin molecules inside the membrane of

polymersomes, and neglected the statistical character of the self-assembly process of polymersome formation.

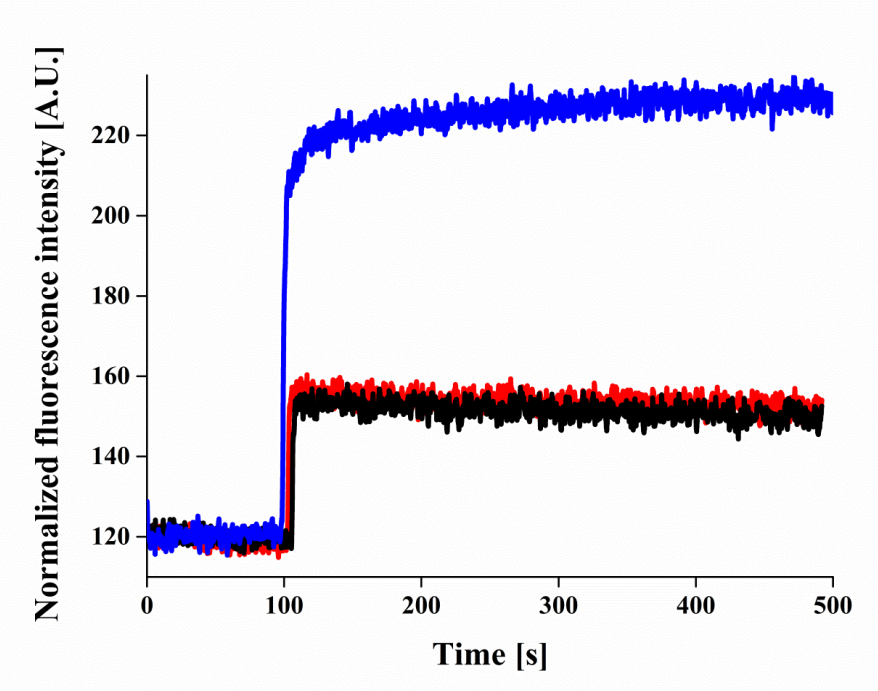

Fig. 30. Ca^{2+} influx through $A_6B_{44}A_6$ polymer membrane. ACG-loaded $A_6B_{44}A_6$ polymersomes (black curve), with EtOH (red curve), at the optimum concentration of 3.74 μM ionomycin (blue curve), in the presence of 830 μM $CaCl_2$

This results in aprox. $9.14 \cdot 10^3$ ionomycin molecules/polymersome for the initial amount of 3.74 μM ionomycin, and $2.28 \cdot 10^{11}$ polymersomes (obtained from light scattering data).

Further increases in ionomycin concentration up to 10.40 μM resulted in a lower increase in the fluorescence intensity of the encapsulated ACG. This indicates that a high amount of ionomycin influences the transport of Ca^{2+} ions through the polymersome membrane by nonspecific attachment of ionomycin molecules on its external surface or by formation of 1:2 Ca-ionomycin complexes (Figure 31). Only 80% of the initial ionomycin amount (10.4 μM) was inserted in polymersome membrane (Figure 32). At higher initial concentration of ionomycin (15 μM) a significant fraction of polymersomes did not preserve their architecture (Figure 31), resulting in leakage of the entrapped dye, as observed by the very high fluorescence intensity (Figure 31).

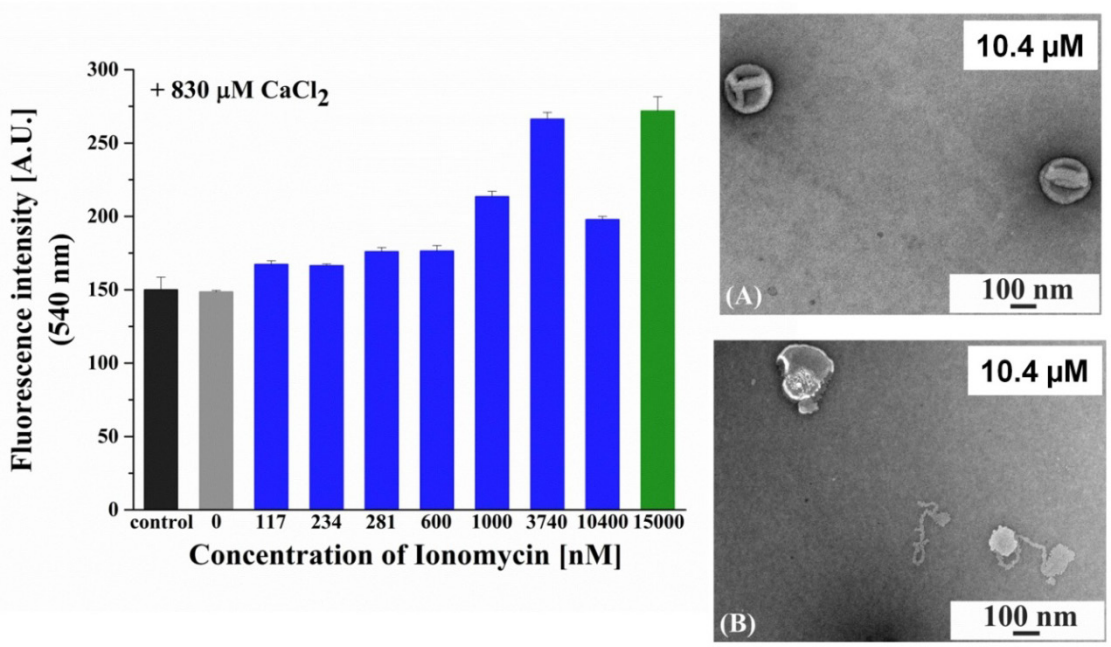

Fig. 31. Influence of ionomycin concentration on membrane permeabilization of $A_6B_{44}A_6$ polymersomes. The concentration of $CaCl_2$ was maintained constant at 830 µM for ACG loaded $A_6B_{44}A_6$ polymersomes (black bar), in the presence of ethanol (grey bar) and increasing concentrations of ionomycin (blue and green bars). Error bars are shown as standard deviations of three individual measurements. Ionomycin insertion in polymersome membrane, given as percentage. TEM micrograph of ACG loaded polymersomes of $A_6B_{44}A_6$ in the presence of 10.4 µM (A) and 15 µM ionomycin (B).

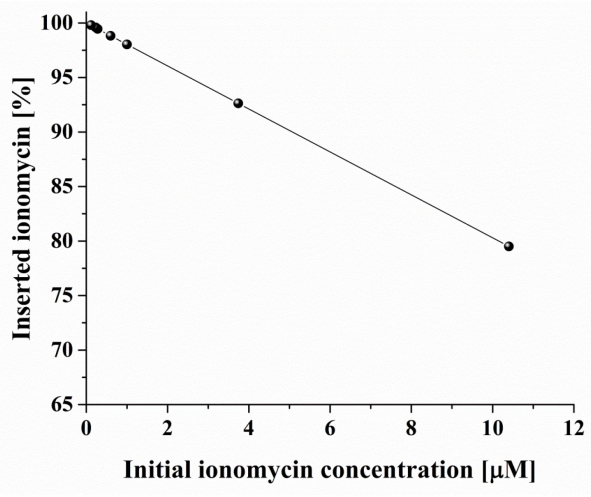

Fig. 32. Ionomycin insertion in polymersome membrane, given as percentage.

To obtain insights into the the efficiency of calcium influx through the ionomycin ion-carrier in the first short period of time (≤15 s), we used stopped–flow spectroscopy (Figure 33). Ina very simplistic way, in a stopped-flow device, two or more (depending on the configuration of the setup) species (dyes, proteins, cells etc) are injected in a mixing chamber to monitor their interaction kintetics (conformational changes, osmotic changes, bindings, ion influxes through membranes) in real time through the change in the spectrophotometric signal intensity (light scattering, absorbance, fluorescence) [151]. In our case, an increase in the fluorescence intensity of the ACG in polymersomes upon insertion of 3.74 μM ionomycin was observed. Ca^{2+} ions are transported at a fast rate through the functional inserted ionomycin, resulting in an instant Ca^{2+}–selective and permeable polymer membrane. By using a double-exponential equation, stopped-flow data was analysed to take into account both fractions of ACG (encapsulated and attached to the membrane):

$$A(t) = \Delta A_1 \cdot \exp(k_1 \cdot t) + \Delta A_2 \cdot \exp(k_2 \cdot t) + A_\infty \quad (12)$$

where k_1 and k_2 are the observed rate constants for the first and second components of the double–exponential reaction, respectively, and ΔA_1 and ΔA_2, are the corresponding amplitudes for the first and second components of the double–exponential reaction. A_∞ represents the final value of the fluorescence intensity.

The change over time in the intensity of the fluorescence signal upon mixing the ACG-containing polymersomes with $CaCl_2$ solution indicates that there are two kinetic processes taking place. The kinetic parameter of the first exponential term ($k_1 \approx 4\ s^{-1}$) obtained from a sudden increase in fluorescence intensity had similar values for ACG-containing polymersomes, ACG-containing polymersomes upon addition of EtOH, and Polsp (Table 10).
Therefore this parameter describes the interaction of Ca^{2+} ions with ACG molecules attached on the outer surface of the polymersome membrane. The kinetic time constant of the second exponential term (k_2) is ~50 times slower than for ACG-containing polymersomes without ionomycin ($k_2 \approx 0.8\ s^{-1}$) in the presence of $CaCl_2$. When ACG-containing polymersomes were in the presence of ionomycin, k_2 was three times higher ($k_2 = 0.27\ s^{-1}$) in the presence of $CaCl_2$, indicating that transport of Ca^{2+} ions through the membrane occurs as a result of functional insertion of ionomycin. In addition, both the amplitude of the second time rate (ΔA_2), related to

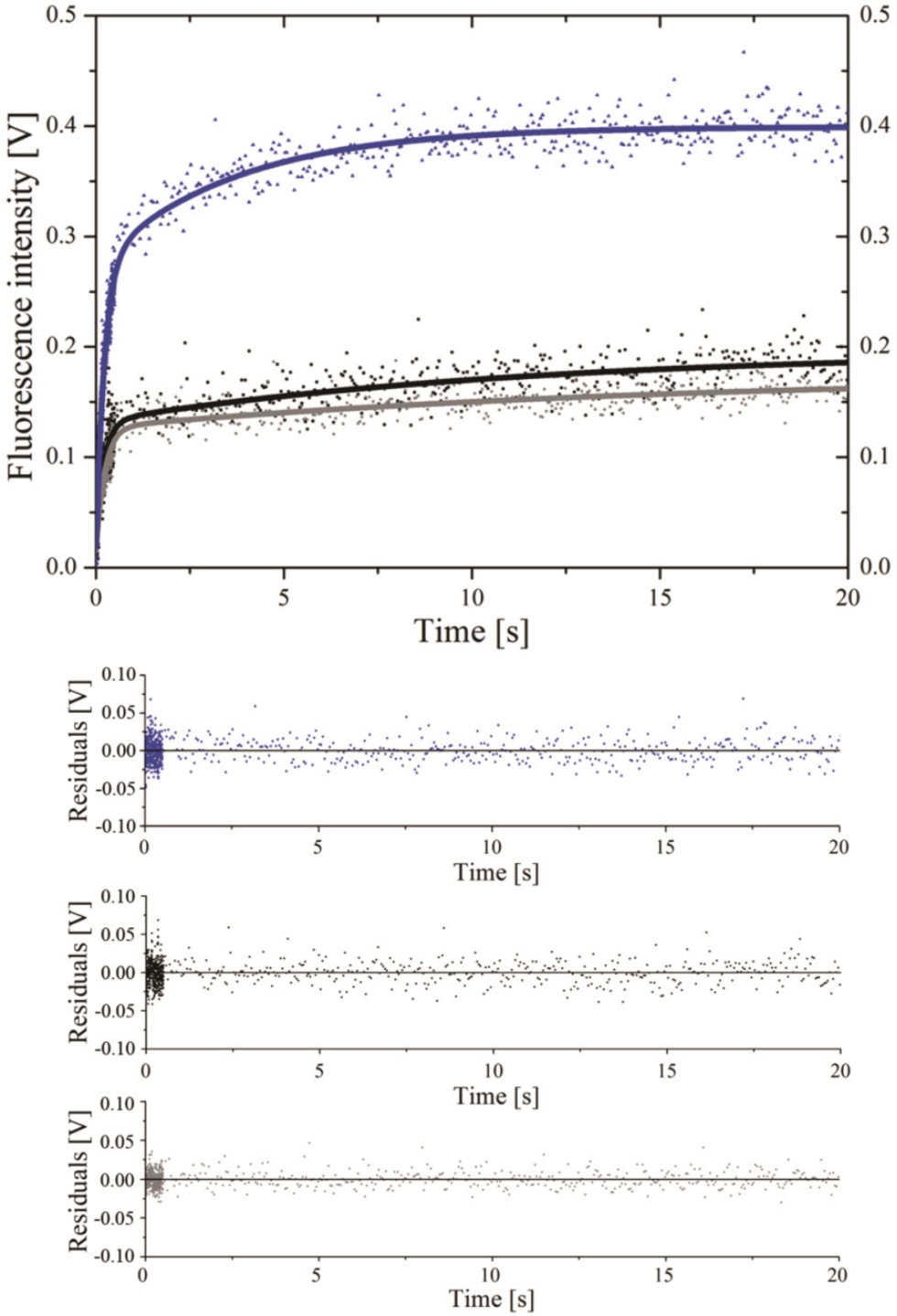

Fig. 33. Fluorescence intensity increase of ACG-loaded $A_6B_{44}A_6$ polymersomes observed by stopped-flow spectroscopy - before (black and grey curves), and after insertion of ionomycin (blue curve). Residuals for fits to a double exponential equation are shown in the lower panel.

the change in the signal intensity of the encapsulated dye, and the amplitude (ΔA_1), related to the dye attached to the membrane, are almost double for the Polsp compared to the ACG-containing polymersomes without ionomycin (Table 10). The higher value of ΔA_2 in the case of Polsp is related to the freely diffusing dye molecules inside the polymersome cavity, which react with Ca^{2+} ions that diffuse through the ionomycin. The difference in ΔA_1 values between Polsp and ACG-containing polymersomes, indicates that ACG is also attached to the inner surface of the membrane, as expected due to the symmetric character of membrane formation by the self-assembly process.

Overall, the stopped-flow parameters indicate a selective permeabilization of the membrane by appropriate and functional insertion of ionomycin, and give an insight into the interaction of the selected dye with the polymer membrane.

Table 10. Stopped-flow data analysis. Rate constants (k_1 and k_2) and amplitude changes (ΔA_1 and ΔA_2) were determined from fitting the stopped-flow signal with a double exponential function.

Stopped-flow kinetic parameters	**$A_6B_{44}A_6$ polymersomes with entrapped ACG + $CaCl_2$**	**$A_6B_{44}A_6$ polymersomes with entrapped ACG + EtOH + $CaCl_2$**	**$A_6B_{44}A_6$ polymersomes with entrapped ACG + 3.74 µM Ionomycin + $CaCl_2$**
k_1 [s^{-1}]	4.70	4.35	4.30
k_2 [s^{-1}]	0.09	0.07	0.27
ΔA_1	0.11	0.11	0.26
ΔA_2	0.06	0.05	0.125

The mechanism of permeabilization of the membrane for Ca^{2+} ions upon insertion of ionomycin was further investigated by evaluating diffusion within a very similar triblock copolymer membrane ($A_7B_{49}A_7$) of the fluorescent dye molecule BODIPY, which is similar in size to ionomycin (Figure 34, Table 11). The analysis of the diffusion by z-scan FCS shows that BODIPY has a free-diffusion character ($t_0 = 0$, Figure 34B) as already observed for fluid phase of lipid membranes [79, 152]. This indicates that PMOXA-PDMS-PMOXA triblock copolymer membranes provides a fluid homogenous hydrophobic medium, in which the ionophores are able to freely move. We have recently showed for a library of polymer membranes that the fluidity of such polymersome membranes based on PMOXA-PDMS amphiphilic block copolymers is similar to the fluidity of lipid bilyers [79].

Table 11. Diffusion coefficients of different fluorescent species within polymer and lipid membranes.

Membrane type	Measured species	$M_{w,species}$ [g/mol]	D [μm²/s] (20 °C)
$A_7B_{49}A_7$	SRB-$A_7B_{49}A_7$	5100	1.4 ± 0.1 [79]
	BODIPY 630/650	660	4.7 ± 0.5
POPC	Rhod-PE	1000	12.5 ± 0.5 [79]

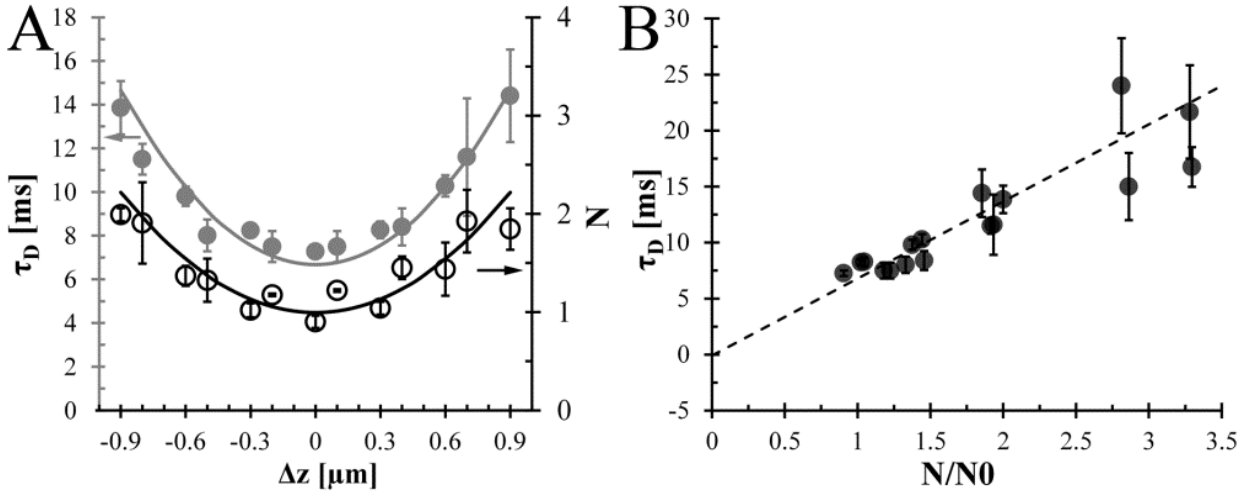

Fig. 34. Diffusion measurements of BODIPY 630/650 within polymersome membrane. A) Z-scan FCS data of BODIPY diffusion within $A_7B_{49}A_7$ membrane. B) Z-scan FCS law showing the free-diffusion character of small hydrophobic molecules.

Additionally, FCS was used to investigate why a slight increase in ACG fluorescence intensity appears in ACG-containing polymersomes without ionomycin after purification by size exclusion chromatography (Figure 35). The short diffusion time of free-diffusing ACG in HEPES buffer ($\tau_{d,ACG}$ = 40 μs) is typical for small molecular mass fluorescent dyes. Interaction of ACG with the polymersome membrane was assessed by adding ACG (20 μM) to empty polymersomes, which initially showed no fluorescence signal. After overnight incubation, the autocorrelation function of the fluorescence signal could be fitted with a bimodal model, which indicates the presence of two different populations of diffusing particles in the solution: a fraction of free ACG, and a second population with a significantly slower diffusion time ($\tau_{d,vesicle} \approx$ 7000 μs). As the second population has diffusion time characteristic of polymersomes

with hydrodynamic radii of 50–100 nm [127], this fraction represents polymersomes to which ACG is attached by nonspecific binding.

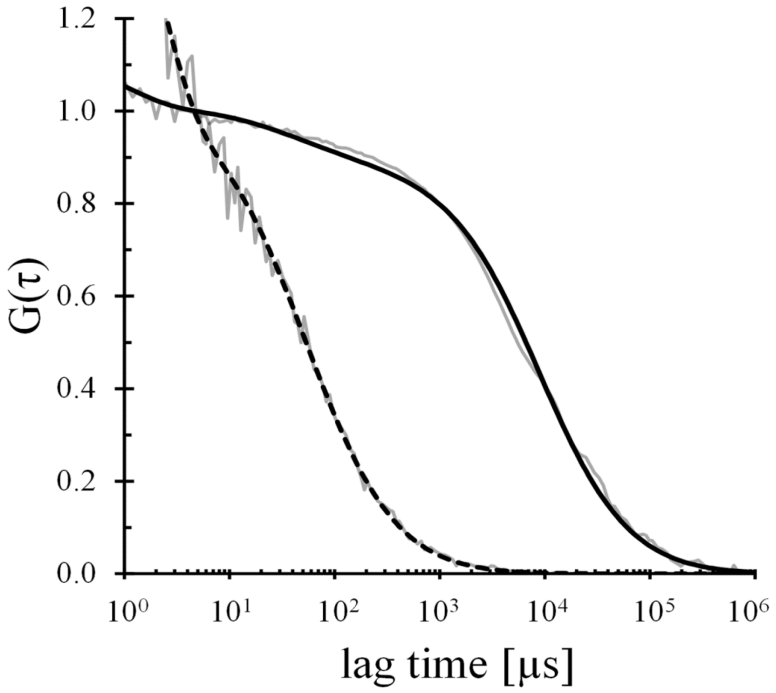

Fig. 35. FCS measurements of ACG interaction with polymersomes. Polymersomes were prepared in absence of ACG. Then ACG was added (20 µM) outside to the polymersomes. After overnight incubation, the diffusion time showed a strong shift to larger particles (polymersome fraction). 90 % of ACG was interacting with the polymersome membrane (high diffusion time – slow diffusing fraction – solid line), while only 10 % of the ACG remained in the solution (fast diffusion time – fast diffusing fraction – dotted line).

To gain more details about the nonspecific interaction of ACG with polymersomes membrane, we formed GUVs with entrapped ACG, and visualized them by confocal laser scanning microscopy (CLSM). CLSM micrographs (Figure 36, left) revealed GUVs containing free ACG molecules in the intravesicular volume. Upon increasing the laser intensity, the encapsulated dye was bleached, and the fluorescence intensity of the GUV membrane clearly indicates that the dye is interacting with the membrane (Figure 36, right). This behaviour was unexpected, due to the hydrophilic nature of ACG, and explains the slight increase of the fluorescence intensity of ACG-containing polymersomes upon addition of $CaCl_2$ (Figure 30, black curve).

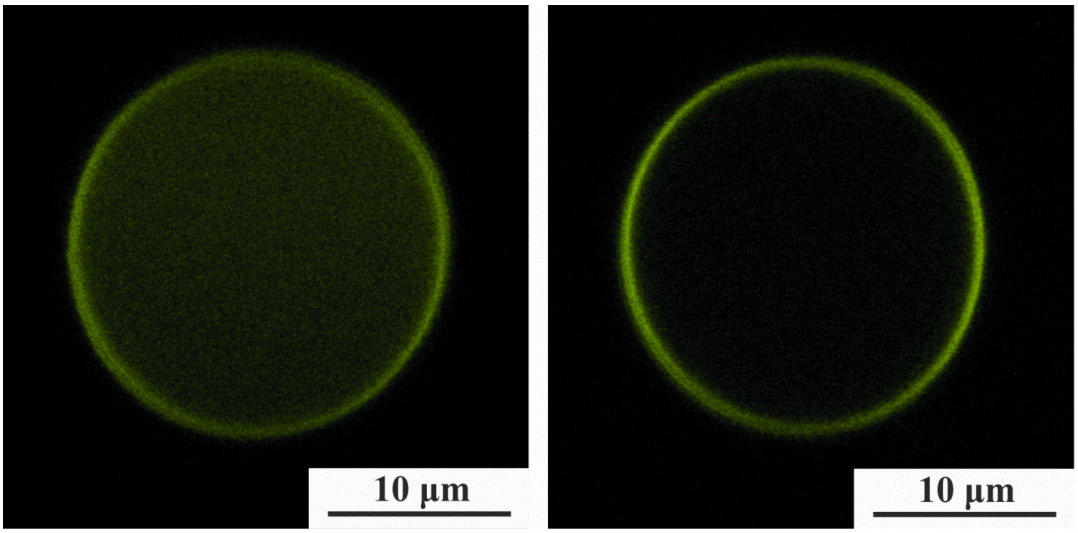

Fig. 36. CLSM micrographs showing ACG interaction with $A_6B_{44}A_6$ GUVs membrane. Left: before bleaching. ACG shows fluorescence inside the vesicle, while outside of the vesicle the ACG concentration is reduced due to dilution of the GUVs into the buffer. Right: After bleaching. The polymeric membrane stays fluorescent, while the free ACG encapsulated in the GUV is bleached. This shows that ACG interacts strongly with the membrane having therefore a strong fluorescence signal emitted from the membrane.

Studies of ionomycin in model liposome membranes revealed a Ca^{2+} permeabilisation of the membrane by formation of Ca-ionomycin complexes, and transport through the membrane [143, 153]. Interestingly, calcium transport through polymersome membranes, which are twice thicker than lipid membranes (10.7 nm thickness), was successful upon insertion of ionomycin, resulting from the appropriate fluid environment of the membrane [79].

2.2 Influence of inserted and functional ionomycin pores in polymersomes with membranes thicker than 10.7 nm

Having permeabilized the membrane of $PMOXA_6$–$PDMS_{44}$–$PMOXA_6$ ($A_6B_{44}A_6$), which has a 10.7 nm thickness, by successful insertion of ionomicin, our interest was to investigate whether increasing the membrane thickness leads to a blocking of Ca^{2+} transport. To do this, two other PMOXA-PDMS triblock block-copolymers were used: $PMOXA_7$–$PDMS_{49}$–$PMOXA_7$ ($A_7B_{49}A_7$) and $PMOXA_{12}$–$PDMS_{63}$–$PMOXA_{12}$ ($A_{12}B_{63}A_{12}$), which self-assemble in aqueous solution into polymersomes with membrane thicknesses of 12.1 and 13.4 nm, respectively [4].
Membrane permeabilization for Ca^{2+} ions was assessed using the conditions optimized for the $A_6B_{44}A_6$ polymer.Using a combination of TEM and light scattering, we evaluated: (i) the self-assembly process of the triblock copolymers in the presence of a Ca^{2+} sensitive dye (ACG), (ii) the integrity of polymersomes upon insertion of ionomycin into the polymer membrane, and (iii) the permeability of polymer membranes in the presence of calcium ions. TEM micrographs revealed the formation of spherical structures in the presence of ACG, with radii around 100 nm for both copolymers (Figure 37A, B). Neither the shape nor size of the spherical assemblies was affected by addition of ionomycin (Figure 37C, E), or ionomycin and $CaCl_2$ (Figure 37D, F).
According to the LS analysis, supramolecular structures with R_g around 100 nm, and ρ values ranging from 0.90 up to 0.93, specific for hollow spheres, were formed (Table 12). Both copolymers self-assemble in polymersomes in the presence of ACG, and their final architecture is preserved upon insertion of ionomycin (3.74 μM), and addition of Ca^{2+} ions (830 μM).

Table 12. Size and stability of 3D assemblies of copolymers with ionomycin, and in the presence of $CaCl_2$

Size and stability of calcium sensing polymersomes	**DLS/SLS**		
	R_g [nm]	**R_h [nm]**	**$\rho = R_g/R_h$**
$A_7B_{49}A_7$ (ACG)	136 ± 3.6 [#]	151 ± 2.0	0.90 ± 0.02
$A_7B_{49}A_7$ (ACG) + ionomycin	127 ± 4.0	139 ± 5.0	0.92 ± 0.01
$A_7B_{49}A_7$ (ACG) + ionomycin + $CaCl_2$	131 ± 1.5	143 ± 2.7	0.91 ± 0.05
$A_{12}B_{63}A_{12}$ (ACG)	136 ± 7.2	152 ± 4.3	0.90 ± 0.01
$A_{12}B_{63}A_{12}$ (ACG) + ionomycin	132 ± 4.1	146 ± 3.0	0.90 ± 0.03
$A_{12}B_{63}A_{12}$ (ACG) + ionomycin + $CaCl_2$	140 ± 2.8	151 ± 2.2	0.93 ± 0.01

[#]*± SD, n=3. An example of DLS/SLS raw data has been presented in Appendix A.*

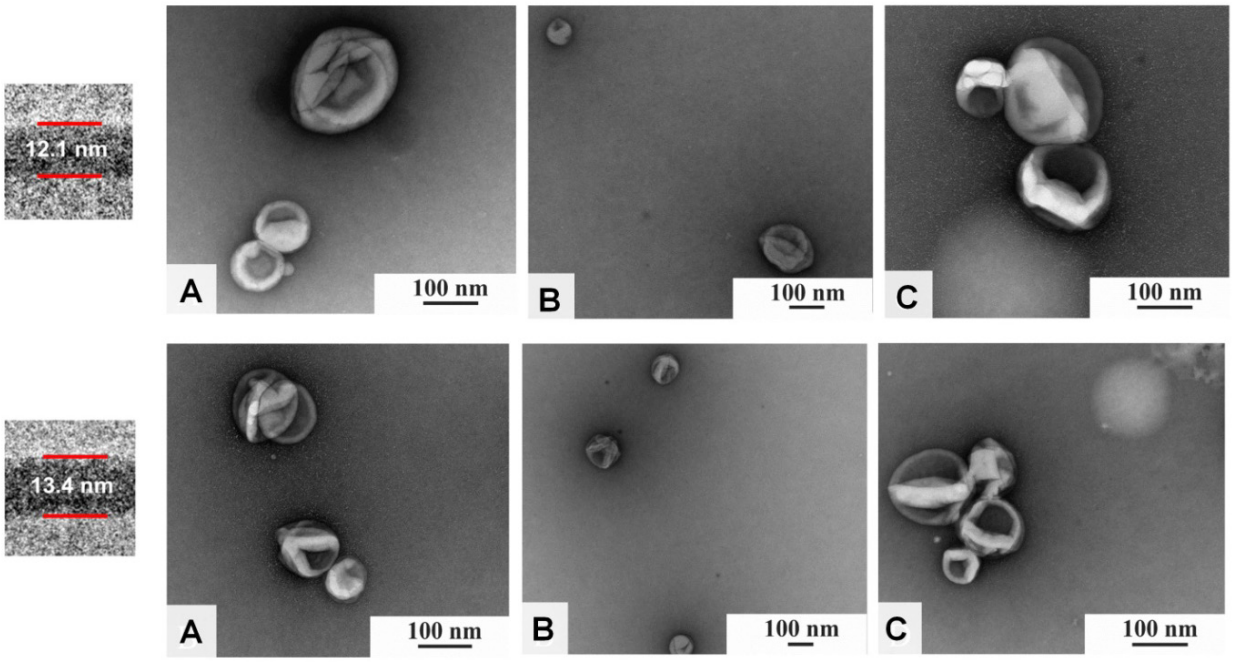

Fig. 37. TEM micrograph of spherical structures of $A_7B_{49}A_7$ (up) and $A_{12}B_{63}A_{12}$ (down): with encapsulated ACG (A), with encapsulated ACG + ionomycin (B), + ionomycin + $CaCl_2$ (C).

The surface (ζ) potential of empty polymersomes was slightly negative (around -2.0 mV) (Table 13), and was not influenced by encapsulation of the dye. More pronounced negative values (in the range -5.0 to -7.0 mV) were obtained in the presence of ionomycin due to its negatively charged carboxylic acid groups, and observation of such a change indicates successful insertion of the ionophore in the synthetic membrane. The presence of Ca^{2+} had no influence on the ζ - potential of polymersomes with inserted ionomycin.

We reported that a fluid homogenous hydrophobic medium is essential for supporting ionomycin movement in a membrane with 10.7 nm thickness [114]. Using the same approach, we evaluated the diffusion of the fluorescent dye molecule BODIPY (similar in size to the non-fluorescent ionomycin) within the $A_7B_{49}A_7$ (12.1 nm thickness) and $A_{12}B_{63}A_{12}$ (13.4 nm thickness) membranes, and determined the diffusion of BODIPY by z-scan FCS in membranes GUVs. The diffusion of BODIPY in the $A_{12}B_{63}A_{12}$ membrane was slightly lower than in the $A_7B_{49}A_7$ membrane (4.4 compared with 4.7 $\mu m^2/s$), but these values indicate that dye diffusion inside the hydrophobic domain, which is of crucial importance for a selective ions permeabilisation of synthetic membranes, was not blocked in the thicker membrane.

Table 13. Surface (ζ) Potential

Samples	ζ [mV] ±SD, n=3
Empty $A_7B_{49}A_7$ polymersomes	-1.7 ± 4.1
$A_7B_{49}A_7$ polymersomes with entrapped ACG	-1.9 ± 1.2
$A_7B_{49}A_7$ polymersomes with entrapped ACG + 3.74 µM ionomycin	-5.2 ± 1.3
$A_7B_{49}A_7$ polymersomes with entrapped ACG + 3.74 µM ionomycin + $CaCl_2$	-5.3 ± 3.5
Empty $A_{12}B_{63}A_{12}$ polymersomes	-2.5 ± 0.9
$A_{12}B_{63}A_{12}$ polymersomes with entrapped ACG	-3.9 ± 2.4
$A_{12}B_{63}A_{12}$ polymersomes with entrapped ACG + 3.74 µM ionomycin	-7.1 ± 2.0
$A_{12}B_{63}A_{12}$ polymersomes with entrapped ACG + 3.74 µM ionomycin + $CaCl_2$	-7.9 ± 1.2

Moreover, the polymer chains in the $A_{12}B_{63}A_{12}$ membrane had similar diffusion character (Figure 38) to the $A_7B_{49}A_{17}$ and $A_6B_{44}A_6$ membranes (1.02 ± 0.04, 1.41 ± 0.04, and 1.89 ± 0.17, respectively) [79]. The slight decrease in diffusion coefficient values with increasing hydrophobic domain size is expected to slightly influence the diffusion of small molecules. As a membrane thickness up to 13.4 nm did not block ionophore movement, we expected that its function of transporting Ca^{2+} across the membrane would not be blocked.

The function of ionomycin was tested in all ACG - loaded polymersomes by stopped - flow spectroscopy. In the absence of ionomycin, all polymersomes had low fluorescence intensity in the presence of 830 µM $CaCl_2$ (Figure 39, left, black curve). The presence of EtOH, the solubilizing agent for the ionophore, did not influence the fluorescence intensity of the encapsulated dye, which thus indicating that it did not affect the membrane (Figure 39, left, red curve). The fluorescence intensity increased significantly when ionomycin (3.74 uM) was added, indicating a transport of Ca^{2+} through the membrane by its successful insertion and function (Figure 39, left, blue curve).

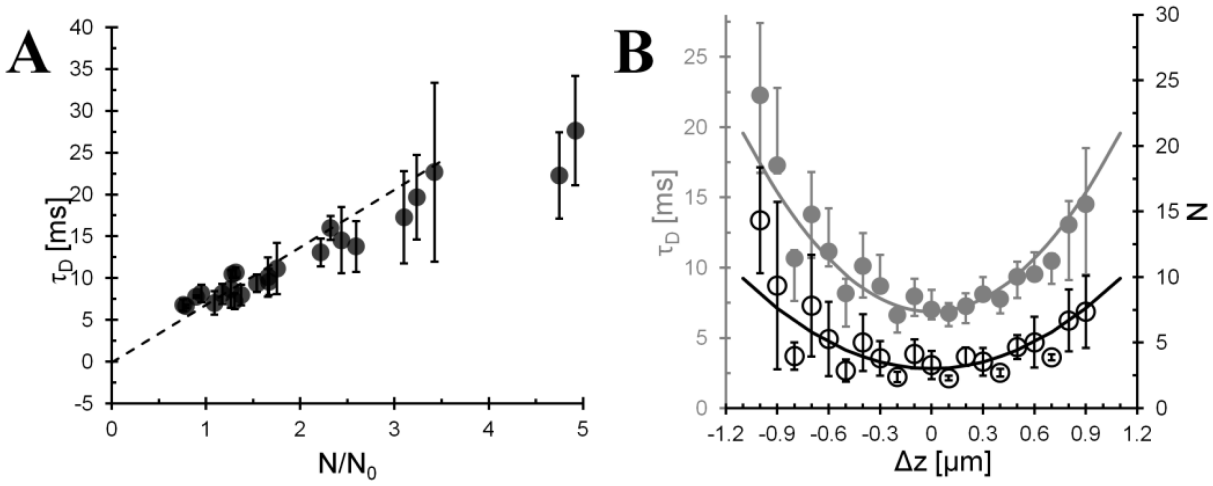

Fig. 38. Diffusion measurements of BODIPY 630/650 within $A_{12}B_{63}A_{12}$ polymersome membranes. A) Typical Z-scan FCS data of BODIPY diffusion within the membrane; B) Z-scan FCS law, showing the free-diffusion character of small hydrophobic molecules.

Additional fluorescence spectroscopy data indicated an increase in the fluorescence intensity of the ACG in polymersomes upon membrane permeabilization with ionomycin (3.74 μM) for both 12.1 (Figure 39, A, right) and 13.4 nm thicknesses (Figure 39, A, right). In the case of the previously tested $A_6B_{44}A_6$ membrane, we observed that a small fraction of the ACG was attached via nonspecific binding, which was suprising because of the hydrophilic nature of the dye. The $A_7B_{49}A_7$ and $A_{12}B_{63}A_{12}$ empty polymersomes incubated with ACG (20 μM) overnight were analysed in a similar manner by FCS, and GUVs-containing ACG visualized by laser scanning microscopy. There was no fluorescence signal in FCS, which indicates a complete removal of the dye, and therefore no nonspecific binding of ACG to the polymersomes membrane. Moreover, measurements of $A_7B_{49}A_7$ and $A_{12}B_{63}A_{12}$ GUVs with entrapped ACG indicated that the dye does not interact with the membrane (Figure 40).

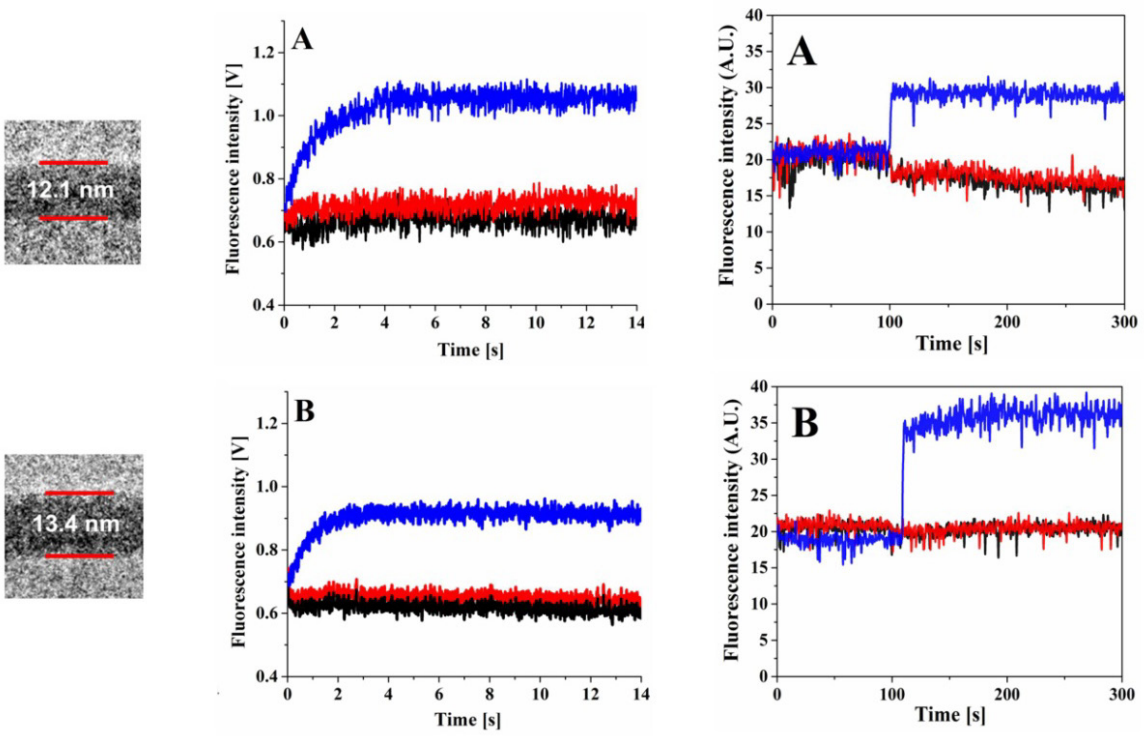

Fig. 39. Ca^{2+} influx through $A_7B_{49}A_7$ (A, left: stopped-flow spectroscopy, right: fluorescence spectroscopy) and $A_{12}B_{63}A_{12}$ (B, left: stopped-flow spectroscopy, right: fluorescence spectroscopy) polymersome membranes. ACG-loaded polymersomes (black curve), with EtOH (red curve), and at the optimum concentration of 3.74 μM ionomycin (blue curve), all in the presence of 830 μM $CaCl_2$.

In case of $A_6B_{44}A_6$, it was necessary to take into account the fact that the dye was both encapsulated and attached to the membrane when analyzing the kinetic parameters obtained by stopped-flow spectroscopy. However, since the dye did not interact with the membrane of $A_7B_{49}A_7$ and $A_{12}B_{63}A_{12}$ polymersomes, the kinetic process was characterized by just the second exponential term (k_2). This was slightly higher for $A_7B_{49}A_7$ than $A_{12}B_{63}A_{12}$ membranes permeabilized with ionomycin (k_2 = 0.12 and 0.11, respectively), but less than half of the $A_6B_{44}A_6$ permeabilized membrane (k_2 = 0.27) [114] (Figure 41).

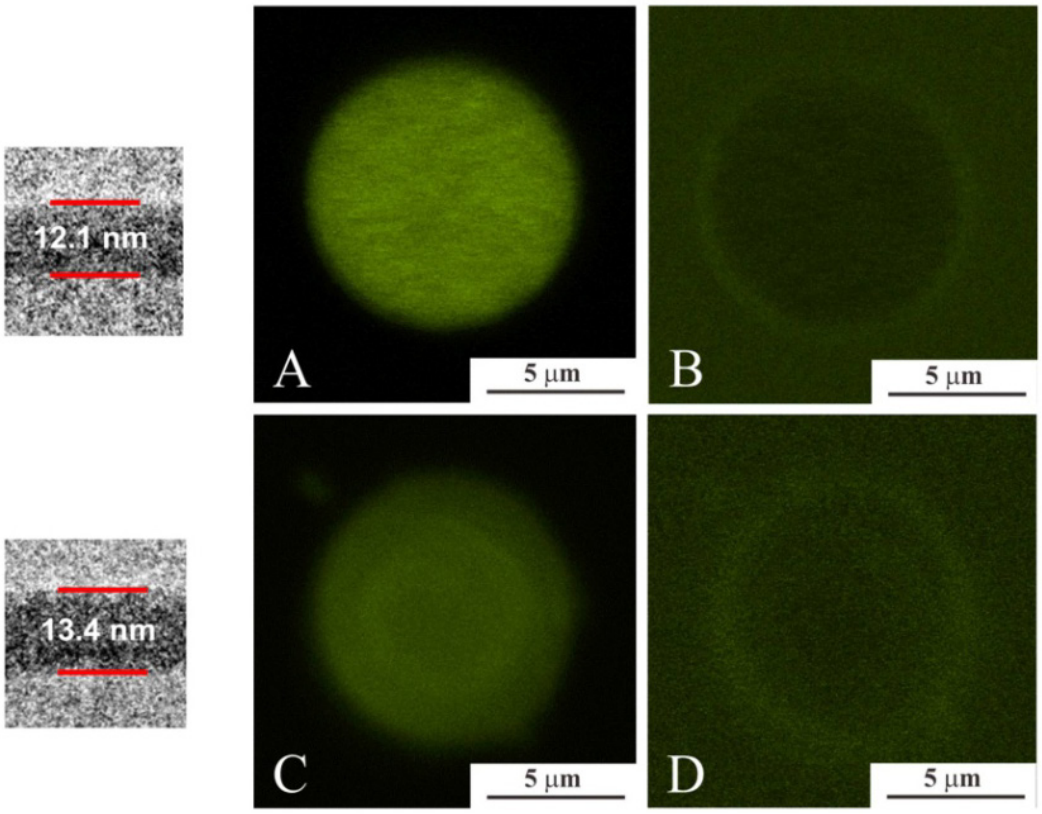

Fig. 40. CLSM micrographs showing ACG interactions with $A_7B_{49}A_7$ (A, B) and $A_{12}B_{63}A_{12}$ (C, D) GUVs membranes. ACG inside $A_7B_{49}A_7$ (A) and $A_{12}B_{63}A_{12}$ GUVs (C) show fluorescence inside the inner cavity, with no fluorescence outside the GUVs, due to a reduced ACG concentration determined by the dilution of the GUVs in buffer. The greenness of the images of $A_7B_{49}A_7$ (B) and $A_{12}B_{63}A_{12}$ (D) after bleaching is because of the necessity of using signal amplification for their visualization. These results demonstrate that ACG has little or no interaction with the membrane, based on a very weak to barely visible fluorescence intensity emitted from the membrane.

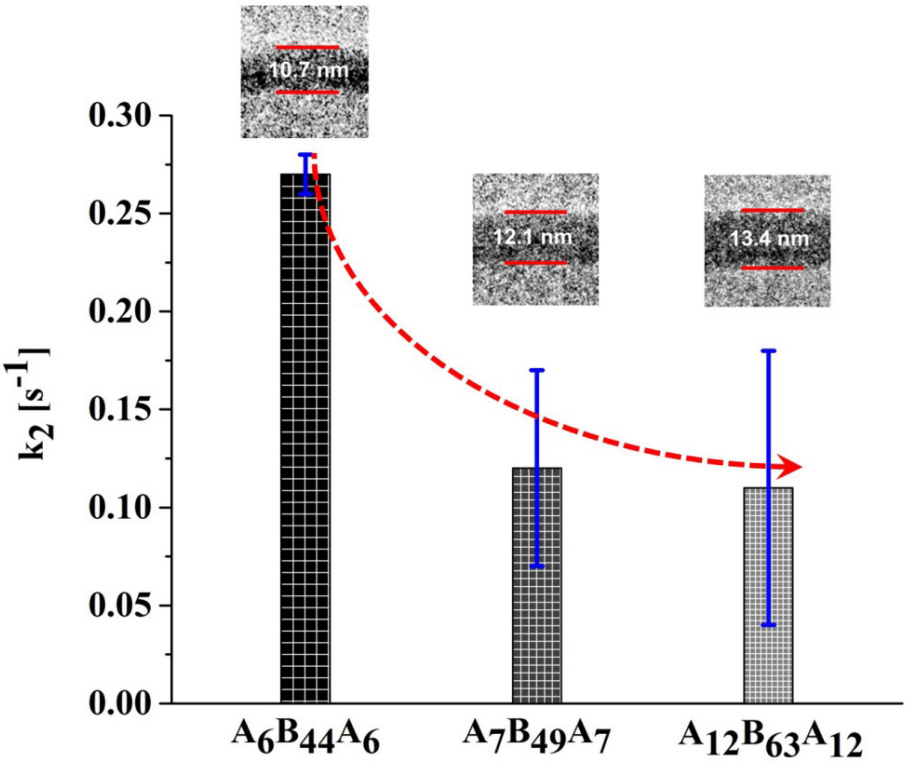

Fig. 41. Kinetic time constants for the second exponential term (k_2) for $A_7B_{49}A_7$ and $A_{12}B_{63}A_{12}$, polymersomes with ionomycin permeabilized membranes, obtained by fitting the stopped-flow signal with a double exponential function. k_2 for $A_6B_{44}A_6$ polymersomes with ionomycin permeabilized membranes is shown for comparison [114]. All $A_xB_yA_x$ polymersomes contained entrapped ACG and mixed with 3.74 μM ionomycin and 830 μM $CaCl_2$.

Thus the transport of Ca^{2+} ions transport across the membrane decreases when the polymer membrane thickness increases, in agreement with the slight differences in the diffusion of BODIPY in the membranes. The correlation of the Ca^{2+} transport with the BODIPY diffusion is in agreement with the diffusion of the polymer chains inside such synthetic membranes [79]. The intrinsic flexibility of the membrane allows both the diffusion of small molecules or ionophores, and the insertion of membrane proteins [75].

3. Conclusions

The viscosity of the hydrophobic domain represents an important factor, which favours the insertion of biopores in synthetic membranes. This has been shown for block copolymers with molecular weights ≤ 2000 g/mol to have similar fluidity to that of natural lipid bilayers. For copolymers with higher molecular weights, chain diffusion was hindered by restricted mobility [79]. However, ion transporters can still move through thick membranes and fulfill their functions as it has been shown for a synthetic membrane with 10.7 nm thickness: ionomycin (with a 1.5 nm diameter) transported Ca^{2+} ions through when inserted in the polymersome membrane made of a 4500 g/mol block copolymer [114]. However, there was no systematic investigation to see whether the ionophores are still able to diffuse through even thicker synthetic membranes, which could affect ionophore function. Whilst channels, biopores or proteins have to adopt a stretched active conformation in order to maintain their function when inserted in membranes with increased thickness [3], ion transporters face the challenge of carrying the ions through a longer hydrophobic path, which might block their diffusion.

The path length for ions through these synthetic membranes was up to 8.9 times higher than the size of the ion-transporter (1.5 nm in diameter), which is a challenging task. Ionomycin was inserted in a membrane with 10.7 nm thickness and preserved its function [114]. The ionophore is still able to perform its function in even thicker membranes (up to 13.4 nm).

The transport of Ca^{2+} ions mediated by the ionophore was not inhibited by the thickness of the membranes, but a decrease was observed, in agreement with the increase in the hydrophobic domain of the membrane. For use in various applications of these synthetic membranes, it is necessary to balance the efficiency of Ca^{2+} transport across the membranes with their mechanic stability, which is related to their thicknesses. Therefore, for applications which require high membrane stability, it is still possible to engineer selective permeability by insertion of ion-transporters, because ion transport is not blocked by thick membranes (up to 13.4 nm).

V. ENZYME REACTION IN CONFINED SPACES AT THE NANOSCALE FOR *IN SITU* GLUCOSE-6-PHOSPHATE PRODUCTION TO ASSIST IN DEFFICIENT RELEVANT METABOLIC PATHWAYS

A publication based on the data discussed in this chapter is in preparation:

M. Lomora, G. Gunkel, S. Mantri, C. G. Palivan, *Enzyme reaction in confined spaces at the nanoscale for in situ glucose-6-phosphate production to assist in deficient relevant metabolic pathways,* **in preparation**.

1. Introduction

Glycolysis (G) and the pentose phosphate pathway (PPP) are two parallel and major metabolic pathways for the generation of energy and formation of nicotinamide adenine dinucleotide phosphate (NADPH). Various significant biological reactions involve NADPH as reducing agent, being an excellent source of electrons for anabolic synthesis of fatty acids, lipids and DNA, important in cellular antioxidation systems, or as substrate for NADPH oxidase that plays key roles in pathological processes by generating reactive oxygen species (ROS) – used for the immune systems to combat infections [154]. In addition, glucose-6-phosphate (G6P) is one of the initiator of G and PPP pathways. In human disorders caused by defects in enzymes, such as phosphoglucomutase, or glucose-6-phosphate dehydrogenase (G6PDH), can lead to glycogen storage diseases [155], manifested by hypoglycemia, glycogen deposition in the liver, growth retardation, hyperuricemia and gout [156].

Altough, there is growing evidence in the association of PGM deficiency towards muscle glycogenosis, a very rare glycolytic disorder designated as glycogenosis type XIV, a consensus for this association and possible treatment options still remains to be established [157, 158]. Glycogenosis type XIV has mainly been characterized by exercise induced intolerance and dissolution of muscle fibres episodes, followed by the release of their contents into the bloodstream (rhabdomyolysis), which might induce health complications, such as kidney failure. An active PGM has not only an important role within the glycolysis and the pentose phosphate pathways in humans, but it is also essential for the synthesis of starch in the chloroplasts of leaves, synthesis of sucrose and cell wall components of plants. Plants take up their nutrients

through the narrow region of soil in direct contact with the root, also known as the rizosphere. This region directly influences plant growth that is mediated through root secretions, associated soil microorganisms, and the activity of accumulated enzymes [159]. It has been shown, for instance, that the lack of PGM activity resulted in a retarded growth in *Arabidopsis* plants [160, 161].

Encapsulation of enzymes in polymeric nanocompartments simultaneously protects them from proteolytic attack and allows them to act *in situ* [162]. Therefore, an elegant manner to engineer sources of G6P is to use nanotechnological systems, which combine active compounds within synthetic compartments to generate nanoreactors and artificial organelles [2, 162, 163]. This chapter contains preliminary experiments that show the production *in situ* of G6P by a nanoreactor containing encapsulated phosphoglucomutase (PGM). The specific substrates and products of PGM can travel through the membrane of the nanoreactor due to its permeabilization by a mixture of engineered α-hemolysin (engineered α-HL), which allows molecules up to 3-4 kDa to pass through, whilst keeping the PGM entrapped inside the inner cavity [164]. PGM reversibly catalyzes production of G6P by isomerization of α-D-glucose-1-phosphate (G1P), using as activators divalent cations (Mg^{2+}) and glucose-1,6-bisphosphate (G1,6-di-PO_4) (Figure 42A). PGM activity has been extensively investigated and the production of G6P is typically detected via an enzyme coupled system, in which G6P is converted to 6-glucose phosphogluconate (6-PG) through the catalytic activity of G6PDH, while reducing nicotinamide adenine dinucleotide phosphate ($NADP^+$) to NADPH, the latter being fluorescent and easy to monitor spectrophotometrically (Figure 42B) [165].

The design and development of a nanoreactor containing encapsulated PGM provides a solution to control the amount and activity of PGM *in situ*, which could lead to the regulation of plant growth which lacks this type of enzyme or as G6P provider for PPP and G pathologies induced by the enzyme mutations or deficiencies.

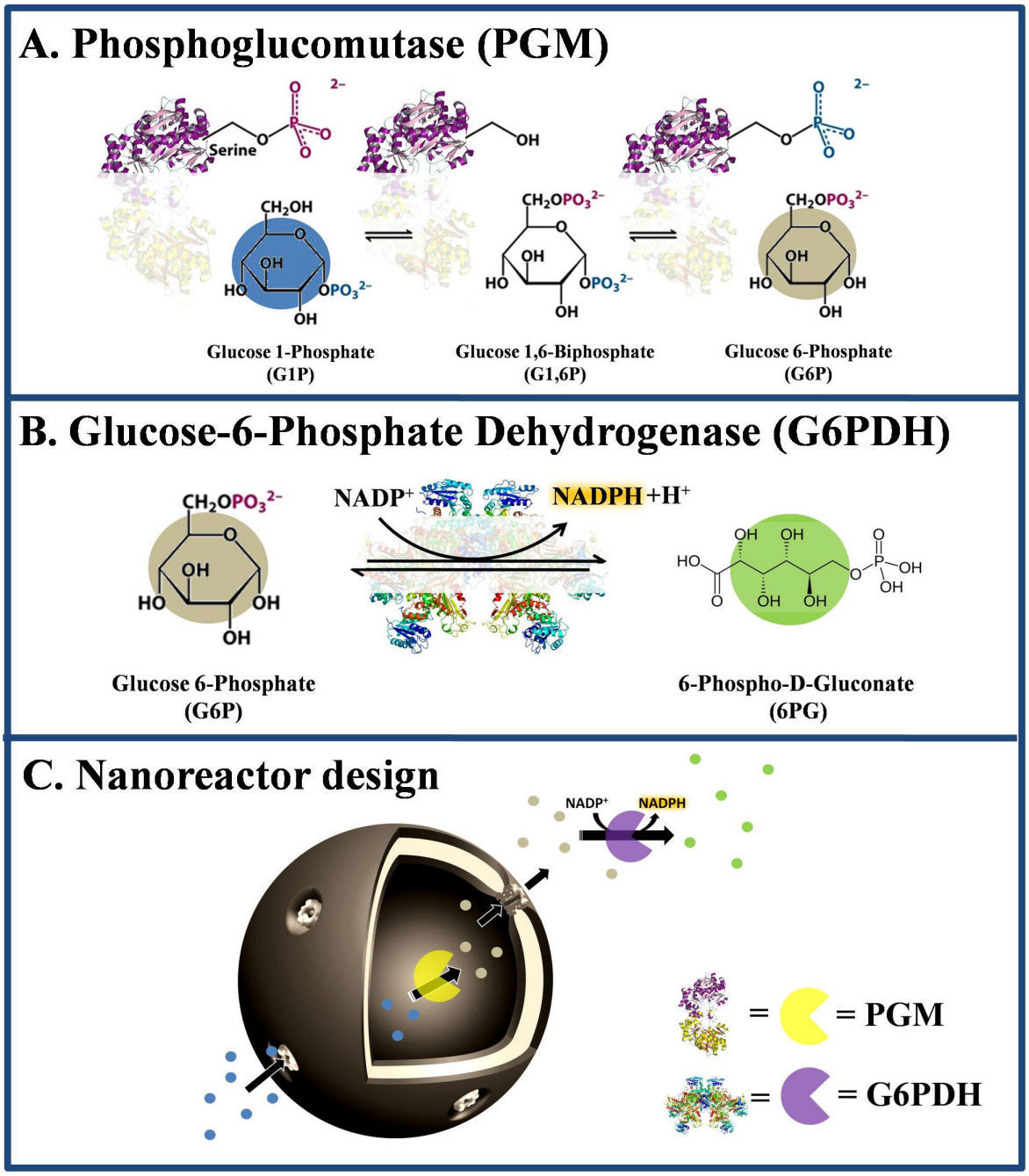

Fig. 42. A. The conversion of glucose 1-phosphate (G1P) to glucose 6-phosphate (G6P) is carried out by an important metabolic enzyme: phosphoglucomutase (PGM). A serine residue of PGM transfers its phosphoryl group to the C-6 hydroxyl group of glucose 1-phosphate. In this way, the glucose 1,6-biphosphate (G1,6-di-PO4) is formed as an intermediary product, with the role to shuttle its C-1 phosphoryl group to the same enzyme serine residue, resulting in the regeneration of PGM and formation of G6P as the final product. The presence of divalent cations

(Mg^{2+}) activators has not been shown for simplicity reasons; **B.** The production of G6P, and thus the PGM enzyme activity, is indirectly monitored through the presence of glucose-6-phosphate dehydrogenase (G6PDH). G6PDH converts G6P to 6-glucose phosphogluconate (6-PG), while reducing nicotinamide adenine dinucleotide phosphate ($NADP^+$) to NADPH, the latter being fluorescent and easy to monitor spectrophotometrically. **C.** Concept design of a polymer nanoreactor (NR), in which PGM (designated in yellow) is encapsulated and protected. The specific G1P substrate (blue solid circle) and products (G1,6-di-PO4 and G1P) of PGM can travel through the membrane of the nanoreactor due its permeabilization by an engineered α-hemolysin (engineered α-HL), which allows molecules up to 3-4 kDa to pass through, whilst keeping the PGM entrapped inside the inner cavity. G1,6-di-PO4 has not been drawn for simplicity reason and because it is an intermediary compounds in the enzymatic reaction, whilst G1P is designated as a solid pale brown circle. Once out of the NR through the engineered α-HL, G6P is converted to 6-PG (solid green circle) through the catalytic activity of G6PDH (purple), while reducing nicotinamide adenine dinucleotide phosphate ($NADP^+$) to fluorescently active NADPH.

2. Results and discussion

2.1. Membrane permeabilization of polymersomes

The design of nanoreactors containing encapsulated enzymes requires that the membrane of polymersome is allowing the passage of necessary substrates and products involved in the chosen enzyme reaction. As polymersome were formed based on the self-assembly of $PMOXA_6$-*b*-$PDMS_{34}$-*b*-$PMOXA_6$ ($A_6B_{34}A_6$), steps to permeabilize their membrane had to be taken. As a biomimetic approach, I chose as a permeabilization route the use of an engineered α-HL, consisting of monomers, dimers, heptamers and heptamer dimers [164].

Prior of using directly polymersomes, liposomes were used as a model system to prove the function of engineered α-HL. Carboxyfluorescein (CF) was entrapped in the inner cavity of liposomes at a quenching concentration (50 mM). To this suspension engineered α-HL was added, as it was known that α-hemolysins easily insert in such type of membranes [166]. The color of the liposome suspension changed from brown to green-yellow in the presence of the engineered α-HL and could be observed with the naked eye, as an indication of dye release and its dilution in the outer environment of liposomes (Figure 43.A).

The formation of liposomes was confirmed via TEM, where vesicular structures were observed with a diameter around 100 nm (Figure 43.B). Addition of 1.35 μg/mL engineered α-HL did not affect the morphology or size of the identified assemblies, confirming that the engineered α-HL is safe to use at this concentration.

As a control, the presence of 6.12×10^{-4} % SDS detergent, present in the solubilization buffer for engineered α-HL, did not induce any dye leakage (Figure 43.C, black curve), this being observed only upon addition of 1.35 μg/mL of engineered α-HL. As a result, we managed to prove that the engineered α-HL is able to successfully insert in the membrane of liposomes and allow the dye to be releaved and increase its fluorescence upon dilution.

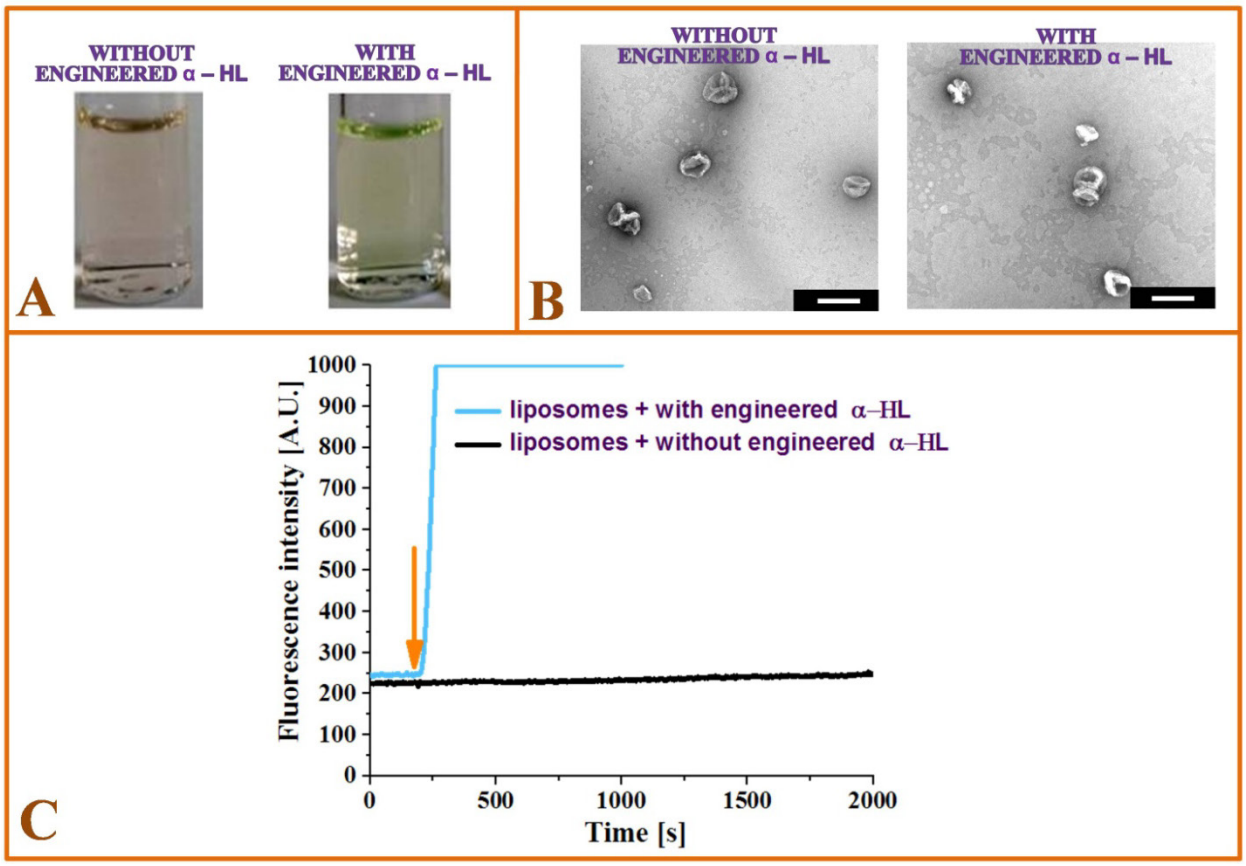

Fig. 43.A. Visible color change in the liposome suspension due to the addition of the engineered α-hemolysin; **B**. Morphology and stability of liposomes with and without engineered α-HL (scale bar: 100 nm); **C**. After the addition of 1.35 µg/mL of engineered α-HL (after around 200 s, as indicated by the orange arrow) dye leakage and increase in fluorescence upon dilution from the liposomes was immediatedly observed (light blue curve). No dye leakage upon addition of SDS detergent only (without engineered α-hemolysin) occurred during 2000 s (black curve).

Using the same conditions for permeabilization as in the case of liposomes, we proceeded to test the insertion of the engineered α-HL for the $A_6B_{34}A_6$ polymersomes containing CF (Figure 44). As in the case of liposomes, TEM revealed vesicular structures with a diameter of around 100-200 nm before and after the addition of the 1.35 µg/mL engineered α-HL. A visible color change from light brown to light green-yellow was observed after addition of the engineered α-HL as for liposomes (Figure 44A).

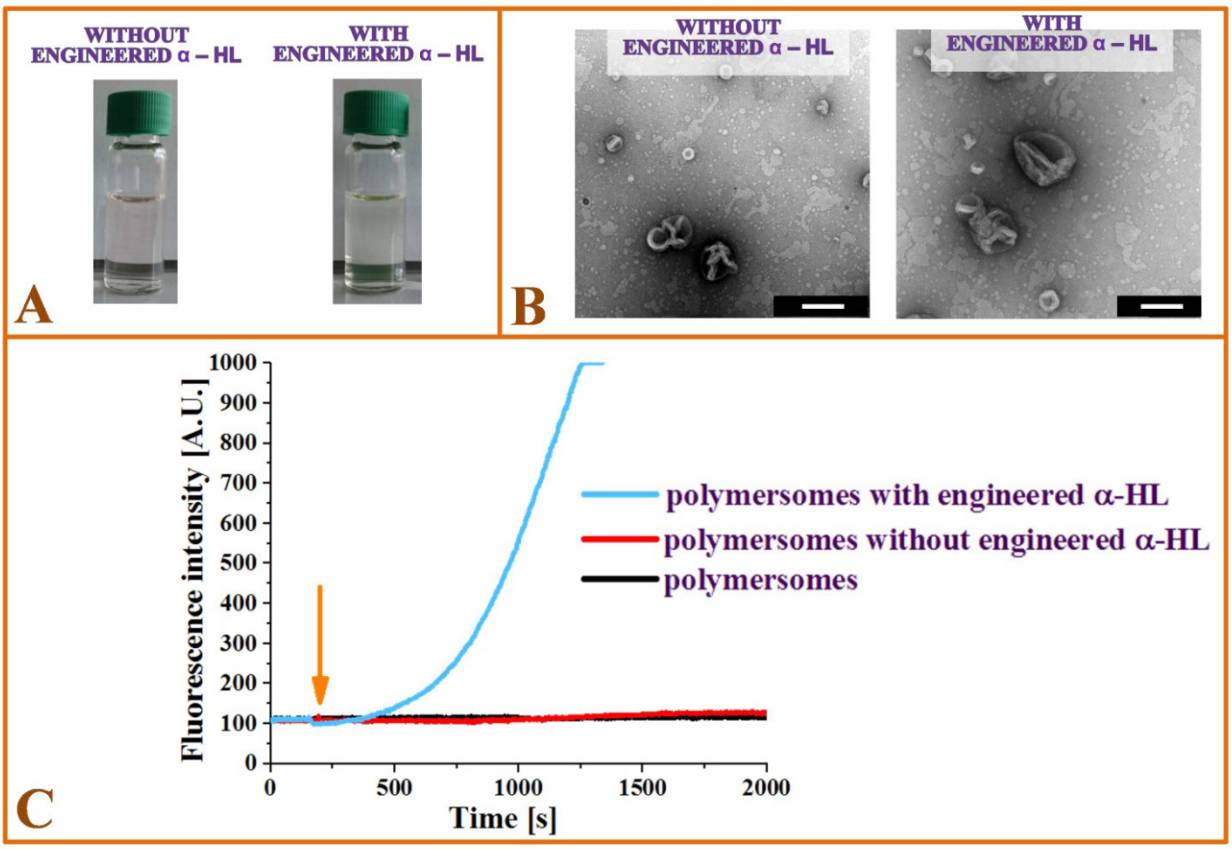

Fig. 44. A. Visible color change in the polymersome suspension due to the addition of the engineered α-hemolysin; **B**. Morphology and stability of polymersomes with and without engineered α-HL (scale bar: 200 nm); **C**. After the addition of 1.35 µg/mL of engineered α-HL (after around 150-200 s, as indicated by the orange arrow), dye leakage and increase in fluorescence upon dilution from the polymersomes was observed after 100-200 s (light blue curve). No dye leakage upon addition of SDS detergent only (without engineered α-hemolysin) occurred during 2000 s. The black curve represents only the polymersomes, without any SDS detergent or engineered α-HL, to identify the initial fluorescence of polymersomes due to the encapsulated dye.

After the addition of 1.35 µg/mL of engineered α-HL (after around 150-200 s, as indicated by the orange arrow), dye leakage and increase in fluorescence upon dilution from the polymersomes was observed after 100-200 s (light blue curve in Fig. 44.C) and not immediatedly as in the case of liposomes. This behavior is expected, because the polymer used self-assemble into polymersomes with a membrane thickness of 9.2 nm [79]. As a consequence, the dye has to travel through an almost double pathlentgh from the inner cavity of polymersomes towards the

extra-vesicular space, as compared with the path of 5 nm (of a typical liposome membrane). In addition, the polymer self-assembly, or the insertion of membrane proteins in a thicker membrane might also impact the final reconstitution process of the membrane proteins. Nevertheless, these results show that the engineered α-HL is able to successfully insert in the membrane of polymersomes as well.

2.2. Influence of increasing concentrations of the engineered α-HL buffer on polymersome integrity

Membrane integrity can be proven by entrapping a dye inside the vesicles, such as polymersomes, at a quenching concentration and then monitoring its spectroscopic properties by dilution upon release [167]. In this case, carboxyfluorescein was encapsulated at a quenching concentration (50 mM) inside $A_6B_{34}A_6$ polymersomes and its release was monitored, which led to an increase in fluorescence intensity [166].

Before testing the influence of the engineered α-HL upon the membrane integrity of the polymersomes, it was essential in identifying whether any dye leakage events occurs in the presence of the engineered α-HL solubilization buffer, containing SDS detergent (Figure 45.A-I). This was necessary, as experimental evidence showed that detergents can solubilize the membrane of polymersomes [168]. Small leakage events of the dye were indeed observed starting with a SDS concentration of $1.26x10^{-3}$ % (v/v) (Figure 45.F and F' inset) with higher influence on the integrity of the polymersome membrane observed upon addition of $2.86x10^{-3}$ % (v/v) SDS (Figure 45.G). The solubilization of the $A_6B_{34}A_6$ polymersome membrane was highest in the presence of $5.91x10^{-3}$ % (v/v) SDS, as a very large amount of CF escaped from the cavity of the vesicles correlated with high fluorescence intensity reaching the limit of the detection (Figure 45.I). Based on these observations, the $6.12x10^{-4}$ % (v/v) concentration of SDS was selected as the safest limit, which does not perturb membrane integrity of polymersomes (Figure 45.E).

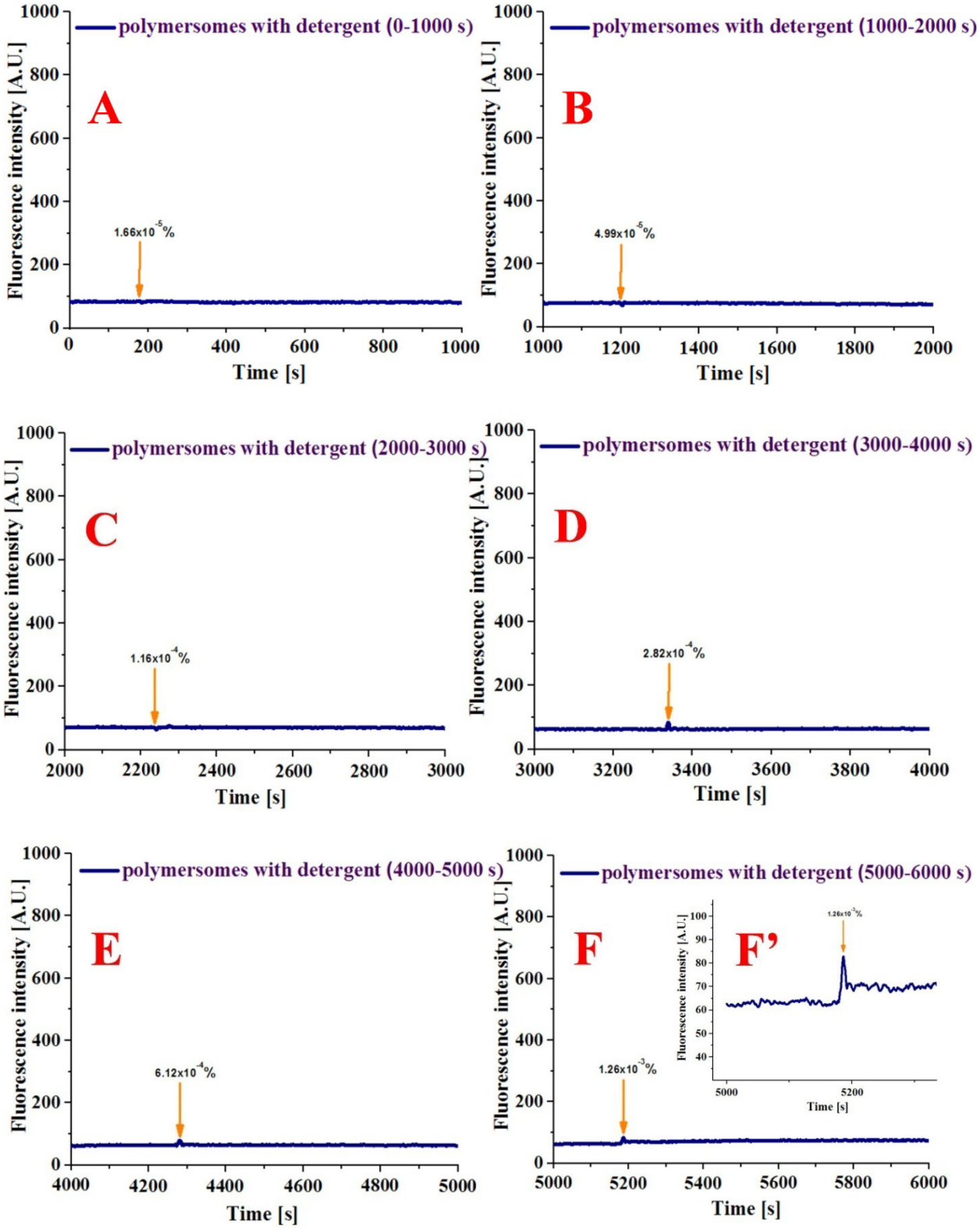
polymersomes with detergent (0-1000 s)
A
1.66x10-5%
Fluorescence intensity [A.U.]
Time [s]
polymersomes with detergent (1000-2000 s)
B
4.99x10-5%
polymersomes with detergent (2000-3000 s)
C
1.16x10-4%
polymersomes with detergent (3000-4000 s)
D
2.82x10-4%
polymersomes with detergent (4000-5000 s)
E
6.12x10-4%
polymersomes with detergent (5000-6000 s)
F
1.26x10-3%
F'
1.26x10-5%

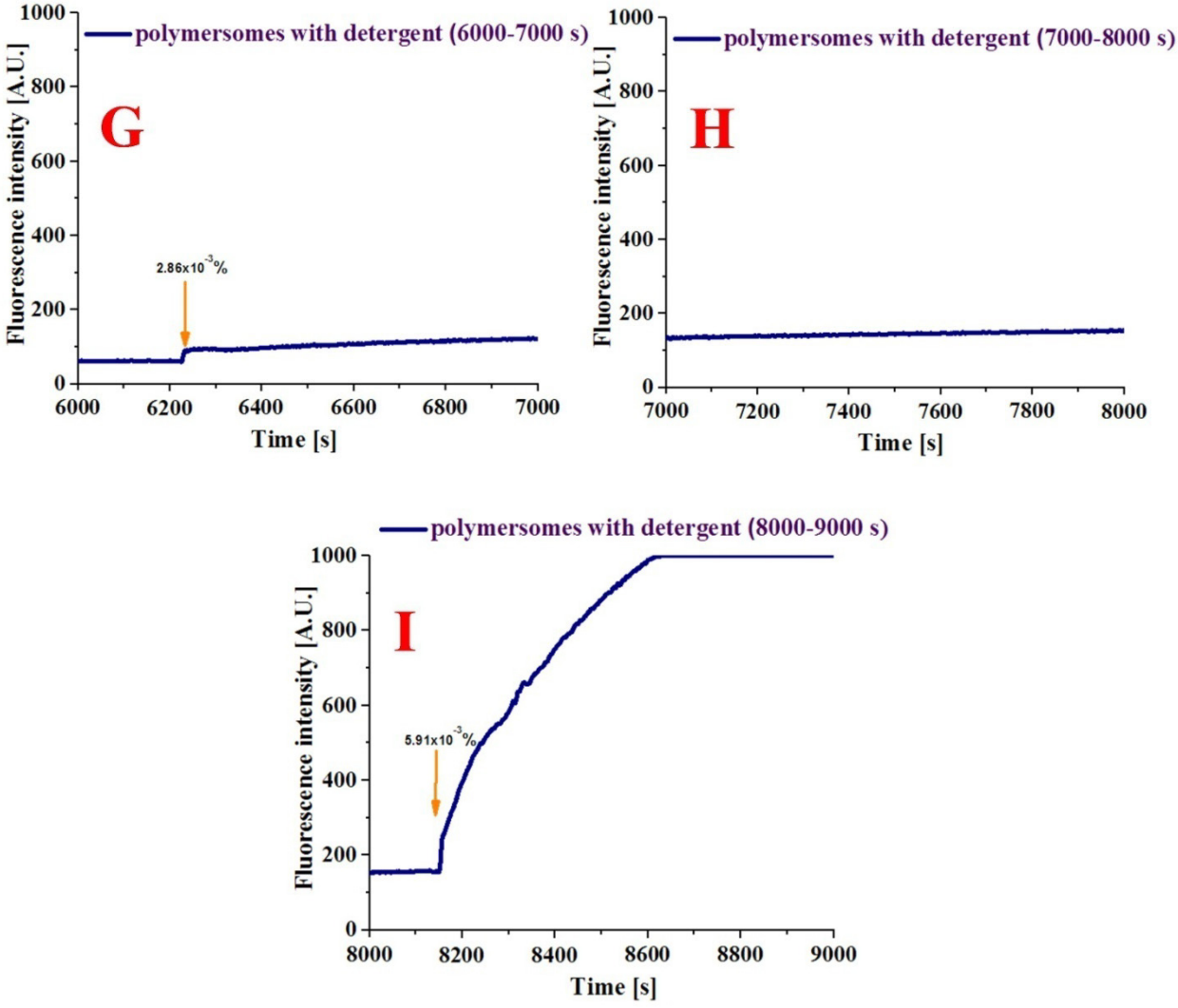

Fig 45. SDS influence at increasing concentrations (%v/v) in the presence of $A_6B_{34}A_6$ polymersomes with encapsulated 6-carboxyfluorescein at a quenching concentration (50 mM). Addition of various increasing concentrations of SDS (indicated by the orange arrow) as follows: $1.66x10^{-5}$ % (**A**), $4.99x10^{-5}$ % (**B**), $1.16x10^{-4}$ % (**C**), $2.82x10^{-4}$ % (**D**), $6.12x10^{-4}$ % (**E**), $1.26x10^{-3}$ % (**F**), $2.86x10^{-3}$ % (**G** and **H**), and $5.91x10^{-3}$ % (**I**), over a period of time of 0-9000 s. The measurement was restarted after each 1000 s, monitoring the release of the dye from the polymersome sample for a total of 2.5 hrs (Figures **A-I**). Inset graph **F'** represents a zoom of graph **F**, for better visualization of the change in fluorescence intensity upon the addition of SDS detergent.

2.3. Morphology, stability, and activity of nanoreactors encapsulating phosphoglucomutase with a membrane permeabilized by engineered α-HL

Enzyme polymer nanoreactors were designed by encapsulating α-phosphoglucomutase (PGM) inside the cavity of the vesicles and add in the extra-vesicular space glucose-6-phosphate dehydrogenase (G6PDH) to produce NADPH starting from α-D-glucose-1-phosphate (G1P).

Prior to PGM encapsulation, the activity of free PGM was monitored by following the production of NADPH as previously described [165]. The enzyme cocktail mixture contained 0.2 U of PGM, 143 mM potassium phosphate: potassium phosphate monobasic (KH_2PO_4) and potassium phosphate dibasic (K_2HPO_4), 0.09 mM ethylenediaminetetraacetic acid (EDTA), $3.6x10^{-4}$ mM G1,6-diPO4, 15 mM $MgCl_2$, 1 U G6PDH, 0.36 mM $NADP^+$, and 33 mM Tris-HCl, pH = 7.50. Over the enzyme cocktail mixture, 0.45 mM G1P (final concentration) was added and the enzymatic reaction was monitored spectrophotometrically. NADPH was produced only when the specific G1P substrate was present in the enzyme cocktail mixture (Figure 46).

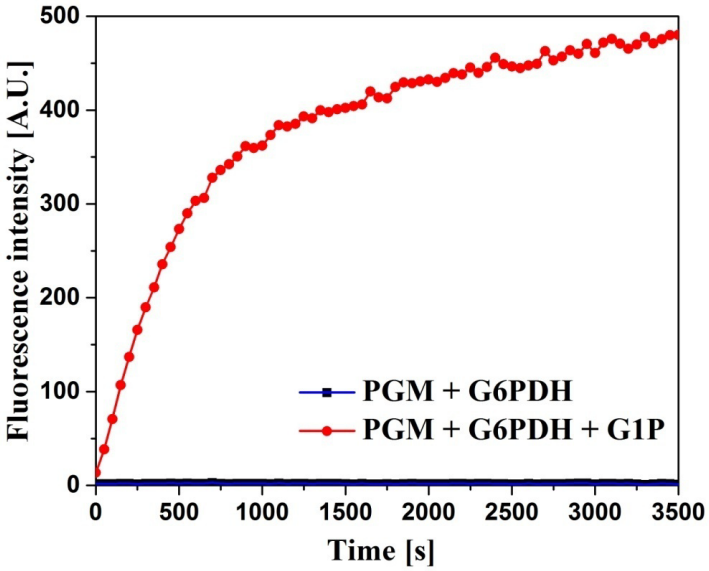

Fig. 46. Free PGM and G6PDH enzymes in solution without G1P substrate (dark blue curve), or with the G1P substrate (red curve).

Nanoreactors were produced by rehydrating over night a $A_6B_{34}A_6$ block copolymer film with the enzyme cocktail mixture, using 10 U of PGM instead of 1 U PGM and in the absence of G6PDH, followed by extrusion with 200 nm pore filters and separation of the nanoreactors from the non-

encapsulated PGM. The permeabilization of the nanoreactors was induced by direct addition of engineered α-HL.

TEM micrographs confirmed formation of spherical structures with a diameter of 100-200 nm in the presence of PGM, therefore this enzyme or the enzyme cocktail mixture used for the self-assembly did not affect the formation of $A_6B_{34}A_6$ nanoreactors, nor the presence of $6.12x10^{-4}$ % SDS or 0.675 µg/mL of engineered α-HL (Figure 47).

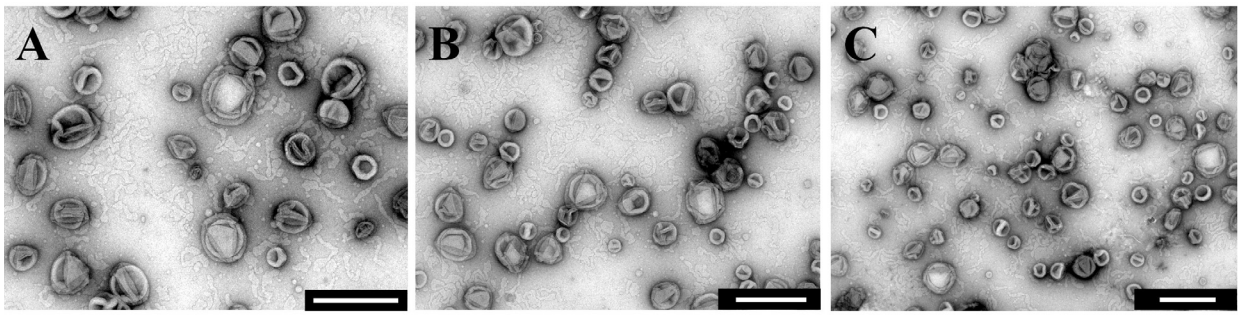

Fig. 47. Representative TEM micrographs depicting $A_6B_{34}A_6$ nanoreactors containing PGM (**A**), $A_6B_{34}A_6$ nanoreactors with PGM and $6.12x10^{-4}$ % SDS detergent (**B**), or in the presence of the 0.675 µg/mL engineered α-HL (**C**). Scale bar: 200 nm.

Additionally, light scattering data confirmed the sizes of the spherical structures observed in TEM with sizes around 160 nm (Table 14). No significant change in the size of the spherical samples was observed in the nanoreactors containing PGM with $6.12x10^{-4}$ % SDS detergent, or with the 0.675 µg/mL engineered α-HL after 1.38 hrs, confirming the stability of the system and offering more confidence in the observed changes in the fluorescence intensity.

Once formed, nanoreactors containing PGM **Table 14.** DLS data of 3D assemblies of $A_6B_{34}A_6$ with the encapsulated enzyme, presence of detergent or engineered α-HL.

Sample	**Diameter [nm]**
$A_6B_{34}A_6$ + PGM	167.2 ± 2.0
$A_6B_{34}A_6$ + PGM + SDS detergent	164.2 ± 1.4
$A_6B_{34}A_6$ + PGM + engineered α-HL	161.0 ± 2.1

were mixed with 1 U G6PDH enzyme and the cascade reaction was monitored via formation of NADPH. In control sample, no change was observed in fluorescence intensity, when G1P was added in the PGM polymer nanoreactors mixture with $6.12x10^{-4}$ % SDS detergent (Figure 48A-E, black curve). The fluorescence kept itself stable for 1.38 hrs, showing that the G1P substrate cannot cross the vesicles membrane and initiate the cascade reaction. When G1P was added to the PGM nanoreactors mixture containing 0.675 µg/mL engineered α-HL, an increase in fluorescence intensity was observed after aproximatedly 300 s, confirming the permeabilization of the nanoreactors membrane, which initiates the entire cascade reaction (Figure 48A-E, cyan curve).

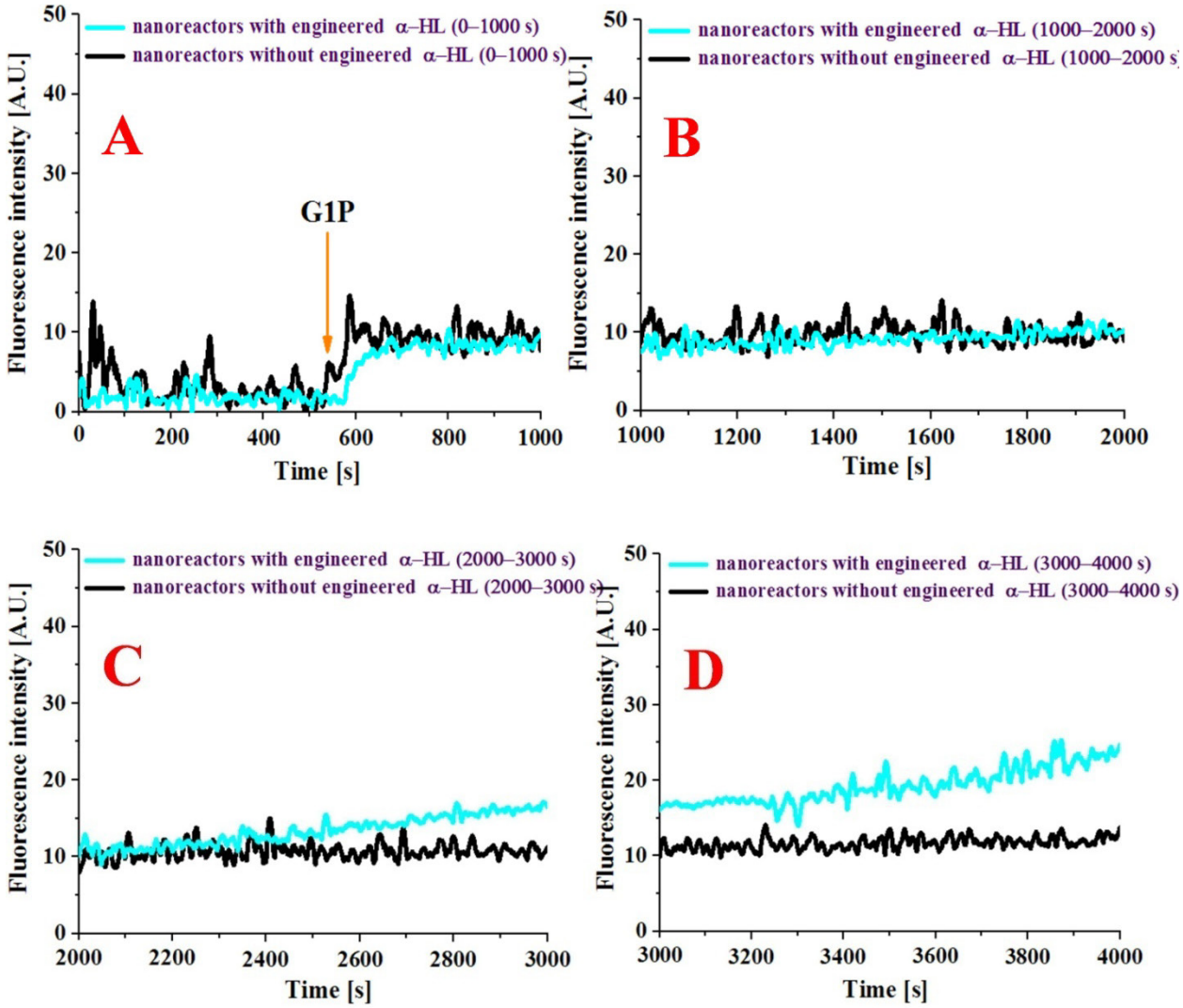

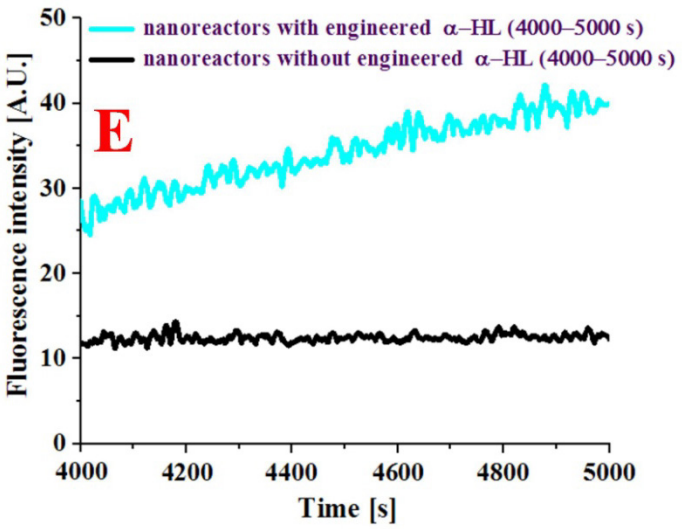

Fig. 48. Nanoreactors containing PGM in the presence of 6.12×10^{-4} % SDS (black curve) or 0.675 µg/mL of engineered α-HL (cyan curve) over a time period of 0-5000 s (**A-E**). Measurement was restarted after each 1000 s, monitoring the formation of NAPDH based on the increase in fluorescence intensity for a total of 1.38 hrs (**A-E**). Addition of SDS detergent or G1P substrate occurred after around 560 s, as indicated by the orange arrow.

3. Conclusions and outlook

We successfully designed polymer nanoreactors by encapsulation of phosphoglucomutase and insertion of a mixture of engineered α-hemolysins in their membrane. Moreover, these nanoreactors produced G6P, which was indirectly detected with a G6PDH enzyme found outside the vesicular space, via the formation of fluorescently NADPH. These nanoreactors produced G6P, a relevant metabolic compound which could aid in an incomplete glycolysis, pentose phosphate pathway, or a complex biological reaction, in which phosphoglucomutase is mutated or deficient.

In the near future, these nanoreactors will be optimized in terms of PGM encapsulation efficiency and control of the amount of enzyme to be encapsulated in relation with the stability and intended activity of the final nanoreactor will be investigated. It would be interesting to optimize and compare the activity of the nanoreactors containing PGM with the relevant activity in which this enzyme acts in its natural environment, as well as whether the nanoreactors containing PGM could replace or even improve biological or complex metabolic pathways in which phosphoglucomutase is mutated or deficient.

VI. ACTIVE BIO-HYBRID COMPARTMENTS ON SURFACES

X. Zhang, **M. Lomora**, T. Einfalt, W. Meier, N. Klein, D. Schneider, and C. G. Palivan, *Active surfaces engineered by immobilizing protein-polymer nanoreactors for selectively detecting sugar alcohols*, Biomaterials, **2016**, 89, 79-88.

My own contribution to this project was to express and purify the E. coli glycerol facilitator (GlpF) protein, maintaining the communication and sending samples to confirm our results with our collaborators, helping with the experiments related to the insertion of GlpF inside the synthetic membranes, contributing to the writing and critically analyzing the manuscript and creating the concept figure. As a result, only a summary of the project is described in this chapter.

1. Introduction

This chapter offers a general overview of the versatility of NRs' design via an example of their attachment on solid support for engineering sensitive "active surfaces". These nanoreactors are based on PMOXA-*b*-PDMS-*b*-PMOXA polymersomes in which specific membrane proteins are inserted in the membrane and enzymes sensitive to sugar alcohols are encapsulated inside the cavity. The specific membrane proteins chosen are able to selectively allow diffusion of sugar alcohols into the inner cavity of the polymersomes, thus initiating an enzymatic reaction used for sensitive and selective sugar alcohol biosensing. As a model channel protein for selective transport of sugar alcohols through the synthetic membrane, E. coli glycerol facilitator (GlpF) was selected, which conducts sugar alcohols with a high degree of stereo selectivity [169–172]. Inside the polymer nanoreactors we encapsulated ribitol 2-dehydrogenase (RDH), an enzyme that catalyzes a variety of sugar alcohol reactions [173, 174] (Figure 49). Therefore this "smart" combination of biomolecules serves to obtain a selective transport through the membrane of sugar alcohols, and their detection. Additionally, to obtain "active surfaces" for detecting sugar alcohols, the nanoreactors optimized in solution were then immobilized on a solid support: aldehyde groups exposed at the compartment external surface reacted via an aldehyde-amino reaction with glass surfaces chemically modified with amino groups. The design of polymer

nanoreactors followed by their immobilization on a solid support to produce “active surfaces”, act in this case as selective biosensors for sugar alcohols with both time and selectivity dependent precision.

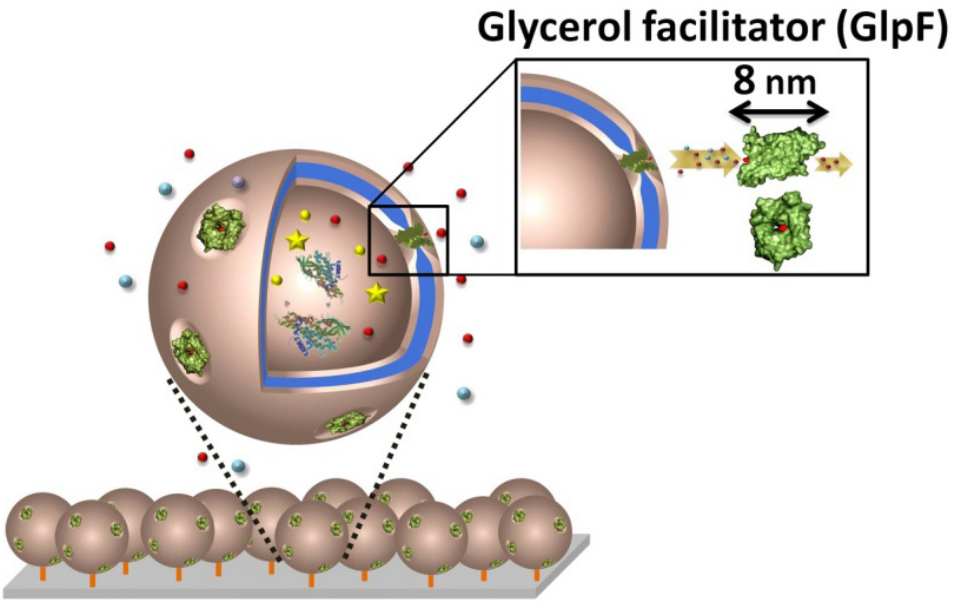

Fig 49. Design of an “active surface” serving as a sugar alcohol biosensor based on immobilized protein-polymersome nanoreactors with reconstituted membrane protein (GlpF) for selective transport of sugar alcohols, and encapsulated enzymes (RDH) for sensitive detection of sugar alcohols.

2. Results and discussion

2.1. Activity of GlpF nanoreactors in solution

NRs with selective permeability were obtained by insertion of GlpF, able to transport various sugar alcohols [169–172] into the membrane of PMOXA$_6$-*b*-PDMS$_{42}$-*b*-PMOXA$_6$ (A$_6$B$_{42}$A$_6$) polymersomes. For an enzyme able to sense the presence of sugar alcohols in situ, ribitol dehydrogenase (RDH) was encapsulated into the cavity of polymersomes [173, 174]. RDH converts ribitol with oxidized nicotinamide adenine dinucleotide (NAD^+) to D-ribulose, and reduced nicotinamide adenine dinucleotide (NADH).

Quantitative detection of ribitol with GlpF-nanoreactors was possible for a concentration range of 1.5 - 9 mM (Figure 50), where the change in absorbance intensity was proportional to the

amount of added ribitol (reaction time 15 min). All endpoints were in agreement with the theoretical values calculated using the extinction coefficient of NADH at 340 nm, an important characteristic for an analytical use of our biosensor. The K_m value (7.9 mM) of the reaction of the encapsulated RDH with ribitol was in agreement with the values previously obtained for free RDH [175], which indicates that the encapsulated enzyme preserved its catalytic activity. Since the concentration of sugar alcohols in biology or food products is in the milli-molar range, this biosensor well suited for the development of medical applications [176].

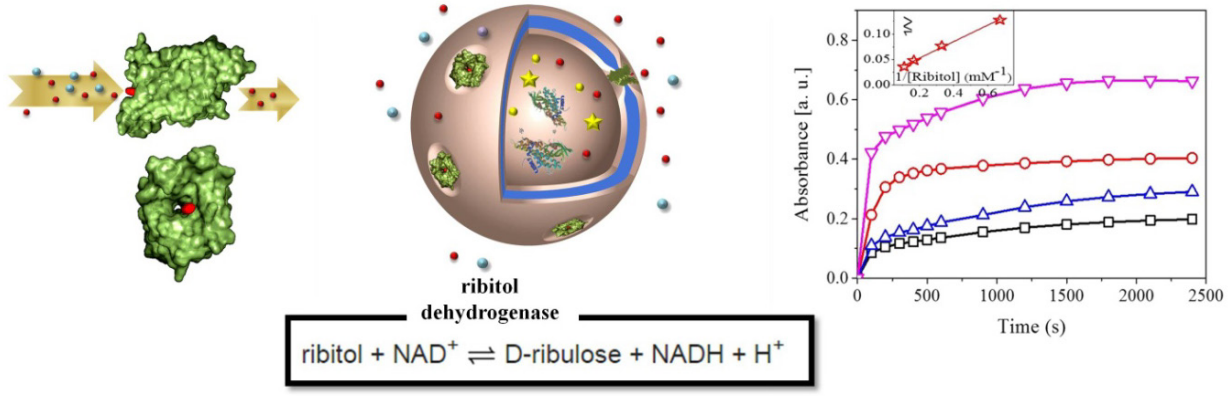

Fig. 50. Molecular representation for the GlpF used for permeabilization of the polymer nanoreactors (left); Enzymatic reaction used for the design of the GlpF-nanoreactor (middle); Conversion of ribitol by RDH-nanoreactors with inserted GlpF in solution with ribitol at different concentrations: 1.5 mM (black □), 3 mM (blue Δ), 6 mM (red ○) and 9 mM (pink open ▼) (right).

2.2. Immobilization on solid support

To obtain "active surfaces" for detecting sugar alcohols, GlpF nanoreactors were immobilized on glass solid supports, and their activity was further investigated after immobilization. Immobilization of nanoreactors was based on Schiff base formation between aldehyde groups exposed at the outer surface of nanoreactors and amino groups with which the support surface is functionalized [113]. For this purpose polymersomes were self-assembled from a mixture of non-functionalized copolymers ($PMOXA_6$-*b*-$PDMS_{42}$-*b*-$PMOXA_6$) and 5% functionalized copolymers ($PMOXA_7$-*b*-$PDMS_{44}$-*b*-$PMOXA_7$) with aldehyde end groups to provide the possibility of immobilizing polymersomes onto glass surfaces, chemically modified with amino

groups, via an aldehyde-amino reaction. After immobilizing the nanoreactors on the glass surface, the surface was rinsed several times with bidistilled water in order to remove any unimmobilized polymersomes. Both SEM and atomic force microscopy (AFM) images recorded arbitrary throughout the surface containing immobilized nanoreactors indicate the presence of spherical objects (Figure 51). SEM micrographs (Figure 51A) revealed that the solid surface was nonhomogeneously covered by spherical objects with diameters around 100 - 150 nm, in agreement with the AFM scan under air (Figure 51B). Rinsing the surface with bidistilled water did not remove the attached nanoreactors, which were covalently bound via amine bonds. In addition, the height of the collapsed polymersomes based on the magnified height images and the corresponding cross-section profiles (Figure 51C), was determined to be ~ 7 nm, which is close to the thickness of two overlapping polymer layers in the dry state.

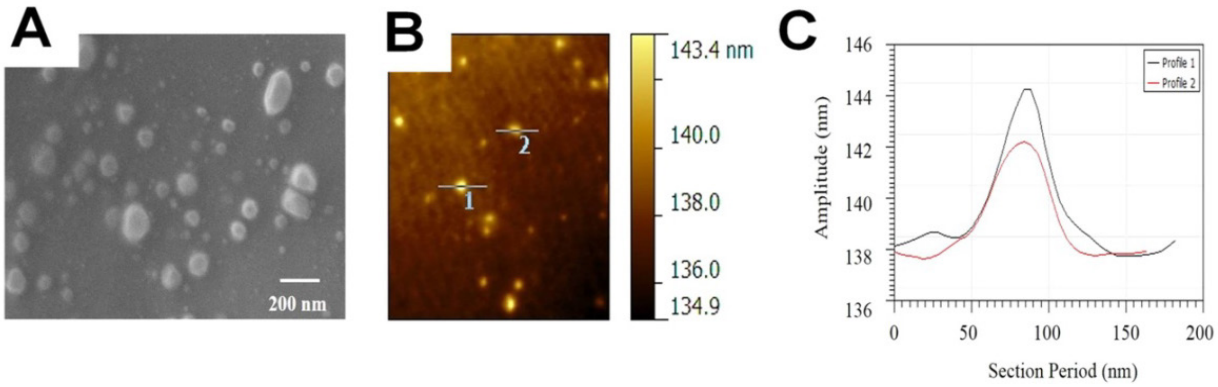

Fig. 51. A) SEM images of nanoreactors covalently immobilized on an amino functionalized glass surface; B) Overview AFM image of the immobilized nanoreactorson an amino functionalized glass surface, and C) height curve of two selected nanoreactors.

2.3. Function of the “active surfaces”

As during the enzymatic reaction involving the chosen enzyme (RDH) NADH is produced, which is fluorescent (with an emission wavelength at 445 nm), it was used as a probe to evaluate the activity after immobilization of GlpF-nanoreactors on a solid support by confocal laser scanning microscopy (CLSM). CLSM images of the surface containing immobilized nanoreactors without GlpF after incubation with ribitol for 20 min showed no fluorescence (Figure 52A), while surfaces with immobilized nanoreactors and GlpF showed a bright fluorescence of the surface (Figure 52B). The cross scratch part of the surface, where no nanoreactors were present after rinsing with water, showed no fluorescence (Figure 52B). Therefore, NRs preserved their enzymatic activity after immobilization on the glass surface, and thus could function as active biosensing surfaces for sugar alcohols.

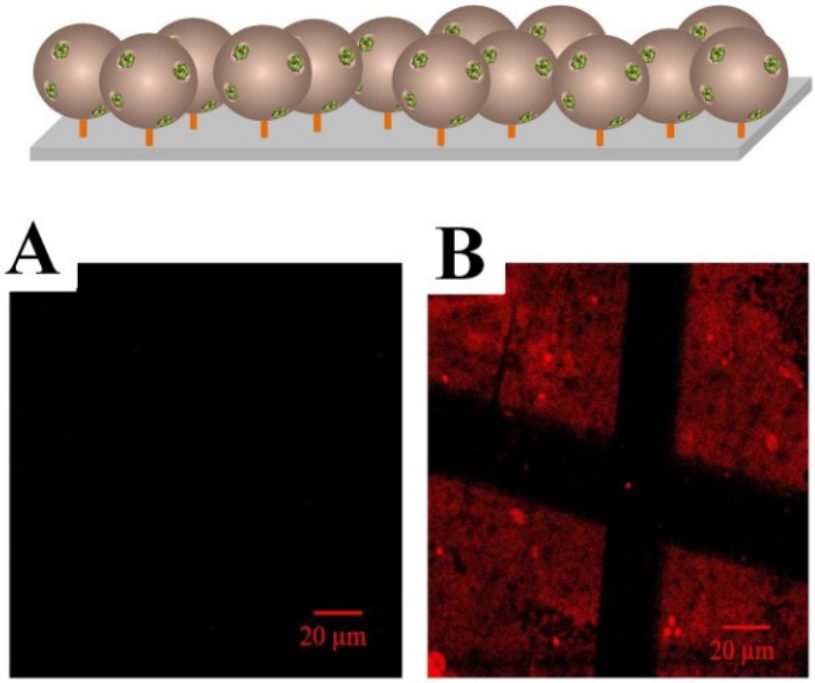

Fig. 52. CLSM micrographs of A) the active surface with immobilized nanoreactors without inserted GlpF, and B) with inserted GlpF.

3. Conclusions

We have developed “active surfaces” for selective biosensing of sugar alcohols based on immobilization of nanoreactors with specific membrane proteins inserted in their membranes, and sugar alcohol sensitive enzymes encapsulated in their cavities. Interestingly, the artificial surrounding within such a copolymer membrane and the high membrane thickness did not affect the function of the reconstituted GlpF, which allowed selective flux of sugar alcohols into the inner cavity of the nanoreactors, where the encapsulated enzymes serve as biosensing entities. An advantage of encapsulating the enzymes inside polymersomes is their protection from a potentially harmful environment, whilst preserving their catalytic activity. This smart approach prolongs the life-time of the enzymatic biosensor. Such protein-polymer nanoreactors with selective permeability offer the opportunity of monitoring the concentration of biologically relevant sugar alcohols and support biosensing approaches in a variety of domains, such as medical, biochemical or industrial. In addition, their immobilization on solid supports provides efficient “active surfaces” due to the rapid change in their fluorescence intensity in the presence of sugar alcohols. The concept of polymer compartments with selective permeability by inserting specific membrane proteins can be easily extended to the biosensing of other molecules by a simple change of membrane protein and encapsulated enzyme.

VII. OVERALL CONCLUSIONS AND OUTLOOK

This thesis presents the basis for the development of nano-scaled biosensors, nanoreactors and active surfaces based on the interaction of block copolymers that form supra-molecular assemblies (polymersomes) and biomolecules (biopores, ion-carriers, enzymes) in solution or on solid supports.

Chapter III dealt with presenting engineered polymersomes which allowed the passage of protons and monovalent ions, such as Na^+ and K^+, through the insertion of a pore protein gramicidin (gA). It was a very cumbersome process to identify the proper conditions for the observation of permeabilizaton events for the polymersome membranes assembled from $PMOXA_x$-$PDMS_y$-$PMOXA_x$ copolymers. Indeed, for this particular pore and type of membranes, gramicidin of approximately 2.6 nm in length inserted and maintained its function up to a membrane thickness of 12.1 nm. Therefore, a limit of insertion and function of the pore was identified (< 13.4 nm for $PMOXA_x$-$PDMS_y$-$PMOXA_x$ polymersome membrane thickness), without affecting the architecture of the polyersomes. The results presented within this body of work raises even more interesting questions and challenging tasks to be explored in terms of identifying other unknown functions of the pore in the presence of these types of synthetic membranes. Aspects to be considered using the conditions identified in this work might include further investigations related to the ability of gA: to transport monovalent cations in synthetic membranes with different thicknesses, to transport other types of ions than monovalent ions, being accepted within the scientific community that the channel is normally blocked in the presence of divalent cations (like Ca^{2+}) when inserted in lipid membranes, a detailed kinetic study of ion transport through the channels under the same conditions as presented here. There is still a fascinating territory to be discovered only in this case!

With regard to ionomycin (**Chapter IV**) and its interation with membranes composed of $PMOXA_x$-$PDMS_y$-$PMOXA_x$, it was possible to observe influx of Ca^{2+} ions through selected synthetic membranes. It needs to be stressed that ionomycin is an ion carrier and does not form pores or “holes” like gA, instead it travels through the hydrophobic part of the membrane to transport divalent cations from the extra-vesicular space to the inner cavity of the polymersomes and vice-versa, until an equilibrium of ions is reached. This was observed by using sensitive

fluorescent dyes, such as ACG, that increase its fluorescence in the presence of Ca^{2+}. A slower diffusion of these divalent cations was observed once the polymersome membranes were increased from 10.7 nm to 13.4 nm, from which we assumed that the ionophore had to travel longer, or its movement was impeded by a stronger entanglement of the polymer chains, through a thicker membrane. These polymersomes with preserved architecture and engineered ion selective permeability are wonderful candidates for the development of biosensors in applications in which changes in the environment, such as variations of pH, or ions concentration are required, as well as for the design of nanoreactors.

Chapter V presents preliminary data of nanoreactors with membranes permeable to molecules of up to 3-4 kDa, due to the presence of an engineered mixture of α-hemolysins. The focus is on designing a cascade enzymatic reaction which, under the protection of the cavity of the innocuous $PMOXA_x$-$PDMS_y$-$PMOXA_x$ polymersomes, should act as a provider of metabolic energy at the nanoscale. Like this, a controlled production of NAPH *in situ* can be obtained and find applications, like replacing an impaired metabolic pathway, in which the chosen enzyme (phosphoglucomutase) could be deficient. These amazing results might provide the starting point for the development of a novel system in biomedical applications, as for instance in enzyme replacement therapy. Futher optimization of the presented nanoreactor is needed to be in line with the intended application.

Furthermore, these systems can find exciting applications in the cellular world, as candidates for artificial organelles, or polymersome-in-polymersome systems, with particular attention towards improvements of the encapsulation efficiency (of biomacromolecules and also small polymersomes), cell uptake and addressing specific pathologic conditions. An additional challenge is the enhancement of mechanical stability of polymersomes after internalisation in cells. The current examples show a promising and elegant way to assemble complex systems using simple biomimetic strategies that allow gaining a deeper understanding of the biological processes and the synthetic tools designed. Moreover, the engineered polymersomes can be attached on solid support, as the example discussed in the final chapter of this thesis (**Chapter VI**) shows. By creating the proper membrane protein-polymersome membrane-enzymatic reaction-solid support combination, versatile solutions can be identified for tackling current issues in fields like biomedicine, catalysis, or environmental research.

The experience I have gained in working with polymersomes, in terms of their self-assembly and the encapsulation of biomolecules inside their cavity, will be a valuable tool for my future research carrer. I hope I could expand and compare this expertise with the investigation of other types of micro-/nanocompatments, such as LbL (layer-by-layer) capsules prepared by polyelectrolytes and their interaction with hydrogels and cells. This will allow me to gain training in more versatile tools to design micro-/nanodevices in combination with cells seeded in protective hydrogel scaffolds for the treatment of specific diseases, which I would like to develop in the nearest future.

VIII. EXPERIMENTAL SECTION

This chapter includes all materials, methods and characterization techniques, reproduced or modified from ref. [3] Copyright (2017) with permission from Elsevier, ref. [4] Copyright John Wiley and Sons, ref. [114] CC-BY-NC 3.0 license, and ref. [115] Copyright (2017) with permission from Elsevier.

Materials and methods

Gramicidin from Bacillus aneurinolyctus (Bacillus brevis), linear polypeptide antibiotic complex A mixture of gramicidins A, B, C, and D, 8-hydroxypyrene-1,3,6-trisulfonic acid trisodium salt (pyranine), 5(6)-carboxyfluorescein, monosodium phosphate (NaH_2PO_4), potassium phosphate dibasic (K_2HPO_4), potassium phosphate monobasic (KH_2PO_4), sodium chloride (NaCl), sodium hydroxide (NaOH), hydrochloric acid (HCl), ethanol (EtOH), and dimethyl sulfoxide (DMSO), C_2H_6OS, N–(2–hydroxyethyl)piperazine–N′–(2–ethanesulfonic acid) sodium salt (HEPES), calcium chloride dihydrate ($CaCl_2 \cdot 2H_2O$) were obtained from Sigma Aldrich and was used as received. 6-(((4,4-difluoro-5-(2-thienyl)-4-bora-3a,4a-diaza-s-indacene-3-yl)styryloxy)acetyl) aminohexanoic acid, succinimidyl ester (BODIPY) 630/650 fluorophore was purchased from Molecular Probes. Asante Natrium Green-2 (ANG-2), Asante Potassium Green-2 (APG-2), and Asante Calcium Green (ACG) K^+ salt were purchased from TEFLabs Inc. Ionomycin was purchased from Alomone Labs. Atto 488 maleimide from ATTO-TEC GmbH (Germany), and n-octyl-β-d-glucopyranoside (β-OG) from Anatrace (USA). His-tagged recombinant Enterobacter aerogenes ribitol 2-dehydrogenase (RDH) was acquired from Cusabio Biotech Co., Ltd (China). All reagents were used as received without further purifications unless otherwise stated.

Preparation of polymersomes and insertion of gA

Polymersomes were prepared at room temperature from different triblock copolymers $PMOXA_x$-$PDMS_y$-$PMOXA_x$, by film hydration method [177]. To produce a thin film, 5 mg of the block copolymer was dissolved in 1 mL of ethanol and subsequently evaporated under reduced pressure (150 mbar) to render a thin film. This film was further rehydrated with: a) 1 mL of pyranine solution 0.5 mM in 10 mM NaH_2PO_4, 132 mM NaCl buffer (pH 8.2); b) 1 mL of 250 μg/mL APG-2 solution in sodium buffer (10 mM NaH_2PO_4, 132 mM NaCl, pH 7.0), or c) 1 mL of 250 μg/mL ANG-2 solution in potassium buffer (10 mM KH_2PO_4, 132 mM KCl, pH 7.0). The

polymer suspensions were stirred overnight at RT and afterwards extruded through a 200 nm pore-size polycarbonate (PC) membrane (Merck, Germany), using an Avanti mini-extruder (Avanti Polar Lipids, USA). Any free dye was separated from polymersomes containing entrapped dye by passage through HiTrap desalting columns (Sephadex G-25 Superfine, GE Healthcare, UK) or 20 cm^3 in-house prepacked column (Sepharose 2B, Sigma Aldrich). gA biopores were inserted in polymer membrane by direct addition of 10 µL 0.08 mg/mL to 0.45 mg/mL gA in DMSO:EtOH, 1:1 ratio (solvent) to the pyranine (ANG-2, or APG-2) loaded polymersomes solutions.

The concentration of pyranine encapsulated in polymersomes was determined by UV-vis spectroscopy, $\lambda = 456$ nm.

Preparation of giant unilamellar vesicles (GUVs) and insertion of gA

GUVs were formed by the electroformation technique [178] using a Nanion Vesicle Prep Pro setup (Nanion Technologies, Munich, Germany). Briefly, 50 µL of a 4 mg/ml polymer stock solution in EtOH was spread on an indium tin oxide (ITO) coated glass slide to form a smooth polymer film on the glass surface, followed by drying for 45 min in high vacuum. By using an O-ring , a closed chamber was formed filled with a solution containing 100 mM sucrose, 10 mM K_2HPO_4/KH_2PO_4, pH 5.5 and 0.05 mM 5(6)-carboxyfluorescein (Sigma). Electroformation was performed overnight, in dark at RT (2.0 V, 3.0 Hz).

For imaging, GUVs containing gA were formed by addition of 0.7 µL 0.32 mg/mL gA (567 nM final concentration) to GUVs solution. gA insertion was tested by changing the pH with 1 µL of 0.4 M NaOH. The intrinsic permeability of GUVs to proton influx was verified by incubating solutions of GUVs with 0.7 µL DMSO:EtOH (1:1) ratio solvent, and 1 µL 0.4 M of NaOH.

Preparation of polymersomes and insertion of ionomycin

Polymersomes were prepared by the film hydration method [70] at room temperature using $PMOXA_x$–$PDMS_y$–$PMOXA_x$ triblock copolymer [79]. Briefly, for each sample, 5 mg of the block copolymer was dissolved in 1 mL of ethanol and subsequently evaporated under reduced pressure (150 mbar) to render a thin film. This film was then rehydrated with: i) 1 mL HEPES buffer (20 mM HEPES, 50 mM NaCl, pH = 7.4) (empty polymersomes), or ii) 1 mL of 20 µM

ACG solution in HEPES buffer (polymersomes with entrapped ACG). The polymer suspensions were stirred overnight at room temperature (RT) and afterwards extruded (13 times) through a 200 nm pore–size polycarbonate (PC) membrane (Merck, Germany), using an Avanti mini–extruder (Avanti Polar Lipids, USA). Extravesicular dye was separated from polymersomes that contained entrapped dye by passage through a 20 cm^3 in–house prepacked size exclusion column (Sepharose 2B, Sigma Aldrich). Ionomycin was added to the polymersomes mixture from a stock solution of ionomycin in EtOH (1.17 mM).

Efficiency of the ACG entrapment process in polymersomes

The concentration of encapsulated ACG in polymersomes was determined by UV–VIS spectroscopy at λ = 517 nm. For this, a value of 24310 $M^{-1}cm^{-1}$ for the extinction coefficient of ACG in HEPES buffer was obtained based on a calibration curve for the dye. The entrapment efficiency of the process (EEP) was determined as a percentage of the ratio between the concentration of ACG in polymersomes after encapsulation and purification (c_{ep}) and the initial concentration of ACG used for the film rehydration (c_i) [70]:

$$EEP[\%] = \frac{c_{ep}}{c_i} \cdot 100 \quad (13)$$

Preparation of giant unilamellar vesicles (GUVs) with ACG

For the generation of giant unilamellar polymeric vesicles (GUVs), 30 µL of the polymer dissolved in EtOH (4 mg/ml) was spread on an ITO – coated glass plate. The polymer solution was dried in high vacuum for 2 h in order to form a smooth polymer film on the glass surface. A chamber was formed with an O–ring and filled with 100 mM sucrose solution containing 20 µM of ACG. The chamber was closed with a second ITO – coated glass plate facing the ITO side to the solution, and then exposed to an AC current (2.5 V, 3.0 Hz) overnight at 20 °C.

Preparation of polymersomes/liposomes with 5(6)-Carboxyfluorescein (CF) or PGM

Polymersomes were prepared at room temperature from $PMOXA_6$-$PDMS_{34}$-$PMOXA_6$, triblock copolymer, by film hydration method [177]. To produce a thin film, 5 mg of the block copolymer was dissolved in 1 mL of ethanol and subsequently evaporated under reduced pressure (150 mbar) to render a thin film. This film was further rehydrated with 1 mL 50 mM

5(6)-Carboxyfluorescein (CF) in buffer A (150 mM NaCl, 2.7 mM KCl, 10 mM Na_2HPO_4, 2 mM KH_2PO_4, pH=8.0). The polymer suspensions were stirred overnight at RT.

To produce enzyme containing polymersomes, the polymer films were rehydrated with 1 mL of 10 U PGM, 143 mM K-PO4 (KH_2PO_4+K_2HPO_4), 9x10-2 mM EDTA, $3.6x10^{-4}$ mM G1,6-di-PO4, 0.36 mM $NADP^+$, 33 mM Tris-HCl, pH = 7.50.

Meanwhile, liposomes were prepared according to a previously published procedure [166]. Shortly, 20 mg of L-α-phosphatidylcholine from soybean, type IV-S (Sigma) were solubilized in 1 mL $CHCl_3$ in a 2.5 mL green capped glass vial. The organic solvent was removed afterwards under a stream of Ar, followed by 3 hours drying under vacuum in a Varian 801 Thermocouple Vacuum Pressure/Harrick Plasma cleaner. The resulted lipid thin film was rehydrated with 300 µL 50 mM CF in buffer A, followed by gentle stirring overnight at RT. The following day, the lipid suspension was 5 times frozen/thawed using liquid N2/370C water bath. The suspensions were afterwards extruded through a 200 nm (liposomes) or 100 nm (polymersomes) pore -size polycarbonate (PC) membrane (Merck, Germany), using an Avanti mini-extruder (Avanti Polar Lipids, USA). Any free dye was separated from polymersomes or 1:10 diluted liposomes in buffer B (300 mM NaCl, 2.7 mM KCl, 10 mM Na_2HPO_4, 2 mM KH_2PO_4, pH=8.0) containing entrapped dye by eluting them in buffer B through HiTrap desalting columns (Sephadex G-25 Superfine, GE Healthcare, UK). The non-encapsulated enzyme was removed by eluting the polymersomes with enzyme sample with 45 mM K-PO_4, 33 mM Tris-HCl, pH = 7.40 using a 20 cm^3 in-house prepacked column (Sepharose 2B, Sigma Aldrich).

Engineered α-hemolysin to induce leakage into the membranes of polymersomes and liposomes

The engineered α-hemolysins used herein has been expressed and purified via Ni^{2+}-NTA chromatography as previously described [164], with a final buffer composition of 300 mM NaCl, 50 mM Tris.HCl, 0.1% (v/v) SDS, pH = 8.0 (**engineered α-HL**). The engineered α-HL was used by direct addition over the polymersome and liposomes suspensions. A total initial concentration of the engineered α-HL was determined using the BCA assay (Thermo Scientific), or directly via measuring the absorbance at 280 nm with a NanoDrop 2000c Spectrophotometer. In order to avoid any interference from the engineered α-HL initial solubilization buffer during

the concentration measurements, the protein samples were washed with phosphate-buffered saline (PBS) by passing them 5 times through 10k cut-off filters (Millipore).

GlpF expression and purification

The plasmid pRSET-His-GlpF was transformed into *E. coli* BL21(DE3) cells (Agilent Technologies, USA). Expression from this plasmid results in production of the GlpF protein with a N-terminally added deca-histidine tail. The transformed cells were plated on selective LB agar plates with 100 μg mL^{-1} ampicilin and incubated overnight. Then single colonies were used to inoculate LB medium with 100 μg mL^{-1} ampicillin, and cells were grown at 37 °C until an OD_{600} of 1.2 - 1.3 was reached. 500 μM isopropyl β-D-1-thiogalactopyranoside (IPTG, Sigma Aldrich) was added to induce protein expression and cells were allowed to grow for 3 more hours. Then cells were harvested by centrifugation, resuspended in 50 mM phosphate buffer (pH 8.0) with 300 mM NaCl and 10% glycerol (Sigma Aldrich), and lysed by tip sonification at 4 °C. Cellular debris was removed by centrifugation at 3000 g (15 min at 4 °C), and membranes were subsequently separated from soluble proteins by centrifugation at 110,000g for 1 h. Precipitated membranes were solubilized in 50 mM phosphate buffer (pH 8.0), 300 mM NaCl, and 10% glycerol, and membrane proteins extracted by addition of 50 mM OG. After incubation for 1 h at room temperature, undissolved material was removed by centrifugation. Solubilized proteins were mixed with Ni-NTA agarose (Qiagen, Germany) and incubated for 1 h at room temperature. The Ni-NTA agarose was washed with 20 column volumes of solubilization buffer containing 80 mM imidazole (Sigma Aldrich). His-tagged proteins were then eluted with 1 mL of solubilization buffer containing 300 mM imidazole. Protein concentrations were determined by measuring the absorbance at 280 nm using the calculated molar extinction coefficient of 38305 $M^{-1}cm^{-1}$. Protein concentrations were determined using the BCA protein assay (Fisher Scientific GmbH, Germany). For SDS-PAGE analyses, 8 μL of the eluted protein solutions were incubated in sample buffer at 37°C for 30 min, and the 10% SDS-gels were run for 2 h at a current of 25 mA.

Preparation of GlpF-containing polymersomes

Polymer nanorectors containing GlpF and RDH were prepared by a minor modification of the film rehydration method described previously [91]. 4 mg of $PMOXA_6$-*b*-$PDMS_{42}$-*b*-$PMOXA_6$ copolymer were dissolved in 1 mL ethanol in round-bottom flasks, then placed in a rotary vacuum evaporator (40 ºC, 1 hour, 170 rpm for solvent removal) until a thin film was formed. The thin polymer film was rehydrated using 1 mL of 10 µg mL^{-1} RDH solution in phosphate buffer solution (pH 9), and 0.05 mg ml^{-1} GlpF in 0.2 % OG and left over-night under magnetic stirring at 4 ºC. Polymersomes were extruded by passing them at least 11 times through 400 nm, followed by 200 nm pore-sized polycarbonate (PC) membranes (Merck, Germany) mounted in an Avanti mini-extruder (Avanti Polar Lipids, USA). To remove OG solubilizing GlpF and facilitate the insertion of GlpF into the polymersome membrane, solutions were first dialyzed against PBS buffer at 4ºC for 24 hours, changing the buffer every 8 hours, with molecular cut-off of 8-10 kDa MWCO dialysis membranes (Spectrum Laboratories, Inc. USA). Subsequently, solutions were dialyzed against PBS buffer at 4 °C for at least 24 hours, changing the buffer 4 times per day, using molecular cut-off of 300 kDa MWCO dialysis membranes to remove the non-encapsulated RDH.

Activity of RDH nanoreactors

RDH activity was determined in bulk by spectrophotometric measurement of the change in absorbance of NADH at 340 nm, using a standard assay mixture for substrate oxidation contained in a final volume of 1 mL at room temperature: 100 µmol phosphate buffer solution at pH 9.0, 1.8 µmol NAD^+ and 0.02 – 0.2 U RDH. The reaction was started by the addition of ribitol. One unit (U) of enzyme activity is defined as the amount of enzyme required to oxidize 1 µmol NAD^+ per min under standard assay conditions.

Immobilization of RDH nanoreactors

RDH nanoreactors able to be immobilized on a solid support were prepared as described above, but with a mixture of 5% aldehyde-terminated $PMOXA_7$-*b*-$PDMS_{44}$-*b*-$PMOXA_7$ copolymer and 95% $PMOXA_6$-*b*-$PDMS_{42}$-*b*-$PMOXA_6$ copolymer in PBS buffer containing a 0.3% (w/v) 2-picoline borane complex at room temperature.

Immobilization of NRs was performed by adapting to glass substrates (Thermos Scientific, Gerhard Menzel GmbH) a procedure described previously [113]. The amino functional groups exposed at the glass surface were obtained by immersing the glass surface in a solution of 3-aminopropyltriethoxysilane (APTES) under water-free and oxygen-free conditions. Then, NRs with exposed aldehyde groups were immobilized on functionalized glass surfaces by placing the glass substrates in a freshly-prepared PBS buffer solution containing NRs and 0.3% sodium cyanoborohydride at room temperature. After 12 h of reaction, the solid substrates were extensively rinsed with bidistilled water and dried under a stream of nitrogen prior to scanning electron microscopy (SEM) or atomic force microscopy (AFM) measurements.

Characterization techniques

Light scattering (LS)

Dynamic (DLS) and static (SLS) light-scattering experiments were performed on an ALV (Langen, Germany) goniometer equipped with an ALV He-Ne laser (JDS Uniphase, wavelength λ = 632.8 nm). Polymersome emulsions were serially diluted to polymer concentrations ranging from 1.25 mg/mL to 0.07 mg/mL, and measured in 10 mm cylindrical quartz cells at angles of 30-150°, 293 K ± 0.5 K. The photon intensity auto-correlation function g2(t) was determined with an ALV-5000E correlator (scattering angles between 30° and 150°). A non–linear decay–time analysis supported by regularized inverse Laplace transform of g2(t) (CONTIN algorithm) was used to analyze the DLS data and to evaluate the apparent hydrodynamic radius (R_h) of polymersomes. The angle–dependent apparent diffusion coefficient was extrapolated to zero momentum transfer (q^2) using the ALV/Static and dynamic FIT and PLOT 4.31 software. Angle and concentration–dependent SLS data were analyzed using Guinier plots and used to determine the apparent molecular weight ($M_{w,agg}$), the radius of gyration (R_g), and the second virial coefficient (A_2) of the polymersomes. The structural parameter (ρ) and the average aggregation number (N_{agg}) of self-assembled structures were calculated using the following equations:

$$\rho = \frac{R_g}{R_h} \tag{14}$$

$$N_{agg} = \frac{M_{w,agg}}{M_w} \tag{15}$$

where M_w is the average molecular weight of $PMOXA_x$–$PDMS_y$–$PMOXA_x$ triblock copolymers.

Transmission electron microscopy (TEM)

5 µL of polymersome solutions were adsorbed for 1 min on glow-discharged carbon-coated copper grids. The samples were blotted, washed and negatively stained with 2% uranyl acetate solution. Micrographs were obtained using a transmission electron microscope (Philips Morgagni 268D).

Cryogenic transmission electron microscopy

An unextruded polymer suspension of $A_7B_{42}A_7$ in a Hepes buffer (20 mM Hepes, pH 7.4, 50 mM NaCl) at a concentration of 5 mg/ml was deposited on glow-discharged holey carbon grids (Quantifoil, Germany) and blotted before quick-freezing in liquid ethane using a Vitribot plunging-freezing device (FEI, USA). Grids were stored in liquid nitrogen before transfer them to a cryo-holder (Gatan, USA). Imaging was performed on a Philips CM200 FEG TEM at 200 kV accelerating voltage in low-dose mode with a defocus value of -2 µm for membrane thickness measurements. The membrane thickness was calculated as mean values ± SD (n=112) using Image J software (U. S. National Institutes of Health, Bethesda, Maryland, USA) [79].

Scanning electron microscopy (SEM)

SEM was performed with a Hitachi S-4800 FEG (Hitachi, Ltd., Japan), operated at 5 kV accelerating voltage. Before SEM measurements, the samples of NRs or NRs immobilized on glass surfaces were sputter-coated with platinum to minimize the overall change.

Atomic force microscopy (AFM)

AFM measurements were performed in a tapping mode under air using an Agilent 5100 AFM/SPM microscope (PicoLe System, Molecular Imaging). Images were recorded using silicon cantilevers (PPP-NCHR, Nanosensors) with a nominal spring constant of 42 N m^{-1} and a resonance frequency of 200-500 kHz, and collected with a resolution of 512 × 512 pixels at a scan rate of 0.5 line s^{-1}.

Fluorescence correlation spectroscopy (FCS)

FCS measurements were performed at 20°C on a Zeiss LSM 510-META/Confcor2 laser-scanning microscope equipped with a 458 nm Argon/2 laser and a 40×water-immersion objective (Zeiss C/Apochromat 40X, NA 1.2). Excitation power was P_L = 15 mW, and the excitation transmission was 10%. The diameter of the pinhole was set to 66 µm. For each measurement, 10 µL of sample solution, containing polymersomes with entrapped pyranine was used directly after the purification step, and placed on glass slides. For FCS, spectra were recorded over 10 s, and each measurement was repeated 10 times.

For polymersomes with ACG measurements, the diameter of the pinhole was set to 74 µm, and the diffusion time for ACG (25 nM) in Hepes buffer was fixed in the fitting procedure. Empty polymersomes were incubated overnight with 20 µM ACG at RT, then 10 µL of these solutions were placed on microscopy glass slides, and FCS measured at an excitation transmission of 10 % over 20 x 10 s. Autocorrelation functions were fitted with a two–component model including triplet state [179]. From the two–component fitting model, the percentages of fast–diffusing (free ACG) and slow–diffusing fractions (ACG–containing polymersomes) were obtained.

Z-scan FCS: GUV membranes were stained with Bodipy 630/650 NHS ester (Thermo Fisher Scientific Inc; Waltham, MA, USA) by the addition of 5 µL of a 25 nM Bodipy stock solution in buffer to the immobilized GUVs on the glass surface. Z-scans were recorded as previously described [79], except that a He–Ne laser was used (λ = 633 nm, 1% transmission at 15 mW).

UV-vis Spectroscopy

UV-vis spectroscopy measurements were carried out on a Specord 210 Plus spectrophotometer, Analytic Jena AG, Germany, or on a SpectraMaxPlus 384 (Molecular Devices, Sunnyvale, USA) using a 96–well absorbance microplate.

Fluorescence spectroscopy

The fluorescence measurements were carried out on a LS 55 Fluorescence Spectrometer from Perkin Elmer with a FL Winlab Software. Polymersomes loaded with pyranine, APG-2, and ANG-2 with or without gA solutions were added in a 1 cm path length quartz cuvette, placed in a thermostated stirred single cell holder. A small stirrer was placed in the cuvette to assure

thorough and gentle mixing of reagents, as well as accurate temperature work. An excitation wavelength of 454 nm and an emission of 511 nm were used for pyranine, with slits set at 7.5 nm. ANG-2 and APG-2 dyes were excited at 511 nm and had an emission of 540 nm.
Diluted polymersome solutions containing entrapped ACG without, and with ionomycin, and in the presence of $CaCl_2$, were excited at $\lambda = 517$ nm and emission was monitored at $\lambda = 540$ nm.

Stopped-flow spectroscopy with fluorescence detection

Stopped-flow experiments were performed on a stopped-flow apparatus (Bio-Logic SAS, France). Polymersomes loaded with pyranine, with or without gA solutions were automatically injected in a 1.5 mm light path cuvette, with blackened edges to reduce light scattering in fluorescence configuration. The monochromator was set at 454 nm and a cut-off filter of 475 nm was used during all measurements.
Samples consisting of polymersome suspensions loaded with ACG, without or with ionomycin, were injected into a SX20 stopped–flow apparatus (Applied Photophysics, UK), using a monochromator set at 517 nm and a cut–off filter of 530 nm.

Surface (ζ) potential measurements

The ζ-potential of: (i) free calcium sensitive dye (ACG), (ii) empty polymersome solutions without ionomycin, in the absence of calcium ions, (iii) polymersomes with entrapped ACG solutions without ionomycin, in the absence of calcium ions, (iv) polymersomes with entrapped ACG solutions with ionomycin, in the absence of calcium ions, and (v) polymersomes with entrapped ACG solutions with ionomycin, in the presence of calcium ions was investigated. We used disposable folded capillary cells placed in a Zetasizer Nano ZSP (Malvern Instruments), at 25 °C.

Confocal Laser Scanning Microscopy (CLSM)

CLSM experiments were performed on a confocal laser scanning microscope (Zeiss LSM 510-META/Confocor2, Carl Zeiss, Jena, Germany). An Argon/2 laser ($\lambda = 488$ nm, 30 mW, 25% power output, 0.5% transmission) as the excitation source. A main dichromatic beam splitter (HFT 488/543), a secondary dichroic beam splitter (NFT 515) and a band pass filter (BP 505-530) were used in all experiments. In case of BODIPY, a He-Ne laser ($\lambda = 633$ nm) was used as

the excitation source with a transmission of 15%, and main dichromatic beam splitter (HFT UV/488/543/633), a secondary dichroic beam splitter (NFT 545) and a band pass filter (LP 650).The images were recorded with a water immersion objective (C-Apochromat 40x/1.2W). Each sample was scanned unidirectionally using an automatically controlled time series with a cycle delay of 5s.

GUV solutions were diluted in 60 mM K_2HPO_4/KH_2PO_4 buffer and transferred to plasma-cleaned 8-well borosilicate microscopy chambers (ThermoFischer Scientific). For visualization purposes, GUV membranes were stained with Bodipy 630/650.

GUVs with ACG measurements were performed using an Argon/2 laser (λ = 514 nm) and a 40×water–immersion objective (Zeiss C/Apochromat 40X, NA 1.2). Excitation power of the laser was 15 mW and the excitation transmission was set to 10 %. For imaging of GUVs, the laser beam was guided through a dichromatic beam splitter (HFT 514), a secondary dichroic beam splitter (NFT 515), and a low pass filter (LP 530). GUVs were immobilized on microscopy slides by diluting the GUVs (sucrose solution) in HEPES buffer; the GUVs sink to the bottom of the glass slide and adhere on the surface. Images were taken before and after bleaching for 3 s at 100 % transmission.

IX. REFERENCES

[1] Cutkosky, M.R. Climbing with adhesion: From bioinspiration to biounderstanding. *Interface focus*, **2015**, *5,* 1-9.

[2] Tanner, P.; Balasubramanian, V.; Palivan, C.G. Aiding nature's organelles: artificial peroxisomes play their role. *Nano letters*, **2013**, *13,* 2875–2883.

[3] Lomora, M.; Garni, M.; Itel, F.; Tanner, P.; Spulber, M.; Palivan, C.G. Polymersomes with engineered ion selective permeability as stimuli-responsive nanocompartments with preserved architecture. *Biomaterials*, **2015**, *53,* 406–414.

[4] Lomora, M.; Dinu, I.A.; Itel, F.; Rigo, S.; Spulber, M.; Palivan, C.G. Does Membrane thickness affect the transport of selective ions mediated by ionophores in synthetic membranes? *Macromolecular rapid communications*, **2015**, *36,* 1929–1934.

[5] Soyer, O.S. *Evolutionary systems biology;* Springer, New York, **2012**.

[6] Akbarzadeh, A.; Rezaei-Sadabady, R.; Davaran, S.; Joo, S.W.; Zarghami, N.; Hanifehpour, Y.; Samiei, M.; Kouhi, M.; Nejati-Koshki, K. Liposome: Classification, preparation, and applications. *Nanoscale research letters*, **2013**, *8,* 1-9.

[7] Torchilin, V.P. Recent advances with liposomes as pharmaceutical carriers. *Nature reviews. Drug discovery*, **2005**, *4,* 145–160.

[8] Kirby, C.; Clarke, J.; Gregoriadis, G. Effect of the cholesterol content of small unilamellar liposomes on their stability in vivo and in vitro. *The Biochemical journal*, **1980**, *186,* 591–598.

[9] Briuglia, M.-L.; Rotella, C.; McFarlane, A.; Lamprou, D.A. Influence of cholesterol on liposome stability and on in vitro drug release. *Drug delivery and translational research*, **2015**, *5,* 231–242.

[10] Grit, M.; Crommelin, D.J. Chemical stability of liposomes: Implications for their physical stability. *Chemistry and physics of lipids*, **1993**, *64,* 3–18.

[11] Tamai, H.; Okutsu, N.; Tokuyama, Y.; Shimizu, E.; Miyagi, S.; Shulga, S.; Danilov, V.I.; Kurita, N. A coarse grained molecular dynamics study on the structure and stability of small-sized liposomes. *Molecular simulation*, **2015**, *42,* 122–130.

[12] Discher, D.E.; Eisenberg, A. Polymer vesicles. *Science*, **2002**, *297,* 967–973.

[13] Discher, D.E.; Ahmed, F. Polymersomes. *Annual review of biomedical engineering*, **2006**, *8,* 323–341.

[14] Alexandridis, P.; Lindman, B. *Amphiphilic block copolymers: Self-assembly and applications;* Elsevier: Amsterdam, **2000**.

[15] Whitesides, G.M.; Grzybowski, B. Self-assembly at all scales. *Science*, **2002**, *295,* 2418–2421.

[16] Du, J.; O'Reilly, R.K. Advances and challenges in smart and functional polymer vesicles. *Soft matter*, **2009**, *5,* 3544–3561.

[17] Kita-Tokarczyk, K.; Grumelard, J.; Haefele, T.; Meier, W. Block copolymer vesicles - Using concepts from polymer chemistry to mimic biomembranes. *Polymer*, **2005**, *46,* 3540–3563.

[18] Rikken, R.S.M.; Engelkamp, H.; Nolte, R.J.M.; Maan, J.C.; van Hest, J.C.M.; Wilson, D.A.; Christianen, P.C.M. Shaping polymersomes into predictable morphologies via out-of-equilibrium self-assembly. *Nature communications*, **2016**, *7,* 1–7.

[19] Chambon, P.; Blanazs, A.; Battaglia, G.; Armes, S.P. Facile synthesis of methacrylic ABC triblock copolymer vesicles by RAFT aqueous dispersion polymerization. *Macromolecules*, **2012**, *45,* 5081–5090.

[20] Antonietti, M.; Förster, S. Vesicles and liposomes: A self-assembly principle beyond lipids. *Adv. mater.*, **2003**, *15,* 1323–1333.

[21] Postupalenko, V.; Tomaz, E.; Lomora, M.; Dinu, I.A.; Palivan, G.C. *Bio-nanoreactors: From confined reaction spaces to artificial organelles, in Samahe Sadjadi (ed.), Organic nanoreactors: From molecular to supramolecular organic compounds;* Academic Press, Elsevier: London, 341-371, **2016**.

[22] Discher, B.M. Polymersomes: Tough vesicles made from diblock copolymers. *Science*, **1999**, *284,* 1143–1146.

[23] Du, Y.; Chen, W.; Zheng, M.; Meng, F.; Zhong, Z. pH-sensitive degradable chimaeric polymersomes for the intracellular release of doxorubicin hydrochloride. *Biomaterials*, **2012**, *33,* 7291–7299.

[24] Kim, H.-O.; Kim, E.; An, Y.; Choi, J.; Jang, E.; Choi, E.B.; Kukreja, A.; Kim, M.-H.; Kang, B.; Kim, D.-J.; Suh, J.-S.; Huh, Y.-M.; Haam, S. A biodegradable polymersome containing

Bcl-xL siRNA and doxorubicin as a dual delivery vehicle for a synergistic anticancer effect. *Macromolecular bioscience*, **2013**, *13,* 745–754.

[25] Massignani, M.; Lomas, H.; Battaglia, G. Polymersomes: A synthetic biological approach to encapsulation and delivery. In: *Modern techniques for nano- and microreactors/-reactions*. Caruso, F., Ed.; Springer, Berlin, **2010**; Vol. *229*; pp. 115–154.

[26] Le Meins, J.-F.; Schatz, C.; Lecommandoux, S.; Sandre, O. Hybrid polymer/lipid vesicles: State of the art and future perspectives. *Materials today*, **2013**, *16,* 397–402.

[27] Pata, V.; Dan, N. The effect of chain length on protein solubilization in polymer-based vesicles (polymersomes). *Biophysical journal*, **2003**, *85,* 2111–2118.

[28] Men, Y.; Peng, F.; Tu, Y.; van Hest, Jan C. M.; Wilson, D.A. Methods for production of uniform small-sized polymersome with rigid membrane. *Polym. chem.*, **2016**, *7,* 3977–3982.

[29] Liu, G.; Ma, S.; Li, S.; Cheng, R.; Meng, F.; Liu, H.; Zhong, Z. The highly efficient delivery of exogenous proteins into cells mediated by biodegradable chimaeric polymersomes. *Biomaterials*, **2010**, *31,* 7575–7585.

[30] Cheng, R.; Meng, F.; Ma, S.; Xu, H.; Liu, H.; Jing, X.; Zhong, Z. Reduction and temperature dual-responsive crosslinked polymersomes for targeted intracellular protein delivery. *J. mater. chem.*, **2011**, *21,* 19013–19020.

[31] Canton, I.; Massignani, M.; Patikarnmonthon, N.; Chierico, L.; Robertson, J.; Renshaw, S.A.; Warren, N.J.; Madsen, J.P.; Armes, S.P.; Lewis, A.L.; Battaglia, G. Fully synthetic polymer vesicles for intracellular delivery of antibodies in live cells. *FASEB journal*, **2013**, *27,* 98–108.

[32] Zhang, J.; Wu, L.; Meng, F.; Wang, Z.; Deng, C.; Liu, H.; Zhong, Z. pH and reduction dual-bioresponsive polymersomes for efficient intracellular protein delivery. *Langmuir*, **2012**, *28,* 2056–2065.

[33] Stano, A.; Scott, E.A.; Dane, K.Y.; Swartz, M.A.; Hubbell, J.A. Tunable T cell immunity towards a protein antigen using polymersomes vs. solid-core nanoparticles. *Biomaterials*, **2013**, *34,* 4339–4346.

[34] Tang, R.; Kim, C.S.; Solfiell, D.J.; Rana, S.; Mout, R.; Velazquez-Delgado, E.M.; Chompoosor, A.; Jeong, Y.; Yan, B.; Zhu, Z.-J.; Kim, C.; Hardy, J.A.; Rotello, V.M. Direct delivery of functional proteins and enzymes to the cytosol using nanoparticle-stabilized nanocapsules. *ACS nano*, **2013**, *7,* 6667–6673.

[35] Gaitzsch, J.; Canton, I.; Appelhans, D.; Battaglia, G.; Voit, B. Cellular interactions with photo-cross-linked and pH-sensitive polymersomes: biocompatibility and uptake studies. *Biomacromolecules*, **2012**, *13,* 4188–4195.

[36] Huang, Z.; Teng, W.; Liu, L.; Wang, L.; Wang, Q.; Dong, Y. Efficient cytosolic delivery mediated by polymersomes facilely prepared from a degradable, amphiphilic, and amphoteric copolymer. *Nanotechnology*, **2013**, *24,* 1–14.

[37] Matini, T.; Francini, N.; Battocchio, A.; Spain, S.G.; Mantovani, G.; Vicent, M.J.; Sanchis, J.; Gallon, E.; Mastrotto, F.; Salmaso, S.; Caliceti, P.; Alexander, C. Synthesis and characterization of variable conformation pH responsive block co-polymers for nucleic acid delivery and targeted cell entry. *Polym. chem.*, **2014**, *5,* 1626–1636.

[38] Nardin, C.; Thoeni, S.; Widmer, J.; Winterhalter, M.; Meier, W. Nanoreactors based on (polymerized) ABA-triblock copolymer vesicles. *Chem. commun.*, **2000,** 1433–1434.

[39] Ben-Haim, N.; Broz, P.; Marsch, S.; Meier, W.; Hunziker, P. Cell-specific integration of artificial organelles based on functionalized polymer vesicles. *Nano letters*, **2008**, *8,* 1368–1373.

[40] van Dongen, S.; Verdurmen, W.; Peters, R.; Nolte, R.; Brock, R.; van Hest, J. Cellular integration of an enzyme-loaded polymersome nanoreactor. *Angewandte chemie*, **2010**, *49,* 7213–7216.

[41] Peters, R.; Marguet, M.; Marais, S.; Fraaije, M.W.; van Hest, J.; Lecommandoux, S. Cascade reactions in multicompartmentalized polymersomes. *Angewandte chemie*, **2014**, *53,* 146–150.

[42] Napoli, A.; Boerakker, M.J.; Tirelli, N.; Nolte, R.J.M.; Sommerdijk, N. A. J. M.; Hubbell, J.A. Glucose-oxidase based self-destructing polymeric vesicles. *Langmuir*, **2004**, *20,* 3487–3491.

[43] Kim, K.T.; Cornelissen, Jeroen J. L. M.; Nolte, R.J.M.; van Hest, Jan C. M. A polymersome nanoreactor with controllable permeability induced by stimuli-responsive block Copolymers. *Adv. mater.*, **2009**, *21,* 2787–2791.

[44] Carlsen, A.; Glaser, N.; Le Meins, J.-F.; Lecommandoux, S. Block copolymer vesicle permeability measured by osmotic swelling and shrinking. *Langmuir*, **2011**, *27,* 4884–4890.

[45] Spulber, M.; Najer, A.; Winkelbach, K.; Glaied, O.; Waser, M.; Pieles, U.; Meier, W.; Bruns, N. Photoreaction of a hydroxyalkyphenone with the membrane of polymersomes: a

versatile method to generate semipermeable nanoreactors. *Journal of the american chemical society*, **2013**, *135,* 9204–9212.

[46] Gaitzsch, J.; Appelhans, D.; Wang, L.; Battaglia, G.; Voit, B. Synthetic bio-nanoreactor: mechanical and chemical control of polymersome membrane permeability. *Angewandte chemie*, **2012**, *51,* 4448–4451.

[47] Sauer, M.; Meier, W. Polymer nanocontainers with controlled permeability. *Aust. j. chem.*, **2001**, *54,* 149–151.

[48] Nallani, M.; Benito, S.; Onaca, O.; Graff, A.; Lindemann, M.; Winterhalter, M.; Meier, W.; Schwaneberg, U. A nanocompartment system (Synthosome) designed for biotechnological applications. *Journal of biotechnology*, **2006**, *123,* 50–59.

[49] Grzelakowski, M.; Onaca, O.; Rigler, P.; Kumar, M.; Meier, W. Immobilized protein-polymer nanoreactors. *Small*, **2009**, *5,* 2545–2548.

[50] Graff, A.; Sauer, M.; van Gelder, P.; Meier, W. Virus-assisted loading of polymer nanocontainer. *Proceedings of the national academy of sciences of the United States of America*, **2002**, *99,* 5064–5068.

[51] Yu, Y.; Jiang, X.; Gong, S.; Feng, L.; Zhong, Y.; Pang, Z. The proton permeability of self-assembled polymersomes and their neuroprotection by enhancing a neuroprotective peptide across the blood-brain barrier after modification with lactoferrin. *Nanoscale*, **2014**, *6,* 3250–3258.

[52] Cheng, Z.; Tsourkas, A. Paramagnetic porous polymersomes. *Langmuir*, **2008**, *24,* 8169–8173.

[53] Langowska, K.; Palivan, C.G.; Meier, W. Polymer nanoreactors shown to produce and release antibiotics locally. *Chemical communications*, **2013**, *49,* 128–130.

[54] van Dongen, Stijn F M; Nallani, M.; Cornelissen, Jeroen J L M; Nolte, R.J.M.; van Hest, Jan C M. A three-enzyme cascade reaction through positional assembly of enzymes in a polymersome nanoreactor. *Chemistry*, **2009**, *15,* 1107–1114.

[55] Tanner, P.; Onaca, O.; Balasubramanian, V.; Meier, W.; Palivan, C.G. Enzymatic cascade reactions inside polymeric nanocontainers: a means to combat oxidative stress. *Chemistry*, **2011**, *17,* 4552–4560.

[56] Dobrunz, D.; Toma, A.C.; Tanner, P.; Pfohl, T.; Palivan, C.G. Polymer nanoreactors with dual functionality: simultaneous detoxification of peroxynitrite and oxygen transport. *Langmuir*, **2012**, *28,* 15889–15899.

[57] Baumann, P.; Balasubramanian, V.; Onaca-Fischer, O.; Sienkiewicz, A.; Palivan, C.G. Light-responsive polymer nanoreactors: a source of reactive oxygen species on demand. *Nanoscale*, **2013**, *5,* 217–224.

[58] Vocht, C. de; Ranquin, A.; Willaert, R.; van Ginderachter, J.A.; Vanhaecke, T.; Rogiers, V.; Versees, W.; van Gelder, P.; Steyaert, J. Assessment of stability, toxicity and immunogenicity of new polymeric nanoreactors for use in enzyme replacement therapy of MNGIE. *Journal of controlled release*, **2009**, *137,* 246–254.

[59] Chen, Q.; Schonherr, H.; Vancso, G.J. Block-copolymer vesicles as nanoreactors for enzymatic reactions. *Small*, **2009**, *5,* 1436–1445.

[60] Ranquin, A.; Versees, W.; Meier, W.; Steyaert, J.; van Gelder, P. Therapeutic nanoreactors: combining chemistry and biology in a novel triblock copolymer drug delivery system. *Nano letters*, **2005**, *5,* 2220–2224.

[61] Vriezema, D.M.; Garcia, P.M.L.; Sancho Oltra, N.; Hatzakis, N.S.; Kuiper, S.M.; Nolte, R.J.M.; Rowan, A.E.; van Hest, J. Positional assembly of enzymes in polymersome nanoreactors for cascade reactions. *Angewandte chemie*, **2007**, *46,* 7378–7382.

[62] Cordova, A.; Deserno, M.; Gelbart, W.M.; Ben-Shaul, A. Osmotic shock and the strength of viral capsids. *Biophysical journal*, **2003**, *85,* 70–74.

[63] Cornelissen, J.J. Helical superstructures from charged poly(styrene)-poly(isocyanodipeptide) block copolymers. *Science*, **1998**, *280,* 1427–1430.

[64] Hoog, H.M. de; Nallani, M.; Cornelissen, J.J.L.M.; Rowan, A.E.; Nolte, R.J.M.; Arends, I.W.C.E. Biocatalytic oxidation by chloroperoxidase from Caldariomyces fumago in polymersome nanoreactors. *Organic & biomolecular chemistry*, **2009**, *7,* 4604–4610.

[65] Nallani, M.; Hoog, H.-P.M. de; Cornelissen, Jeroen J. L. M.; Palmans, A.R.A.; van Hest, Jan C. M.; Nolte, R.J.M. Polymersome nanoreactors for enzymatic ring-opening polymerization. *Biomacromolecules*, **2007**, *8,* 3723–3728.

[66] Vriezema, D.M.; Hoogboom, J.; Velonia, K.; Takazawa, K.; Christianen, P.C.M.; Maan, J.C.; Rowan, A.E.; Nolte, R.J.M. Vesicles and polymerized vesicles from thiophene-containing rod-coil block copolymers. *Angewandte chemie*, **2003**, *42,* 772–776.

[67] Kuiper, S.M.; Nallani, M.; Vriezema, D.M.; Cornelissen, Jeroen J L M; van Hest, Jan C M; Nolte, R.J.M.; Rowan, A.E. Enzymes containing porous polymersomes as nano reaction vessels for cascade reactions. *Organic & biomolecular chemistry*, **2008**, *6,* 4315–4318.

[68] Louzao, I.; van Hest, Jan C M. Permeability effects on the efficiency of antioxidant nanoreactors. *Biomacromolecules*, **2013**, *14,* 2364–2372.

[69] Spulber, M.; Baumann, P.; Liu, J.; Palivan, C.G. Ceria loaded nanoreactors: a nontoxic superantioxidant system with high stability and efficacy. *Nanoscale*, **2015**, *7,* 1411–1423.

[70] Baumann, P.; Spulber, M.; Dinu, I.A.; Palivan, C.G. Cellular Trojan horse based polymer nanoreactors with light-sensitive activity. *The journal of physical chemistry. B*, **2014**, *118,* 9361–9370.

[71] Onaca, O.; Hughes, D.W.; Balasubramanian, V.; Grzelakowski, M.; Meier, W.; Palivan, C.G. SOD antioxidant nanoreactors: influence of block copolymer composition on the nanoreactor efficiency. *Macromolecular bioscience*, **2010**, *10,* 531–538.

[72] Rosenkranz, T.; Katranidis, A.; Atta, D.; Gregor, I.; Enderlein, J.; Grzelakowski, M.; Rigler, P.; Meier, W.; Fitter, J. Observing proteins as single molecules encapsulated in surface-tethered polymeric nanocontainers. *Chembiochem*, **2009**, *10,* 702–709.

[73] Axthelm, F.; Casse, O.; Koppenol, W.H.; Nauser, T.; Meier, W.; Palivan, C.G. Antioxidant nanoreactor based on superoxide dismutase encapsulated in superoxide-permeable vesicles. *The journal of physical chemistry. B*, **2008**, *112,* 8211–8217.

[74] Dinu, M.V.; Spulber, M.; Renggli, K.; Wu, D.; Monnier, C.A.; Petri-Fink, A.; Bruns, N. Filling polymersomes with polymers by peroxidase-catalyzed atom transfer radical polymerization. *Macromolecular rapid communications*, **2015**, *36,* 507–514.

[75] Itel, F.; Najer, A.; Palivan, C.G.; Meier, W. Dynamics of membrane proteins within synthetic polymer membranes with large hydrophobic mismatch. *Nano letters*, **2015**, *15,* 3871–3878.

[76] Meier, W.; Nardin, C.; Winterhalter, M. Reconstitution of channel proteins in (polymerized) ABA triblock copolymer membranes. *Angew. Chem. Int. Ed.*, **2000**, *39,* 4599–4602.

[77] Kumar, M.; Habel, J.E.O.; Shen, Y.-x.; Meier, W.P.; Walz, T. High-density reconstitution of functional water channels into vesicular and planar block copolymer membranes. *Journal of the American chemical society*, **2012**, *134,* 18631–18637.

[78] Muhammad, N.; Dworeck, T.; Fioroni, M.; Schwaneberg, U. Engineering of the E. coli outer membrane protein FhuA to overcome the hydrophobic mismatch in thick polymeric membranes. *Journal of nanobiotechnology*, **2011**, *9,* 8.

[79] Itel, F.; Chami, M.; Najer, A.; Lörcher, S.; Wu, D.; Dinu, I.A.; Meier, W. Molecular organization and dynamics in polymersome membranes: A lateral diffusion study. *Macromolecules*, **2014**, *47,* 7588–7596.

[80] Srinivas, G.; Discher, D.E.; Klein, M.L. Key roles for chain flexibility in block copolymer membranes that contain pores or make tubes. *Nano letters*, **2005**, *5,* 2343–2349.

[81] Kim, A.J.; Kaucher, M.S.; Davis, K.P.; Peterca, M.; Imam, M.R.; Christian, N.A.; Levine, D.H.; Bates, F.S.; Percec, V.; Hammer, D.A. Proton transport from dendritic helical-pore-incorporated polymersomes. *Adv. funct. mater.*, **2009**, *19,* 2930–2936.

[82] Picker, A.; Nuss, H.; Guenoun, P.; Chevallard, C. Polymer vesicles as microreactors for bioinspired calcium carbonate precipitation. *Langmuir*, **2011**, *27,* 3213–3218.

[83] Sauer, M.; Haefele, T.; Graff, A.; Nardin, C.; Meier, W. Ion-carrier controlled precipitation of calcium phosphate in giant ABA triblock copolymer vesicles. *Chem. commun.*, **2001,** 2452–2453.

[84] Choi, H.-J.; Lee, H.; Montemagno, C.D. Toward hybrid proteo-polymeric vesicles generating a photoinduced proton gradient for biofuel cells. *Nanotechnology*, **2005**, *16,* 1589–1597.

[85] Graff, A.; Fraysse-Ailhas, C.; Palivan, C.G.; Grzelakowski, M.; Friedrich, T.; Vebert, C.; Gescheidt, G.; Meier, W. Amphiphilic copolymer membranes promote NADH: ubiquinone oxidoreductase activity: Towards an electron-transfer nanodevice. *Macromol. chem. phys.*, **2010**, *211,* 229–238.

[86] Kumar, M.; Grzelakowski, M.; Zilles, J.; Clark, M.; Meier, W. Highly permeable polymeric membranes based on the incorporation of the functional water channel protein Aquaporin Z. *Proceedings of the national academy of sciences of the United States of America*, **2007**, *104,* 20719–20724.

[87] Grzelakowski, M.; Cherenet, M.F.; Shen, Y.-x.; Kumar, M. A framework for accurate evaluation of the promise of aquaporin based biomimetic membranes. *Journal of membrane science*, **2015**, *479,* 223–231.

[88] Nallani, M.; Andreasson-Ochsner, M.; Tan, C.-W.D.; Sinner, E.-K.; Wisantoso, Y.; Geifman-Shochat, S.; Hunziker, W. Proteopolymersomes: in vitro production of a membrane protein in polymersome membranes. *Biointerphases*, **2011**, *6,* 153–157.

[89] Broz, P.; Driamov, S.; Ziegler, J.; Ben-Haim, N.; Marsch, S.; Meier, W.; Hunziker, P. Toward intelligent nanosize bioreactors: a pH-switchable, channel-equipped, functional polymer nanocontainer. *Nano letters*, **2006**, *6,* 2349–2353.

[90] Cottenye, N.; Syga, M.-I.; Nosov, S.; Muller, A.H.E.; Ploux, L.; Vebert-Nardin, C. Biological-like vesicular structures self-assembled from DNA-block copolymers. *Chemical communications*, **2012**, *48,* 2615–2617.

[91] Einfalt, T.; Goers, R.; Dinu, I.A.; Najer, A.; Spulber, M.; Onaca-Fischer, O.; Palivan, C.G. Stimuli-triggered activity of nanoreactors by biomimetic engineering polymer membranes. *Nano letters*, **2015**, *15,* 7596–7603.

[92] Messager, L.; Burns, J.R.; Kim, J.; Cecchin, D.; Hindley, J.; Pyne, A.L.B.; Gaitzsch, J.; Battaglia, G.; Howorka, S. Biomimetic hybrid nanocontainers with selective permeability. *Angewandte chemie*, **2016**, *55,* 11106–11109.

[93] Renggli, K.; Baumann, P.; Langowska, K.; Onaca, O.; Bruns, N.; Meier, W. Selective and responsive nanoreactors. *Adv. funct. mater.*, **2011**, *21,* 1241–1259.

[94] Nardin, C.; Widmer, J.; Winterhalter, M.; Meier, W. Amphiphilic block copolymer nanocontainers as bioreactors. *The European physical journal E*, **2001**, *4,* 403–410.

[95] Ihle, S.; Onaca, O.; Rigler, P.; Hauer, B.; Rodríguez-Ropero, F.; Fioroni, M.; Schwaneberg, U. Nanocompartments with a pH release system based on an engineered OmpF channel protein. *Soft matter*, **2011**, *7,* 532–539.

[96] Xie, W.; He, F.; Wang, B.; Chung, T.-S.; Jeyaseelan, K.; Armugam, A.; Tong, Y.W. An aquaporin-based vesicle-embedded polymeric membrane for low energy water filtration. *J. mater. chem. A*, **2013**, *1,* 7592–7600.

[97] Choi, H.-J.; Germain, J.; Montemagno, C.D. Effects of different reconstitution procedures on membrane protein activities in proteopolymersomes. *Nanotechnology*, **2006**, *17,* 1825–1830.

[98] Tsai, M.-F.; Fang, Y.; Miller, C. Sided functions of an arginine-agmatine antiporter oriented in liposomes. *Biochemistry*, **2012**, *51,* 1577–1585.

[99] Hua, D.; Kuang, L.; Liang, H. Self-directed reconstitution of proteorhodopsin with amphiphilic block copolymers induces the formation of hierarchically ordered proteopolymer membrane arrays. *Journal of the American chemical society*, **2011**, *133,* 2354–2357.

[100] Stoenescu, R.; Graff, A.; Meier, W. Asymmetric ABC-triblock copolymer membranes induce a directed insertion of membrane proteins. *Macromolecular bioscience*, **2004**, *4,* 930–935.

[101] Aguilar; Elvira, C.; Gallardo, A.; Vázquez, B.; Román, J.S. Smart polymers and their applications as biomaterials. In: Topics in tissue engineering, N Ashammakhi, R Reis & E Chiellini, Eds., **2007**.

[102] Wang, X.; Hu, J.; Liu, G.; Tian, J.; Wang, H.; Gong, M.; Liu, S. Reversibly switching bilayer permeability and release modules of photochromic polymersomes stabilized by cooperative noncovalent interactions. *Journal of the American chemical society*, **2015**, *137,* 15262–15275.

[103] Wang, X.; Liu, G.; Hu, J.; Zhang, G.; Liu, S. Concurrent block copolymer polymersome stabilization and bilayer permeabilization by stimuli-regulated "traceless" crosslinking. *Angewandte chemie*, **2014**, *53,* 3138–3142.

[104] Gaitzsch, J.; Appelhans, D.; Janke, A.; Strempel, M.; Schwille, P.; Voit, B. Cross-linked and pH sensitive supported polymer bilayers from polymersomes - studies concerning thickness, rigidity and fluidity. *Soft matter*, **2014**, *10,* 75–82.

[105] Yassin, M.A.; Appelhans, D.; Mendes, R.G.; Rummeli, M.H.; Voit, B. pH-dependent release of doxorubicin from fast photo-cross-linkable polymersomes based on benzophenone units. *Chemistry*, **2012**, *18,* 12227–12231.

[106] Grafe, D.; Gaitzsch, J.; Appelhans, D.; Voit, B. Cross-linked polymersomes as nanoreactors for controlled and stabilized single and cascade enzymatic reactions. *Nanoscale*, **2014**, *6,* 10752–10761.

[107] Zhu, Y.; Wang, F.; Zhang, C.; Du, J. Preparation and mechanism insight of nuclear envelope-like polymer vesicles for facile loading of biomacromolecules and enhanced biocatalytic activity. *ACS nano*, **2014**, *8,* 6644–6654.

[108] Yan, Q.; Wang, J.; Yin, Y.; Yuan, J. Breathing polymersomes: CO_2-tuning membrane permeability for size-selective release, separation, and reaction. *Angewandte chemie*, **2013**, *52,* 5070–5073.

[109] Yan, B.; Han, D.; Boissière, O.; Ayotte, P.; Zhao, Y. Manipulation of block copolymer vesicles using CO_2: Dissociation or "breathing". *Soft matter*, **2013**, *9,* 2011.

[110] Feng, A.; Liang, J.; Ji, J.; Dou, J.; Wang, S.; Yuan, J. CO2-breathing and piercing polymersomes as tunable and reversible nanocarriers. *Scientific reports*, **2016**, *6,* 1–10.

[111] Liu, J.; Postupalenko, V.; Lorcher, S.; Wu, D.; Chami, M.; Meier, W.; Palivan, C.G. DNA-mediated self-organization of polymeric nanocompartments leads to interconnected artificial organelles. *Nano letters*, **2016**, *16,* 7128–7136.

[112] Domes, S.; Filiz, V.; Nitsche, J.; Fromsdorf, A.; Forster, S. Covalent attachment of polymersomes to surfaces. *Langmuir*, **2010**, *26,* 6927–6931.

[113] Langowska, K.; Kowal, J.; Palivan, C.G.; Meier, W. A general strategy for creating self-defending surfaces for controlled drug production for long periods of time. *J. mater. chem. B*, **2014**, *2,* 4684.

[114] Lomora, M.; Itel, F.; Dinu, I.A.; Palivan, C.G. Selective ion-permeable membranes by insertion of biopores into polymersomes. *Physical chemistry chemical physics*, **2015**, *17,* 15538–15546.

[115] Zhang, X.; Lomora, M.; Einfalt, T.; Meier, W.; Klein, N.; Schneider, D.; Palivan, C.G. Active surfaces engineered by immobilizing protein-polymer nanoreactors for selectively detecting sugar alcohols. *Biomaterials*, **2016**, *89,* 79–88.

[116] Chadwick, D.J. *Gramicidin and related ion channel-forming peptides;* Wiley: Chichester, **1999**.

[117] Wallace, B. Gramicidin channels and pores. *Annual review of biophysics and biomolecular structure*, **1990**, *19,* 127–157.

[118] Clement, N.R.; Gould, J.M. Pyranine (8-hydroxy-1,3,6-pyrenetrisulfonate) as a probe of internal aqueous hydrogen ion concentration in phospholipid vesicles. *Biochemistry*, **1981**, *20,* 1534–1538.

[119] Jyothi, G.; Mitra, C.K.; Krishnamoorthy, G. Studies on the exchange of gramicidin in liposomes. *Bioelectrochemistry and bioenergetics*, **1991**, *26,* 395–402.

[120] Andersen, O.S. Ion movement through gramicidin A channels. Single-channel measurements at very high potentials. *Biophysical journal*, **1983**, *41,* 119–133.

[121] Helfrich, P.; Jakobsson, E. Calculation of deformation energies and conformations in lipid membranes containing gramicidin channels. *Biophysical journal*, **1990**, *57,* 1075–1084.

[122] Harroun, T.A.; Heller, W.T.; Weiss, T.M.; Yang, L.; Huang, H.W. Experimental evidence for hydrophobic matching and membrane-mediated interactions in lipid bilayers containing gramicidin. *Biophysical journal*, **1999**, *76,* 937–945.

[123] Jing, W.; Wu, Z.; Wang, E. Electrochemical study of gramicidin D forming ion-permeable channels in the bilayer lipid membranes. *Electrochimica acta*, **1998**, *44,* 99–102.

[124] Sychev, S.V.; Barsukov, L.I.; Ivanov, V.T. Conformation of gramicidin A in Triton X-100 micelles from CD and FTIR data: a clean example of antiparallel double beta5.6 helix formation. *Journal of peptide science*, **2013**, *19,* 452–458.

[125] Oliynyk, V.; Mille, C.; Ng, J.B.S.; Ballmoos, C. von; Corkery, R.W.; Bergstrom, L. Selective and ATP-driven transport of ions across supported membranes into nanoporous carriers using gramicidin A and ATP synthase. *Physical chemistry chemical physics*, **2013**, *15,* 2733–2740.

[126] Gonzalez-Perez, A.; Stibius, K.B.; Vissing, T.; Nielsen, C.H.; Mouritsen, O.G. Biomimetic triblock copolymer membrane arrays: a stable template for functional membrane proteins. *Langmuir*, **2009**, *25,* 10447–10450.

[127] Rigler, P.; Meier, W. Encapsulation of fluorescent molecules by functionalized polymeric nanocontainers: investigation by confocal fluorescence imaging and fluorescence correlation spectroscopy. *Journal of the American chemical society*, **2006**, *128,* 367–373.

[128] Schwille, P. Fluorescence Correlation Spectroscopy and Its Potential for Intracellular Applications. *CBB*, **2001**, *34,* 383–408.

[129] Medina, M.A.; Schwille, P. Fluorescence correlation spectroscopy for the detection and study of single molecules in biology. *BioEssays*, **2002**, *24,* 758–764.

[130] Levin, M.K.; Carson, J.H. Fluorescence correlation spectroscopy and quantitative cell biology. *Differentiation; Research in biological diversity*, **2004**, *72,* 1–10.

[131] Kim, S.A.; Heinze, K.G.; Schwille, P. Fluorescence correlation spectroscopy in living cells. *Nature methods*, **2007**, *4,* 963–973.

[132] Rigler, R.; Mets, U.; Widengren, J.; Kask, P. Fluorescence correlation spectroscopy with high count rate and low background: Analysis of translational diffusion. *Eur biophys j.*, **1993**, *22*.

[133] Koynov, K.; Butt, H.-J. Fluorescence correlation spectroscopy in colloid and interface science. *Current opinion in colloid & interface science*, **2012**, *17,* 377–387.

[134] Erbakan, M.; Shen, Y.-x.; Grzelakowski, M.; Butler, P.J.; Kumar, M.; Curtis, W.R. Molecular cloning, overexpression and characterization of a novel water channel protein from Rhodobacter sphaeroides. *PloS one*, **2014**, *9,* e86830.

[135] Mark, J.E.; Allcock, H.R.; West, R. *Inorganic Polymers;* Oxford University Press, **2005**.

[136] Israelachvili, J.; Pashley, R. The hydrophobic interaction is long range, decaying exponentially with distance. *Nature*, **1982**, *300,* 341–342.

[137] Ingolfsson, H.I.; Andersen, O.S. Screening for small molecules' bilayer-modifying potential using a gramicidin-based fluorescence assay. *Assay and drug development technologies*, **2010**, *8,* 427–436.

[138] Kelkar, D.A.; Chattopadhyay, A. The gramicidin ion channel: a model membrane protein. *Biochimica et biophysica acta*, **2007**, *1768,* 2011–2025.

[139] Goulian, M.; Mesquita, O.N.; Fygenson, D.K.; Nielsen, C.; Andersen, O.S.; Libchaber, A. Gramicidin Channel Kinetics under Tension. *Biophysical journal*, **1998**, *74,* 328–337.

[140] Nardin, C.; Hirt, T.; Leukel, J.; Meier, W. Polymerized ABA triblock copolymer vesicles. *Langmuir*, **2000**, *16,* 1035–1041.

[141] Bohunicky, B.; Mousa, S.A. Biosensors: the new wave in cancer diagnosis. *Nanotechnology, science and applications*, **2010**, *4,* 1–10.

[142] Chambers, J.P.; Arulanandam, B.P.; Matta, L.L.; Weis, A.; Valdes, J.J. Biosensor recognition elements. *Current issues in molecular biology*, **2008**, *10,* 1–12.

[143] Fasolato, C.; Pozzan, T. Effect of membrane potential on divalent cation transport catalyzed by the "electroneutral" ionophores A23187 and ionomycin. *The Journal of biological chemistry*, **1989**, *264,* 19630–19636.

[144] Beeler, T.J.; Jona, I.; Martonosi, A. The effect of ionomycin on calcium fluxes in sarcoplasmic reticulum vesicles and liposomes. *The Journal of biological chemistry*, **1979**, *254,* 6229–6231.

[145] Deleers, M.; Couturier, E.; Malaisse, W.J. Ionomycin-mediated calcium transport in rigid and fluid liposomes. *Cell calcium*, **1981**, *2,* 159–171.

[146] Berridge, M.J.; Lipp, P.; Bootman, M.D. The versatility and universality of calcium signalling. *Nature reviews. Molecular cell biology*, **2000**, *1,* 11–21.

[147] Krebs, J.; Michalak, M. *Calcium: A Matter of Life or Death;* Elsevier Science, **2007**.

[148] Gharibi, H.; Moosavi-Movahedi, Z.; Javadian, S.; Nazari, K.; Moosavi-Movahedi, A.A. Vesicular mixed gemini-SDS-hemin-imidazole complex as a peroxidase-like nano artificial enzyme. *The journal of physical chemistry. B*, **2011**, *115,* 4671–4679.

[149] Feng, C.; Ren, C.-l.; Ma, Y.-q. The coexisting phase behavior of thermo-responsive copolymer solutions. *Soft matter*, **2014**, *10,* 5523–5531.

[150] Gao, Z.; Li, Y.; Cooksey, J.P.; Snaddon, T.N.; Schunk, S.; Viseux, E.M.E.; McAteer, S.M.; Kocienski, P.J. A synthesis of an ionomycin calcium complex. *Angewandte chemie*, **2009**, *48,* 5022–5025.

[151] Bagshaw, C.R. Stopped-Flow Techniques. In: *Encyclopedia of Biophysics*. Roberts, G.C.K., Ed.; Springer Berlin Heidelberg: Berlin, Heidelberg, **2013**; pp. 2460–2466.

[152] Heinemann, F.; Schwille, P. Preparation of micrometer-sized free-standing membranes. *Chemphyschem*, **2011**, *12,* 2568–2571.

[153] Erdahl, W.L.; Chapman, C.J.; Taylor, R.W.; Pfeiffer, D.R. Ca2+ transport properties of ionophores A23187, ionomycin, and 4-BrA23187 in a well defined model system. *Biophysical journal*, **1994**, *66,* 1678–1693.

[154] Ying, W. NAD^+/NADH and $NADP^+$/NADPH in cellular functions and cell death: Regulation and biological consequences. *Antioxidants & redox signaling*, **2008**, *10,* 179–206.

[155] Jang, W.; Gomer, R.H. Exposure of cells to a cell number-counting factor decreases the activity of glucose-6-phosphatase to decrease intracellular glucose levels in Dictyostelium discoideum. *Eukaryotic cell*, **2005**, *4,* 72–81.

[156] Cohn, R.M.; Herman, R.H.; Zakim, D. Glucose 6-phosphatase: a multifunctional enzyme. *The American journal of clinical nutrition*, **1969**, *22,* 1204–1210.

[157] Tegtmeyer, L.C.; Rust, S.; van Scherpenzeel, M.; Ng, B.G.; Losfeld, M.-E.; Timal, S.; Raymond, K.; He, P.; Ichikawa, M.; Veltman, J.; Huijben, K.; Shin, Y.S.; Sharma, V.; Adamowicz, M.; Lammens, M.; Reunert, J.; Witten, A.; Schrapers, E.; Matthijs, G.; Jaeken,

J.; Rymen, D.; Stojkovic, T.; Laforet, P.; Petit, F.; Aumaitre, O.; Czarnowska, E.; Piraud, M.; Podskarbi, T.; Stanley, C.A.; Matalon, R.; Burda, P.; Seyyedi, S.; Debus, V.; Socha, P.; Sykut-Cegielska, J.; van Spronsen, F.; Meirleir, L. de; Vajro, P.; DeClue, T.; Ficicioglu, C.; Wada, Y.; Wevers, R.A.; Vanderschaeghe, D.; Callewaert, N.; Fingerhut, R.; van Schaftingen, E.; Freeze, H.H.; Morava, E.; Lefeber, D.J.; Marquardt, T. Multiple phenotypes in phosphoglucomutase 1 deficiency. *The New England journal of medicine*, **2014**, *370,* 533–542.

[158] Stojkovic, T.; Vissing, J.; Petit, F.; Piraud, M.; Orngreen, M.C.; Andersen, G.; Claeys, K.G.; Wary, C.; Hogrel, J.-Y.; Laforet, P. Muscle glycogenosis due to phosphoglucomutase 1 deficiency. *The New England journal of medicine*, **2009**, *361,* 425–427.

[159] Gianfreda, L. Enzymes of importance to rhizosphere processes. *J. soil sci. plant nutr.*, **2015,** 283–306.

[160] Malinova, I.; Kunz, H.-H.; Alseekh, S.; Herbst, K.; Fernie, A.R.; Gierth, M.; Fettke, J. Reduction of the cytosolic phosphoglucomutase in Arabidopsis reveals impact on plant growth, seed and root development, and carbohydrate partitioning. *Plos one*, **2014**, *9,*1-11.

[161] Koornneef, M.; Meinke, D. The development of Arabidopsis as a model plant. *The plant journal*, **2010**, *61,* 909–921.

[162] Palivan, C.G.; Goers, R.; Najer, A.; Zhang, X.; Car, A.; Meier, W. Bioinspired polymer vesicles and membranes for biological and medical applications. *Chemical society reviews*, **2016**, *45,* 377–411.

[163] Torchilin, V.P. *Handbook of nanobiomedical research: Fundamentals, applications, and recent developments;* World Scientific: Singapore, New Jersey, **2014**.

[164] Mantri, S.; Sapra, K.T.; Cheley, S.; Sharp, T.H.; Bayley, H. An engineered dimeric protein pore that spans adjacent lipid bilayers. *Nature communications*, **2013**, *4,* 1–10.

[165] Paradowska, K.; Surdy, A.; Ginalska, G. α-Phosphoglucomutase from Escherichia coli ATCC 25922 – pilot studies. *Annales Universitates Mariae Curie-Skłodowska, Pharmacia, sectio DDD*, *1,* 125–135.

[166] Raychaudhuri, P.; Li, Q.; Mason, A.; Mikhailova, E.; Heron, A.J.; Bayley, H. Fluorinated amphiphiles control the insertion of alpha-hemolysin pores into lipid bilayers. *Biochemistry*, **2011**, *50,* 1599–1606.

[167] Ladokhin, A.S.; Wimley, W.C.; White, S.H. Leakage of membrane vesicle contents: Determination of mechanism using fluorescence requenching. *Biophysical journal*, **1995**, *69,* 1964–1971.

[168] Pata, V.; Ahmed, F.; Discher, D.E.; Dan, N. Membrane solubilization by detergent: resistance conferred by thickness. *Langmuir*, **2004**, *20,* 3888–3893.

[169] Cymer, F.; Schneider, D. A single glutamate residue controls the oligomerization, function, and stability of the aquaglyceroporin GlpF. *Biochemistry*, **2010**, *49,* 279–286.

[170] Veerappan, A.; Cymer, F.; Klein, N.; Schneider, D. The tetrameric alpha-helical membrane protein GlpF unfolds via a dimeric folding intermediate. *Biochemistry*, **2011**, *50,* 10223–10230.

[171] Fu, D. Structure of a glycerol-conducting channel and the basis for its selectivity. *Science*, **2000**, *290,* 481–486.

[172] Borgnia, M.J.; Agre, P. Reconstitution and functional comparison of purified GlpF and AqpZ, the glycerol and water channels from Escherichia coli. *Proceedings of the national academy of sciences of the United States of America*, **2001**, *98,* 2888–2893.

[173] Poonperm, W.; Takata, G.; Izumori, K. Polyol conversion specificity of Bacillus pallidus. *Bioscience, biotechnology, and biochemistry*, **2008**, *72,* 231–235.

[174] Moon, H.-J.; Tiwari, M.K.; Singh, R.; Kang, Y.C.; Lee, J.-K. Molecular determinants of the cofactor specificity of ribitol dehydrogenase, a short-chain dehydrogenase/reductase. *Applied and environmental microbiology*, **2012**, *78,* 3079–3086.

[175] Moon, H.-J.; Tiwari, M.; Jeya, M.; Lee, J.-K. Cloning and characterization of a ribitol dehydrogenase from Zymomonas mobilis. *Applied microbiology and biotechnology*, **2010**, *87,* 205–214.

[176] Ruskone-Fourmestraux, A.; Attar, A.; Chassard, D.; Coffin, B.; Bornet, F.; Bouhnik, Y. A digestive tolerance study of maltitol after occasional and regular consumption in healthy humans. *European journal of clinical nutrition*, **2003**, *57,* 26–30.

[177] Spulber, M.; Baumann, P.; Saxer, S.S.; Pieles, U.; Meier, W.; Bruns, N. Poly(N-vinylpyrrolidone)-poly(dimethylsiloxane)-based polymersome nanoreactors for laccase-catalyzed biotransformations. *Biomacromolecules*, **2014**, *15,* 1469–1475.

[178] Angelova, M.I.; Dimitrov, D.S. Liposome electroformation. *Faraday discuss. chem. soc.*, **1986**, *81,* 303.

[179] Najer, A.; Wu, D.; Bieri, A.; Brand, F.; Palivan, C.G.; Beck, H.-P.; Meier, W. Nanomimics of host cell membranes block invasion and expose invasive malaria parasites. *ACS nano*, **2014**, *8,* 12560–12571.

X. ACKNOWLEDGEMENTS

I am very grateful to my PhD supervisor Prof. Dr. Cornelia G. Palivan for providing wonderful conditions to do my PhD research and the freedom to be creative within her research group. These last four years have been the most challenging, yet most exciting years of my life, being able to grow professionally and on a personal level. Thank you, Cornelia! Secondly, I am very grateful to Prof. Dr. Wolfgang Meier for his very useful advices and support during my PhD, accepting to be the Examination chair for my defense, as well as for providing the block copolymers. I am very honored to have Prof. Dr. Abhay Pandit (National University of Ireland, Galway) as the co-referee for my PhD thesis and for the effort he is investing in travelling such a long distance just to stop here in Basel for my exam. I am also very grateful as well to Prof. Dr. Abhay Pandit and Keith Feerick (CÚRAM, Centre for Research in Medical Devices, Galway) for the scientific support as part of my carrer development.

I thank Samuel Lörcher, Sven Kasper, and Dr. Adrian Dinu for polymer synthesis. Gabriele Persy, Dr. Adrian Najer, and Christina Zelmer are acknowledged for TEM-measurements, Roland Goers for discussions regarding GUVs, and Mohamed Chami (Center for Cellular Imaging and Nanoanalytics (C-CINA), Biozentrum, University of Basel) for cryo-TEM measurements. I am also very thankful to Dr. B.A. Goodman for editing our manuscripts.

Special thanks go to Serena Rigo and Ina Andrea Ontiveros Casas for preliminary experiments on ionomycin insertion and Dr Reinhard Kissner (Laboratory of Inorganic Chemistry, ETH Zurich) for providing support and useful discussions related to stopped-flow measurements and to Martina Garni for helping with GUVs and CLSM measurements.

I am very thankful to Prof Dr. Dirk Schneider (University of Mainz) for providing the GlpF plasmid and for fruitful discussions. A big big thank you goes to Dr. Noreen Klein and Dr. Elisa Nogueira for guindance in DNA amplification, sequencing, protein expression and purification and for Prof Dr. Marc Creus (University of Basel) for very fruitful discussions regarding the GlpF plasmid. I thank Dr. Timothy Sharpe (Biophysics Facility, Biozentrum, University of Basel) for introducing me to basic biophysical techniques, at the beginning of my PhD.

I am very thankful to Dr. Itel Fabian, Dr. Pascal Tanner, Dr. Mariana Spulber, Dr. Patric Baumann, Dr. Thomas Schuster, Dr. Adrian Najer, Dr. Martin Nussbaumer, Dr. Dalin Wu, and Dr. Ozana Fischer for the introduction in the lab and useful scientific advices during my PhD.

I thank to Dr. Gesine Grabole-Gunkel for the wonderful scientific support and for the prooreading of this thesis together with Dr. Ioana Craciun.

Special thanks go to Prof. Dr. Hagan Bayley (University of Oxford) for enabling the connection to Dr. Shiksha Mantri (ETH Zurich), which produced the mixture of α-hemolysins and with whom I have had very fruitful discussions.

Dr. Christine Strasser, Dr. Hans Flury, and Cedric Graber (Zeiss), as well as Dr. Volker Buschmann (PicoQuant) are highly appreciated for the training opportunities and technical support in confocal microscopy and fluorescence correlation spectroscopy.

PD Dr. med. Stephanie Gros (UKBB) and Dr. Cora-Ann Schoenenberger are thanked for the exciting scientific interactions. I really hope we will be able to continue our amazing collaboration.

Last, but not least, I would like to thank to the entire Meier/Palivan group for the lovely working atmosphere and to Maya Greuter and Daniela Tischhauser for all the administrative support.

Many many thanks to my family and friends: Prof. Dr. Camelia Draghici (Cami, without your encouragements, I would not have embarked to this PhD: Pupilici!), Fabian Itel (your support in the lab was as well priceless!), Chatrina and Corina Caviezel and their parents, David Tora, Jana Tischer, Adeline Cojean, Madalina Stroie, Adrian Dinu, Adrian Najer, Mariana Spulber, Bernadetta + Wojciech + Krosisko Gajewska, Ioana Craciun, to my wonderful Swiss neighbours and the entire CouchSurfing community (special mention to: Dominique Wagner, Jakob Forter, Stephen Tallowitz, and Emmanuel Suffert) from Basel: You have all made my life much much more easier and enjoyable during my PhD!

A BIG BIG thank you, to all and for those I forgot to mention, and keep in touch! ☺

With my very best wishes,
Mihai

XI. APPENDIX

*This appendix has been compiled to serve as a guide with raw data examples obtained from measuring the size of polymersomes, and the diffusion time of free dyes (Oregon Green-488 and pyranine) in solution or polymersomes with encapsulated dye molecules (pyranine) by light scattering (**Appendix A**) and fluorescence correlation spectroscopy (**Appendix B**) techniques. These were obtained by the measurement of a single sample and at least three samples were necessary for statistically relevance and presentation of the final values herein.*

A.Example of DLS/SLS raw data

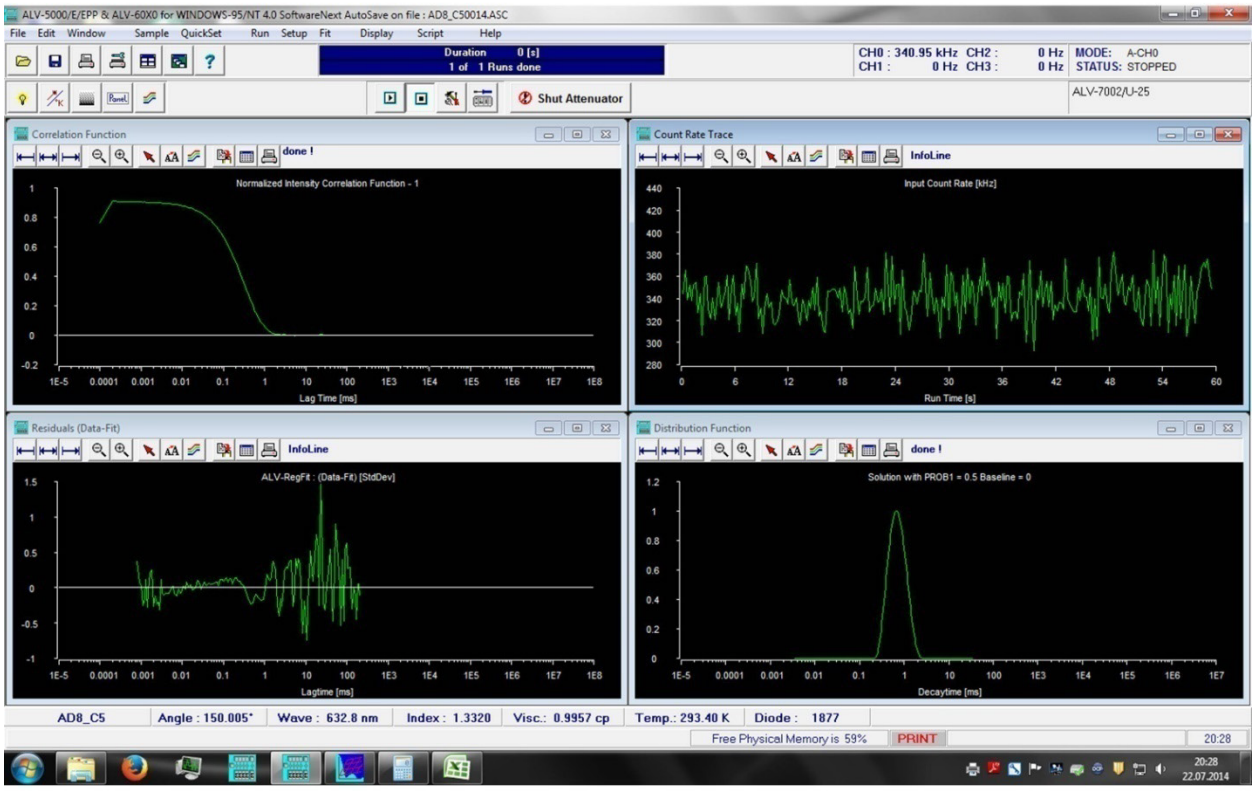

Fig. 53. Light scattering raw data for $A_6B_{44}A_6$ polymersomes with encapsulated pyranine, at a polymer concentration of 0.07 mg/mL: normalized intensity correlation function, count rate, plot of residuals from the data fit, and the distribution function.

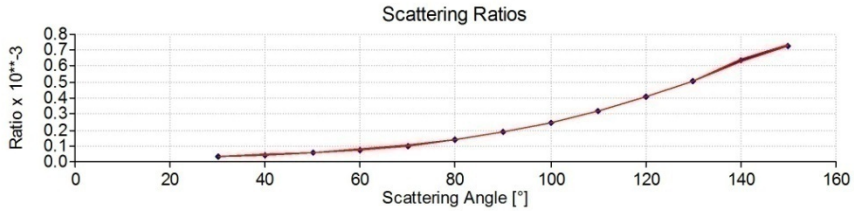

Angle	q²[1/m²]	CR[kHz]	dCR[%]	Imon	dImon[%]	T[K]	dT[%]	Kc/R	dKc/R[%]	Rad[nm]	dRad[%]
30	4.69E+13	367.22	1.52	32808	0.33	293.4	0	3.19E-05	1.19	117.27	2.57
40	8.19E+13	547.577	82.46	74897	84.66	293.4	0	4.41E-05	2.2	112.01	2.39
50	1.25E+14	520.466	2.77	96553	0.16	293.4	0	5.72E-05	2.6	111.31	6.17
60	1.75E+14	386.441	1.39	97359	0.37	293.4	0	7.72E-05	1.02	105.18	2.24
70	2.30E+14	300.485	1.38	96951	0.21	293.4	0	1.01E-04	1.17	104.86	0.93
80	2.89E+14	564.972	1.68	238431	0.38	293.4	0.01	1.39E-04	1.31	102.15	1.87
90	3.50E+14	452.553	1.3	236642	1.03	293.4	0	1.84E-04	0.27	99.79	1.92
100	4.11E+14	378.968	0.28	236939	0.56	293.4	0	2.42E-04	0.28	99.17	2.24
110	4.70E+14	328.01	0.82	239147	0.42	293.4	0	3.19E-04	0.4	96.75	1.1
120	5.25E+14	299.711	0.45	240386	0.56	293.4	0	4.07E-04	0.11	95.53	1.11
130	5.75E+14	290.206	0.27	238940	0.26	293.4	0	5.04E-04	0.01	94.89	1.85
140	6.18E+14	290.117	1.05	238315	0.31	293.4	0	6.36E-04	0.74	94.35	1.73
150	6.53E+14	342.69	1.05	236569	0.42	293.4	0	7.28E-04	0.63	95.98	0.78

Fig. 54. Light scattering raw data for $A_6B_{44}A_6$ polymersomes with encapsulated pyranine, at a polymer concentration of 0.07 mg/mL: Scattering ratio plot and specific raw parameters at 30 -150 ^{0} angles.

A

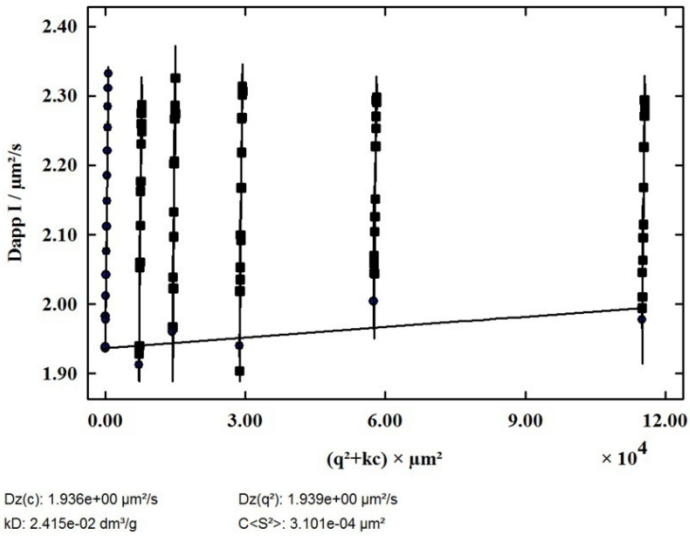

B

Dynamic light scattering, Results of D-II Plot, q2-dep: 1, c-dep: 1, smoothed				
4.31 10/01				
File	Conc/(g/dm³)	Dz(app)/(µm²/s)	C<S²>(app)/µm²	Rh/nm
Conc.=0	0	1.939e	3.10E-04	111.277
AD8_c1.sta	1.25	1.977e	2.63E-04	109.106
AD8_c2.sta	0.625	2.004e	2.39E-04	107.768
AD8_c3.sta	0.3125	1.940e	3.21E-04	111.39
AD8_c4.sta	0.1562	1.959e	2.95E-04	110.141
AD8_c5.sta	0.0781	1.912e	3.24E-04	112.88

Fig. 55. Dynamic light scattering raw data for $A_6B_{44}A_6$ polymersomes with encapsulated pyranine, serially diluted to polymer concentrations ranging from 1.25 mg/mL to 0.07 mg/mL: Guinier plot (A) and results obtained from the fitted data (B).

A

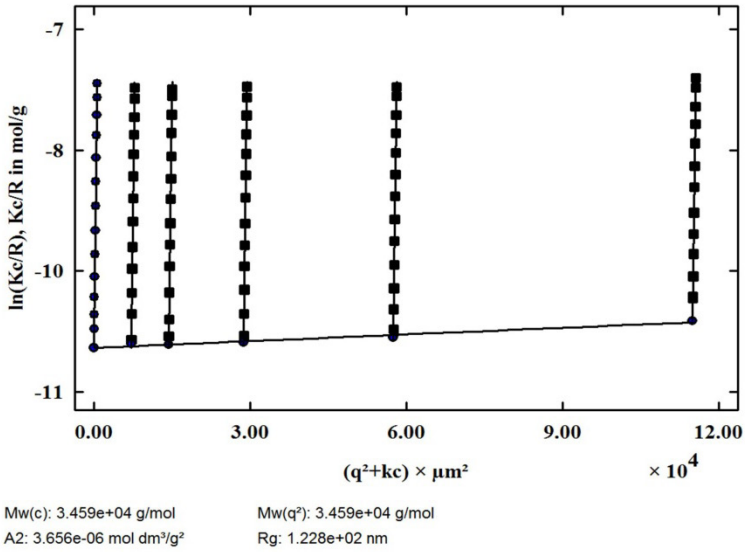

B

Static light scattering, Results of Guinier plot, q2-dep: 1, c-dep: 1, smoothed

4.31 10/01

File	Conc/(g/dm³)	Mw(app)/(g/mol)	<S²>(app)/µm²	Rg(app)/nm
Conc.=0	0	3.46E+04	1.51E-02	122.774
AD8_c1.sta	1.25	2.48E+04	1.40E-02	118.187
AD8_c2.sta	0.625	3.05E+04	1.46E-02	120.68
AD8_c3.sta	0.3125	3.23E+04	1.49E-02	121.86
AD8_c4.sta	0.1562	3.32E+04	1.50E-02	122.361
AD8_c5.sta	0.0781	3.31E+04	1.49E-02	122.154

Fig. 56. Static light scattering raw data for $A_6B_{44}A_6$ polymersomes with encapsulated pyranine, serially diluted to polymer concentrations ranging from 1.25 mg/mL to 0.07 mg/mL: Guinier plot (A) and results obtained from the fitted data (B).

Sample	Conc/(g/dm³)	PDI	Rg/Rh
AD8_c1.sta	1.25	0.135	1.083231
AD8_c2.sta	0.625	0.107	1.119813
AD8_c3.sta	0.3125	0.133	1.093994
AD8_c4.sta	0.1562	0.14	1.110949
AD8_c5.sta	0.0781	0.15	1.082158

Fig. 57. Raw data for $A_6B_{44}A_6$ polymersomes with encapsulated pyranine, serially diluted to polymer concentrations ranging from 1.25 mg/mL to 0.07 mg/mL: PDI and $\rho = R_g/R_h$ values.

B. An example of FCS raw data

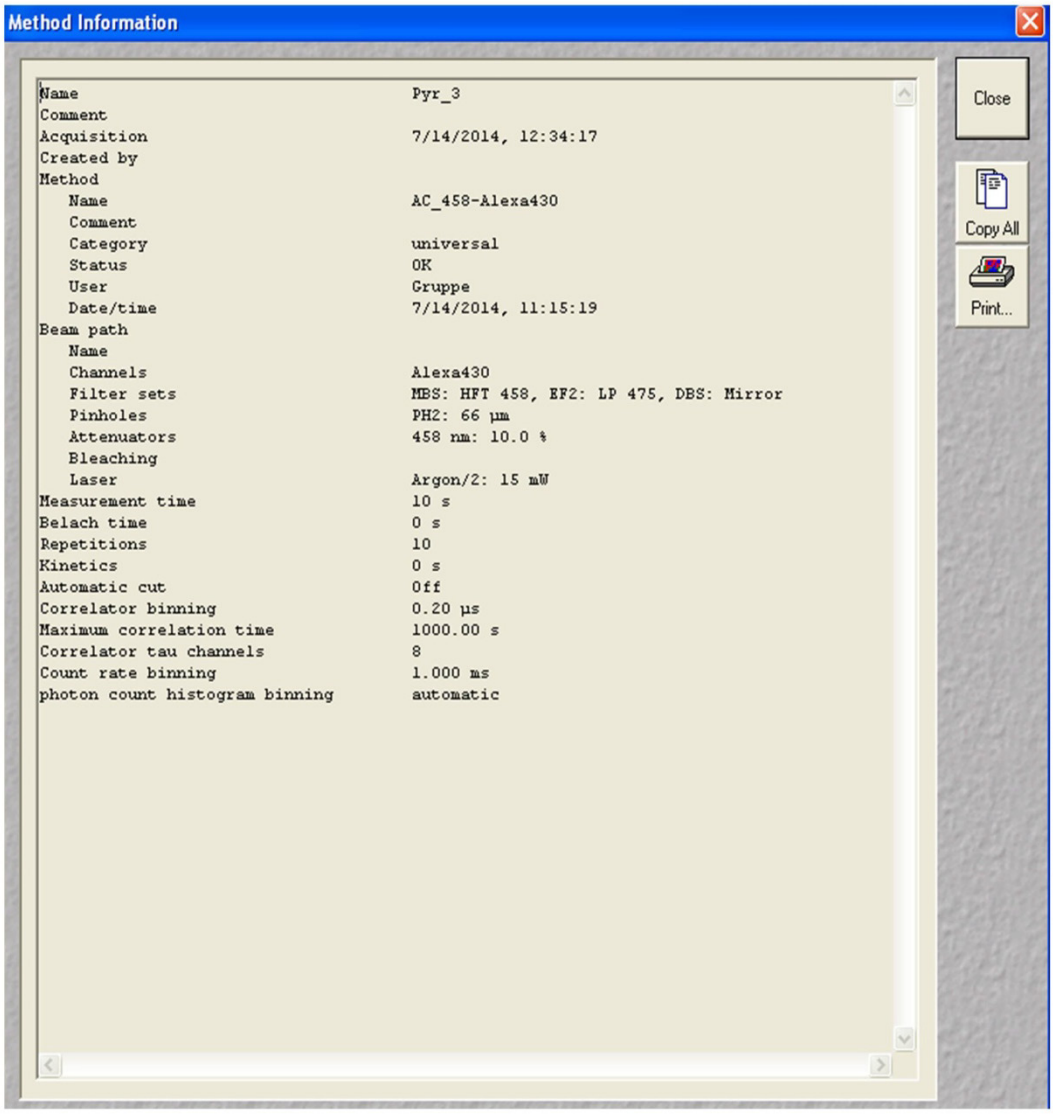

Fig. 58. Method information used for mearing the diffusion time of free pyranine in solution and encapsulated in polymersomes.

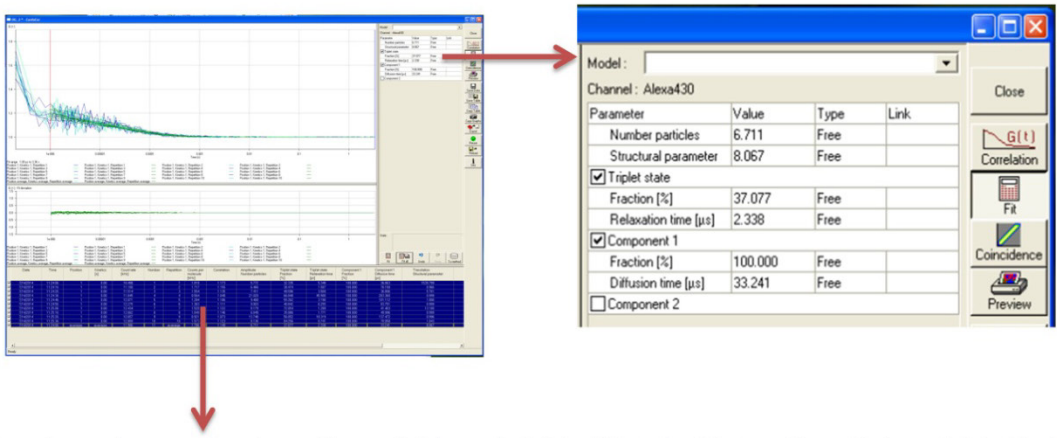

Date	Time	Position	Kinetics [s]	Count rate [kHz]	Number	Repetition	Counts per molecule [kHz]	Correlation	Amplitude Number particles	Triplet state Fraction [%]	Triplet state Relaxation time [µs]	Component 1 Fraction [%]	Component 1 Diffusion time [µs]	Translation Structural	chi ²
7/14/2014	11:24:06	1	0	10.498	1	1	1.819	1.173	5.772	32.335	5.348	100	36.863	1539.799	2.46E-04
7/14/2014	11:24:16	1	0	11.1	2	2	1.717	1.155	6.466	38.474	1.587	100	76.158	0.966	2.86E-04
7/14/2014	11:24:26	1	0	11.514	3	3	1.554	1.135	7.411	49.596	3.568	100	36.806	5.701	1.59E-04
7/14/2014	11:24:36	1	0	11.845	4	4	0.564	1.048	21.02	66.848	45.9	100	283.36	0.999	2.17E-04
7/14/2014	11:24:46	1	0	12.071	5	5	1.284	1.106	9.4	55.262	3.19	100	101.112	1	1.40E-04
7/14/2014	11:24:56	1	0	12.275	6	6	1.363	1.111	9.003	40.842	6.255	100	83.751	0.999	1.53E-04
7/14/2014	11:25:06	1	0	12.434	7	7	1.52	1.122	8.179	72.054	1.289	100	41.403	13.1	1.78E-04
7/14/2014	11:25:16	1	0	12.662	8	8	1.849	1.146	6.849	35.086	1.771	100	49.996	0.999	1.64E-04
7/14/2014	11:25:26	1	0	12.657	9	9	0.921	1.073	13.748	56.052	18.319	100	137.472	0.996	1.34E-04
7/14/2014	11:25:36	1	0	12.8	10	10	1.573	1.123	8.136	84.256	0.741	100	70.058	1.043	1.69E-04
7/14/2014	11:24:06	average	average	11.986	11	average	1.786	1.149	6.711	37.077	2.338	100	33.241	8.067	1.86E-05

Fig. 59. FCS raw data obtained by measuring Oregon Green 488, during the calibration of the FCS instrument.

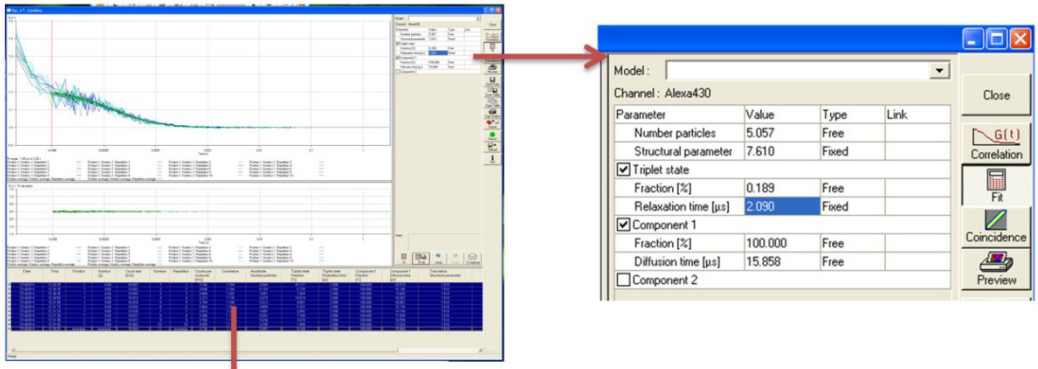

Date	Time	Position	Kinetics [s]	Count rate [kHz]	Number	Repetition	Counts per molecule [kHz]	Correlation	Amplitude Number particles	Triplet state Fraction [%]	Triplet state Relaxation time [µs]	Component 1 Fraction [%]	Component 1 Diffusion time [µs]	Translation Structural parameter	chi ²
7/14/2014	12:30:25	1	0	18.897	1	1	3.106	1.164	6.084	41.117	2.09	100	20.574	7.61	8.66E-05
7/14/2014	12:30:35	1	0	18.803	2	2	3.648	1.194	5.154	0.739	2.09	100	16.106	7.61	1.06E-04
7/14/2014	12:30:45	1	0	18.855	3	3	3.808	1.202	4.951	7.584	2.09	100	14.92	7.61	5.02E-05
7/14/2014	12:30:55	1	0	18.815	4	4	3.313	1.176	5.679	19.074	2.09	100	18.267	7.61	8.27E-05
7/14/2014	12:31:05	1	0	18.97	5	5	3.784	1.199	5.013	9.091	2.09	100	16.887	7.61	7.36E-05
7/14/2014	12:31:15	1	0	18.929	6	6	3.864	1.204	4.898	0.353	2.09	100	15.726	7.61	6.34E-05
7/14/2014	12:31:25	1	0	19.036	7	7	3.81	1.2	4.997	2.652	2.09	100	16.159	7.61	7.65E-05
7/14/2014	12:31:35	1	0	18.837	8	8	3.386	1.18	5.563	7.7	2.09	100	17.594	7.61	5.32E-05
7/14/2014	12:31:45	1	0	18.912	9	9	3.76	1.199	5.03	3.57	2.09	100	16.559	7.61	8.05E-05
7/14/2014	12:31:55	1	0	18.983	10	10	4.035	1.213	4.705	1.989	2.09	100	13.52	7.61	6.32E-05
7/14/2014	12:30:25	average	average	18.904	11	average	3.738	1.198	5.057	0.189	2.09	100	15.858	7.61	3.91E-06

Fig. 60. FCS raw data obtained by measuring pyranine.

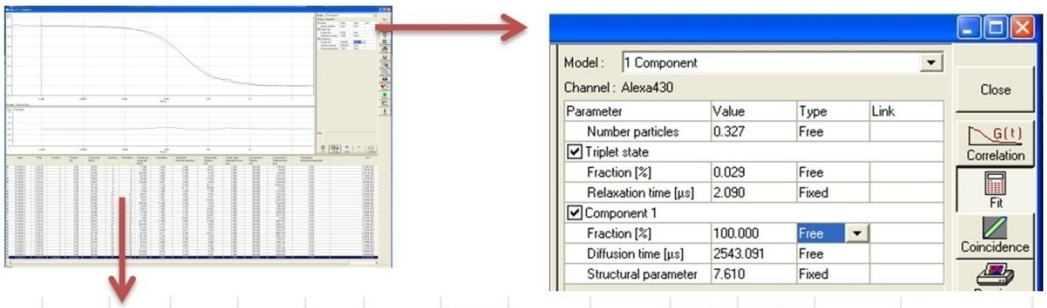

Date	Time	Position	Kinetics [s]	Count rate [kHz]	Number	Repetition	Counts per molecule [kHz]	Correlation	Amplitude Number particles	Triplet state Fraction [%]	Triplet state Relaxation time [µs]	Component 1 Fraction [%]	Component 1 Diffusion time [µs]	Translation Structural parameter	chi²
7/14/2014	13:22:33	1	0	30.954	1	1	77.08	3.49	0.402	0.077	2.09	100	1198.693	7.61	6.28E-03
7/14/2014	13:22:43	1	0	27.561	2	2	1.982	1.072	13.906	38.331	2.09	100	43.694	7.61	2.79E-05
7/14/2014	13:22:53	1	0	30.782	3	3	204.962	7.659	0.15	0.138	2.09	100	423.984	7.61	2.41E-02
7/14/2014	13:23:03	1	0	29.537	4	4	60.793	3.058	0.486	0.104	2.09	100	2170.112	7.61	7.74E-03
7/14/2014	13:23:13	1	0	29.805	5	5	20.456	1.686	1.457	12.928	2.09	100	1426.004	7.61	2.42E-04
7/14/2014	13:23:23	1	0	34.923	6	6	122.954	4.521	0.284	0.02	2.09	100	7422.459	7.61	4.67E-03
7/14/2014	13:23:33	1	0	30.714	7	7	3.751	1.122	8.189	62.111	2.09	100	31569.012	7.61	1.52E-04
7/14/2014	13:23:43	1	0	28.19	8	8	1.687	1.06	16.712	46.008	2.09	100	57.985	7.61	3.42E-05
7/14/2014	13:23:53	1	0	29.179	9	9	17.645	1.605	1.654	7.478	2.09	100	1147.463	7.61	4.73E-04
7/14/2014	13:24:03	1	0	31.275	10	10	48.821	2.561	0.641	0.001	2.09	100	1757.242	7.61	2.63E-03
7/14/2014	13:24:13	1	0	29.86	11	11	20.524	1.687	1.455	0.011	2.09	100	1566.719	7.61	1.01E-03
41834	0.5586	1	0	29.384	12	12	3.672	1.125	8.003	54.607	2.09	100	2443.708	7.61	7.68E-05
7/14/2014	13:24:33	1	0	39.383	13	13	395.338	11.038	0.1	0.079	2.09	100	2522.65	7.61	1.00E-02
7/14/2014	13:24:43	1	0	31.465	14	14	93.958	3.986	0.335	0.394	2.09	100	886.36	7.61	3.70E-03
7/14/2014	13:24:53	1	0	32.198	15	15	25.814	1.802	1.247	20.803	2.09	100	7196.605	7.61	1.03E-03
7/14/2014	13:25:03	1	0	30.692	16	16	14.198	1.463	2.162	22.422	2.09	100	1899.228	7.61	1.96E-04
7/14/2014	13:25:13	1	0	32.09	17	17	11.706	1.365	2.741	24.641	2.09	100	3677.765	7.61	1.09E-04
7/14/2014	13:25:23	1	0	28.231	18	18	1.8	1.064	15.687	59.118	2.09	100	72.289	7.61	4.91E-05
7/14/2014	13:25:33	1	0	44.632	19	19	477.497	11.699	0.093	12.066	2.09	100	2087.782	7.61	2.14E-02
7/14/2014	13:25:43	1	0	39.913	20	20	204.359	6.12	0.195	0.018	2.09	100	2925.437	7.61	3.20E-03
7/14/2014	13:25:53	1	0	34.973	21	21	81.187	3.321	0.431	0.051	2.09	100	2058.509	7.61	3.13E-03
7/14/2014	13:26:03	1	0	32.079	22	22	34.97	2.09	0.917	1.91	2.09	100	1570.223	7.61	1.71E-03
7/14/2014	13:26:13	1	0	37.13	23	23	82.103	3.211	0.452	28.513	2.09	100	8856.344	7.61	6.38E-03
41834	0.559988	1	0	33.747	24	24	145.398	5.309	0.232	0.095	2.09	100	2052.316	7.61	0.008666
7/14/2014	13:26:34	1	0	32.944	25	25	83.154	3.524	0.396	0.016	2.09	100	1130.917	7.61	3.40E-03
7/14/2014	13:26:44	1	0	35.918	26	26	67.516	2.88	0.532	0	2.09	100	1855.136	7.61	7.98E-04
7/14/2014	13:26:54	1	0	32.118	27	27	40.131	2.249	0.8	0.007	2.09	100	2344.177	7.61	1.16E-03
7/14/2014	13:27:04	1	0	34.162	28	28	33.719	1.987	1.013	2.49	2.09	100	1587.939	7.61	3.10E-04
7/14/2014	13:27:14	1	0	40.475	29	29	310.688	8.676	0.13	0.102	2.09	100	1959.398	7.61	4.91E-03
7/14/2014	13:27:24	1	0	39.425	30	30	161.91	5.107	0.243	0.051	2.09	100	2308.303	7.61	1.64E-03
7/14/2014	13:22:33	average	average	34.42	31	average	105.193	4.056	0.327	0.029	2.09	100	2543.091	7.61	6.13E-04

Fig. 61. FCS raw data obtained by measuring $A_6B_{44}A_6$ polymersomes with encapsulated pyranine. Data is evaluated in this case using one component, assuming that there is no free dye in solution.